IOWA STATE UNIVERSITY
Digital Repository

Graduate Theses and Dissertations

Iowa State University Capstones, Theses and Dissertations

2010

An experimental validation of a statistical based damage detection approach

Mitchell Pohlkamp
Iowa State University

Follow this and additional works at: https://lib.dr.iastate.edu/etd

 Part of the Civil and Environmental Engineering Commons

Recommended Citation
Pohlkamp, Mitchell, "An experimental validation of a statistical based damage detection approach" (2010). *Graduate Theses and Dissertations*. 11797.
https://lib.dr.iastate.edu/etd/11797

This Thesis is brought to you for free and open access by the Iowa State University Capstones, Theses and Dissertations at Iowa State University Digital Repository. It has been accepted for inclusion in Graduate Theses and Dissertations by an authorized administrator of Iowa State University Digital Repository. For more information, please contact digirep@iastate.edu.

www.manaraa.com

An experimental validation of a statistical based damage detection approach

by

Mitchell Pohlkamp

A thesis submitted to the graduate faculty

in partial fulfillment of the requirements for the degree of

MASTER OF SCIENCE

Major: Civil Engineering (Structural Engineering)

Program of Study Committee:
Terry J. Wipf, Co-major Professor
Brent M. Phares, Co-major Professor
Loren W. Zachary

Iowa State University

Ames, Iowa

2010

Copyright © Mitchell Pohlkamp, 2010. All rights reserved

www.manaraa.com

TABLE OF CONTENTS

www.manaraa.com

www.manaraa.com

www.manaraa.com

LIST OF FIGURES

www.manaraa.com

www.manaraa.com

LIST OF TABLES

www.manaraa.com

ACKNOWLEDGMENTS

First, I would like to express my most sincere gratitude for all the help given to me by Dr. Brent Phares and Dr. Terry Wipf throughout my years as a graduate student. Without their constant guidance, attention to detail, and their words of encouragement I could not have completed my Master's program. They have taught me much over the past two years that I will continue to use throughout my career and I cannot thank them enough.

I would also like to thank Dr. Zachary for being on my committee, for his suggestions on this thesis, and for helping me achieve my Master's degree.

Much thanks goes out to Doug Wood for his help in the lab and at the bridge. His working knowledge of all things lab and field testing related thoroughly improved the quality of my research and time spent at ISU. Appreciation also goes out to Dr. Lowell Greimann for his extensive research background and inscrutable eye for detail as both were extremely helpful in proceeding in my research and finishing this thesis.

I would like to thank my Town Engineering officemates Casey Faber, Owen Berg, and Thomas Lewin for their constant help in classes and for helping me enjoy my years as a graduate student. There were definitely never any dull moments spent with them. Thanks also go out to my Bridge Engineering officemates Ping Lu, Ashley Cook, Anna Nadermann, and Ursula Deza for their help and support. Special thanks goes out to Ping since without her constant help and guidance I wouldn't be where I am today in my research.

Finally, I would like to extend my deepest gratitude to my parents; their endless support and constant encouragement helped me to become the person I am today.

www.manaraa.com

ABSTRACT

In this thesis, work was completed to validate the accuracy of a developed statistical based damage detection approach. The damage detection approach uses the differences in actual and predicted strains from locations on the bridge caused by heavy five-axle trucks. These differences, called residuals, are then used to construct control charts which compare undamaged and damaged structure data. The validation was achieved by using sacrificial specimens, which modeled damage sensitive locations, were mounted on the bridge and exposed to ambient traffic loads. Different damage levels, simulating cracks or corrosion, were introduced to the sacrificial specimen. Damaged data were compared to undamaged data through the use of control charts and the damage levels were detected. It was also found that damage needed to be close to a sensor in order to be detected by the control chart.

A short sensor attachment study was also completed in this thesis. Issues arose in attaching sensors to concrete therefore multiple sensor attachment techniques were investigated. Through testing in a controlled lab setting it was found that the new techniques were insufficient in transferring strain from the concrete to the sensor. Further study needed to be completed in order to find a satisfactory sensor attachment technique.

www.manaraa.com

CHAPTER 1. INTRODUCTION

The United States infrastructure continues to deteriorate and bridge inspections continue to play a crucial part in ensuring the safety of all who cross over the bridges. As visual inspections of each bridge become more difficult and costly, transportation departments are looking toward other methods of measuring the structural integrity of highway bridges including structural health monitoring (SHM) systems. According to Chintalapudi et al (Chintalapudi, et al. 2006), a structural health monitoring system is one that can autonomously and proactively assess the structural integrity of bridges, buildings, and aerospace vehicles. SHM systems have been in development for many years and are becoming more prominent throughout the United States.

Damage detection, with respect to SHM, is the means of determining if damage exists in the structure by changes in modal parameters, differences in strain, or other changes in behavior over time. The development of damage detection techniques has been ongoing for approximately twenty years and can be as straightforward as determining that damage has occurred somewhere in the structure and as complex as determining the location and severity of the damage. It is generally thought that the use of damage detection techniques may provide ways to increase the safety of the public traveling over the thousands of bridges currently in use.

1.1 General Background: Previous System Development

The precipitous for this work is that in 2005 the Iowa Department of Transportation requested the development of a system that was capable of autonomously detecting damage (specifically the development of fatigue cracks in fracture-critical, two-girder bridges). A SHM system was developed by Wipf, Phares, and Doornink as described in, "Monitoring the Structural Condition of Fracture-Critical Bridges Using Fiber Optic Technology," that uses strain as the monitoring metric (Wipf, Phares and Doornink 2007). The system includes a fiber optic sensor network, data collection and management equipment, wireless communications equipment, and a novel data processing algorithm (Wipf, Phares and Doornink 2007).

The SHM system collects data continuously resulting in large volumes of data that would be impractical for an engineer to discretely analyze. Therefore, the system autonomously identifies

www.manaraa.com

and extracts only the useful sets of strain data; specifically the quasi-static response of the bridge under ambient traffic loads (Wipf, Phares and Doornink 2007). The raw strain data contains many unwanted elements that need to be removed to gain access to the quasi-static live-load response. The process for reducing a continuous data set to the most useful information is described in the following paragraphs.

In a given 24 hour period, temperature variations create a cyclic strain response as is shown in Figure 1.1. The long rolling variation is the result of temperature fluctuations and the short vertical "spikes" are strains resulting from ambient traffic. It was found that if the data were split into approximately one megabyte segments, corresponding to about 27 seconds, temperature variations do not exist. An average baseline can be determined for each 27 second data set. In a process called data zeroing, this average baseline is then subtracted from all data in the 27 second set thereby creating a data set without temperature effects.

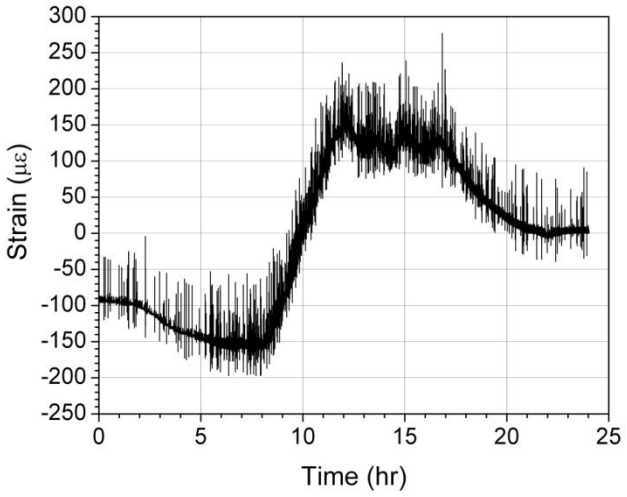

Figure 1.1 24 Hour Strain Record (Wipf, Phares and Doornink 2007)

After data zeroing, the data set contains three components: random noise, the quasi-static vehicular response, and dynamic induced behaviors (Wipf, Phares and Doornink 2007). A lowpass frequency filter is used to remove the noise and dynamic components from the data set since the frequencies of the quasi-static vehicular events are much lower than those of the dynamic responses and noise in the data file, leaving only the quasi-static response. After the

www.manaraa.com

zeroing and filtering is performed, vehicular events are identified within the strain data based on a statistical and structural evaluation of the vehicular response relative to the location of a sensor. After event identification, maximum and minimum strain values, called event extrema, are identified for each event. An event after zeroing, filtering, and extrema identification is shown in Figure 1.2.

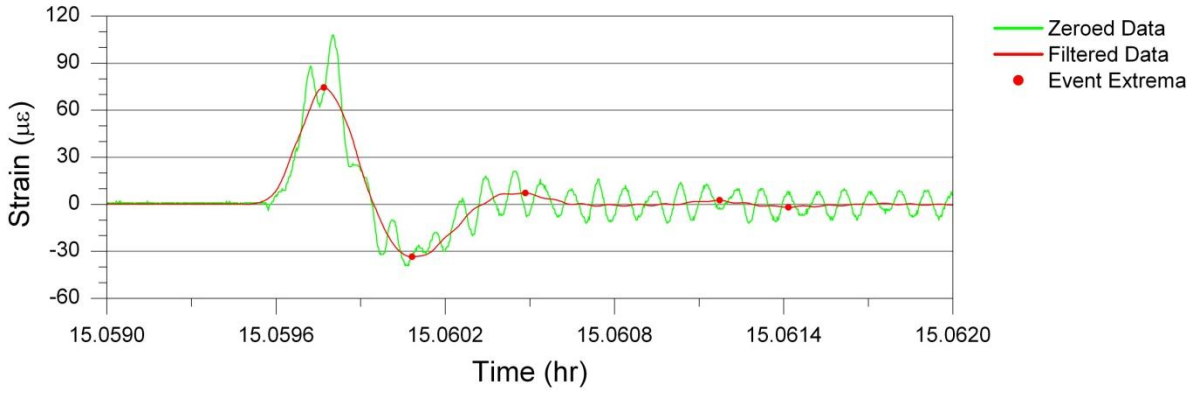

Figure 1.2 Zeroed, Filtered, and Event Extrema Identified Vehicular Event (Wipf, Phares and Doornink 2007)

Strain sensors on the bridge are assigned one of two designations: target sensors (TSs) and non-target sensors (NTSs). In most cases, structural damaged is localized and, therefore, the TSs are those located near where damage might be expected. The NTSs are those located further from the damage sensitive areas and generally relate more to global structural behavior.

The event extrema from two sensors (one TS and one NTS) are matched to form x-y pairs that can be shown on a scatter plot (Figure 1.3). Initial data are collected during a "training" process which defines the "normal" behavior. This process is completed for all applicable and desired sensor pairs. In some cases up to four quadrants of pairs (maximum-maximum, maximum-minimum, minimum-maximum, and minimum-minimum) are present depending on the sensitivity of the sensors to the longitudinal location of the vehicle. Once all scatter plots are created, limits for the data are manually set by an engineer. A typical scatter plot with defined limits is shown in Figure 1.4.

www.manaraa.com

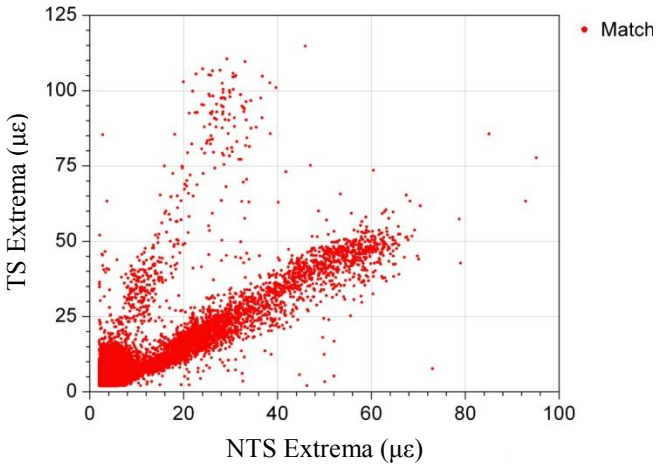

Figure 1.3 Matched Data Points from Two Sensors (Wipf, Phares and Doornink 2007)

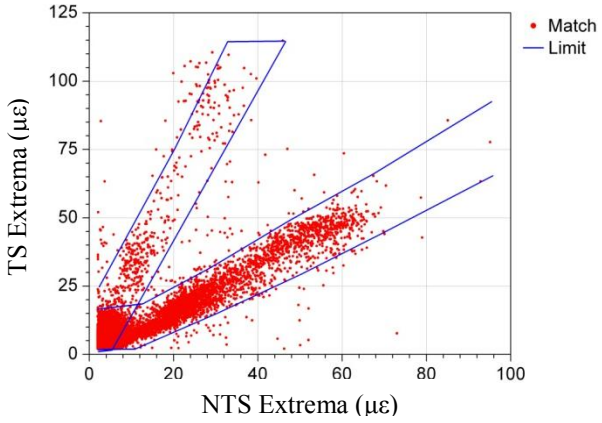

Figure 1.4 Matched Data Points with Applied Limits (Wipf, Phares and Doornink 2007)

Following training, new data are collected from the sensors, zeroed, and filtered using the above discribed methods. The event extrema are paired and compared to the previously established limits. For data points within the set limits, a "pass" assessment is assigned, while for data points outside the set limits, a "fail" assessment is assigned. A relationship pass percentage (RPP) is computed from the data point as follows:

$$RPP\ (\%) = \frac{Number\ of\ "pass"\ assessments}{Total\ number\ of\ assessments} \cdot (100)$$

Numerous RPPs are calculated throughout the monitored time and histograms created. In the histograms from the initial bridge condition, a large grouping of assessments can be expected to

www.manaraa.com

have RPPs near the 100% mark as shown in Figure 1.5. If damage gradually occurs, the large grouping of RPPs can be expected to decrease from near 100% to 0% as time progresses as illustrated in Figure 1.6. If damage occurs suddenly, the histograms can be expected to resemble Figure 1.7 where the RPP changes rapidly.

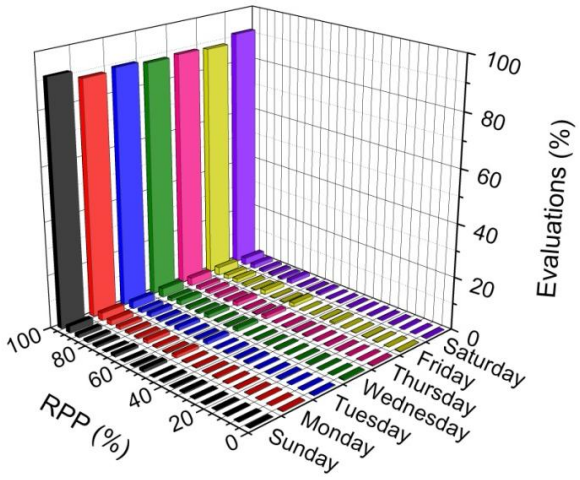

Figure 1.5 Initial Bridge Condition Daily Evaluation Histogram (Wipf, Phares and Doornink 2007)

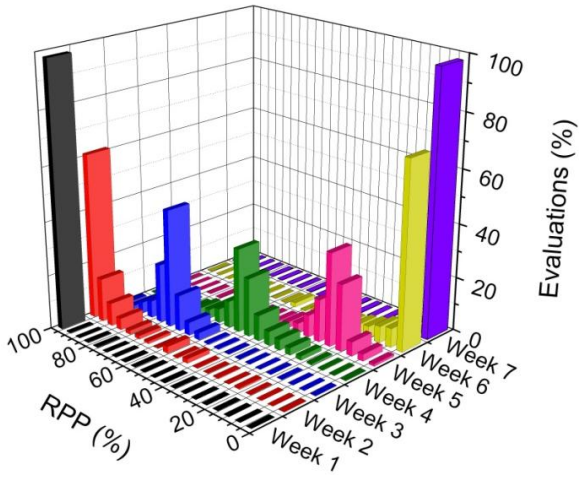

Figure 1.6 Gradually Occurring Damage Daily Assessment Histogram (Wipf, Phares and Doornink 2007)

www.manaraa.com

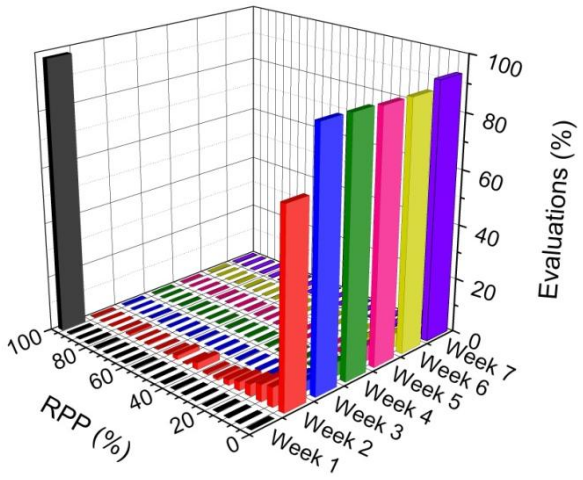

Figure 1.7 Suddenly Occurring Damage Daily Assessment Histogram (Wipf, Phares and Doornink 2007)

In, "Evaluation of a Structural Health Monitoring System for Steel Girder Bridges," Vis developed a finite element model (FE) with simulated damage to analytically verify that, if damage were to occur in a damage sensitive location near a TS, the relationships between TSs and NTSs would change significantly (Vis 2007). A FE model of the bridge was constructed using a commercially available suitable FE software package. Shell63 four node shell elements were used to model both the structural components and the concrete deck. The damage sensitive locations (i.e., locations with high strain concentrations) on the bridge were modeled with refined elements.

The FE model was verified using data obtained from a controlled load test conducted on the subject bridge (Vis 2007). A test truck was driven across the bridge at a crawl speed and data were collected with strain transducers. The position of the truck was recorded at ten foot intervals so that truck position could be aligned with the collected data. Loads equivalent to the test truck were similarly applied to the FE model. The global results from the FE model closely matched the global results obtained from the load test, verifying the FE model accuracy on a global scale. The strains from damage sensitive locations were also compared locally but did not agree as well as the global results. It was therefore concluded that the FE model did not accurately model the damage sensitive locations (Vis 2007). However, it was postulated that the

www.manaraa.com

FE model may sufficiently model changes in load behavior resulting from damage.

Through the use of the FE model, Vis studied three variables impacting the TS-NTS relationships: transverse vehicle location, vehicle configuration, and damage in the bridge. The vehicle's transverse location on the bridge can cause distinct groupings of data on the scatter plots, two of which are shown in Figure 1.8. These groupings of data can be represented by a straight line emanating from the origin of the scatter plot (Vis 2007). The straight lines were also used to represent different vehicular configurations. To show the effects of differing configurations, six truck configurations and loads were applied to the FE model. The lines representing the trucks on the scatter plot are shown in Figure 1.8, illustrating that vehicle configuration also has an effect on the TS-NTS relationship.

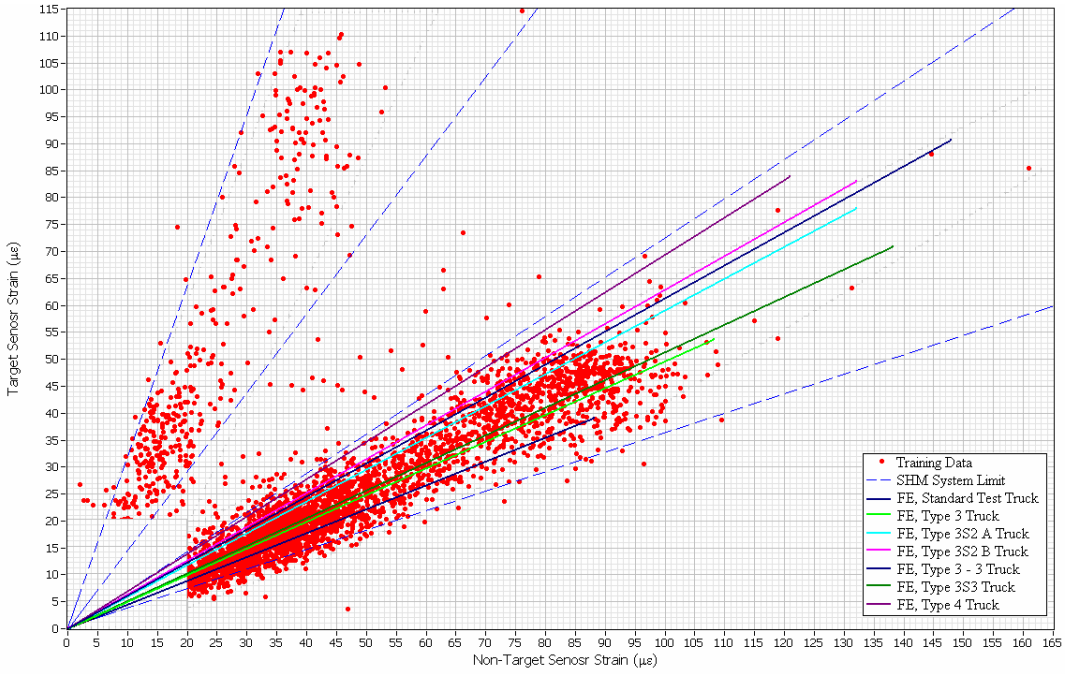

Figure 1.8 Example Scatter Plot with Different Vehicular Configurations (Vis 2007)

Cracks of different sizes were analytically introduced at a damage sensitive location to determine the effects of the cracks on the TS-NTS relationship. As damage was introduced, the slope (i.e., TS-NTS ratio) of the lines changed as the crack length increased as shown in Figure 1.9. To recognize a change in the TS-NTS relationship indicative of damage Vis concluded that the TS-

www.manaraa.com

NTS ratio must pass beyond the range of ratios associated with both transverse vehicular location and different vehicular configurations (Vis 2007). Based upon these results it was concluded that the SHM system will likely be able to identify damage once a crack 1/16 in. in size has developed if a sensor is located near the crack.

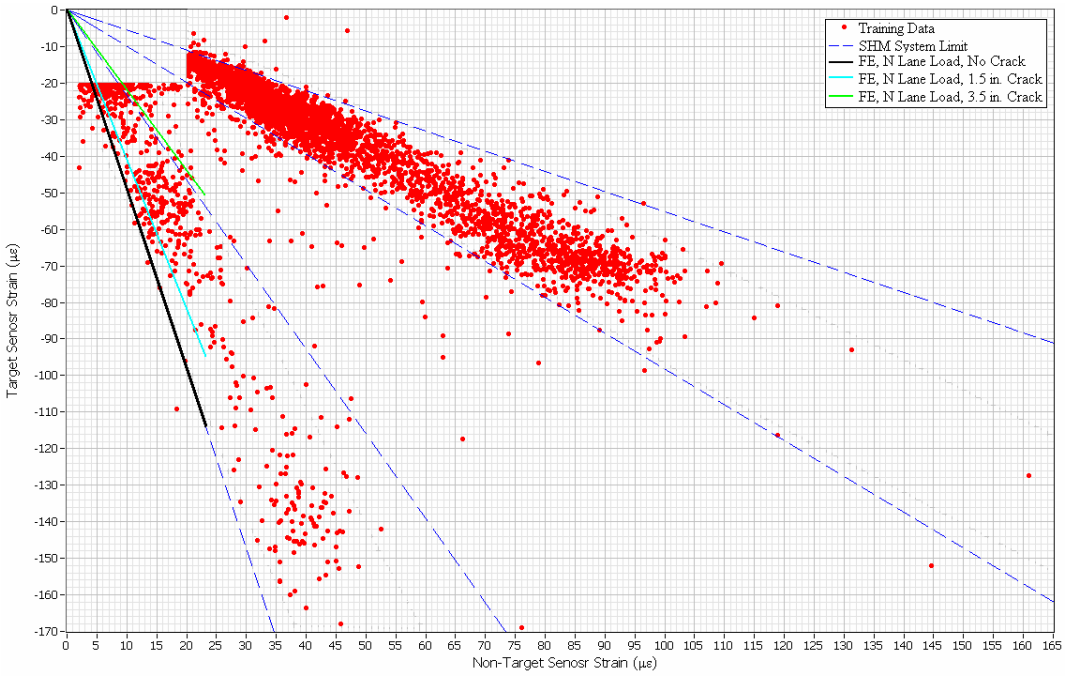

Figure 1.9 Example Scatter Plot with Damage Effects (Vis 2007)

As it was found that is difficult to determine the differences between response changes caused by truck parameters and changes caused by structural damage, a truck parameter detection system and second generation damage detection algorithm were developed by Lu (Lu 2008) as described in, "A Statistical Based Damage Detection Approach for Highway Bridge Structural Health Monitoring." By using only specific truck types the live load induced variability can be reduced. Work completed by Lu (Lu 2008) extends the work previously completed by Wipf, Phares, Doornink (Wipf, Phares and Doornink 2007), and Vis (Vis 2007).

Truck parameters are characteristics of the trucks passing over the bridge and include the travel lane, number of axles, speed, axle spacing, and truck weight group. In the revised algorithm only the strain data that are produced by select truck load conditions are utilized in damage

www.manaraa.com

detection (Lu 2008). To establish a truck parameter detection system, three options were considered: an existing commercial system, the use of the existing sensors on the bridge, and installing new sensors. It was found that commercially available systems were either too expensive or did not integrate into the fiber optic sensor network and were not considered further. To determine the effectiveness of the existing sensor at detecting truck parameters a controlled load test was completed. The results showed that existing sensors could detect tandem axle groups and the steering axle but the differentiation of axles within a group could not be reliably achieved.

Since the existing sensors were not able to detect all the necessary truck parameters for the damage detection algorithm, an investigation into the positions and orientation of deck bottom sensors was performed. A three-dimensional FE model was created of the bridge and trucks crossing the bridge were simulated by applying loads to the nodes of the model along the wheel lines of the truck. For example, the longitudinal strain on the deck bottom produced by a three-axle truck is shown in Figure 1.10. The three peaks indicate there are three axles. It was determined that a good correlation between strain and truck axles existed if longitudinal strain was used and the sensing point was located within two feet of the truck wheel line.

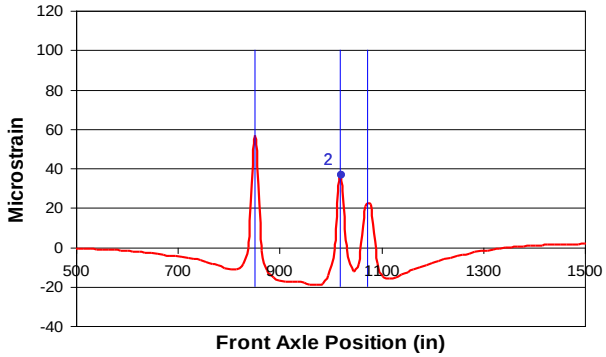

Figure 1.10 Longitudinal Strain from Sensing Point as Truck Passes (Lu 2008)

To confirm the correlation between longitudinal strain and truck axles, a second controlled load test was performed. During this test a three axle truck and a six axle truck crossed the bridge at highway and crawl speeds. A total of 24 deck bottom sensors with two transverse lines of 12 sensors at different longitudinal locations, and 6 girder bottom sensors were used in the load test.

www.manaraa.com

For each truck event, a girder bottom sensor produced one large positive peak if a threshold was properly defined, as shown in Figure 1.11. It was found that the sensor on the girder closest to the vehicle travel lane consistently produced a higher peak strain (above the threshold), thereby determining the truck travel lane. The deck bottom sensors nearest the left wheel line of the right lane truck and the right wheel line of the left lane truck consistently showed the best truck axle detection ability. Data acquisition frequency testing was also completed and it was found that 62.5 Hz was considered to be the minimum frequency required for axle detection (Lu 2008).

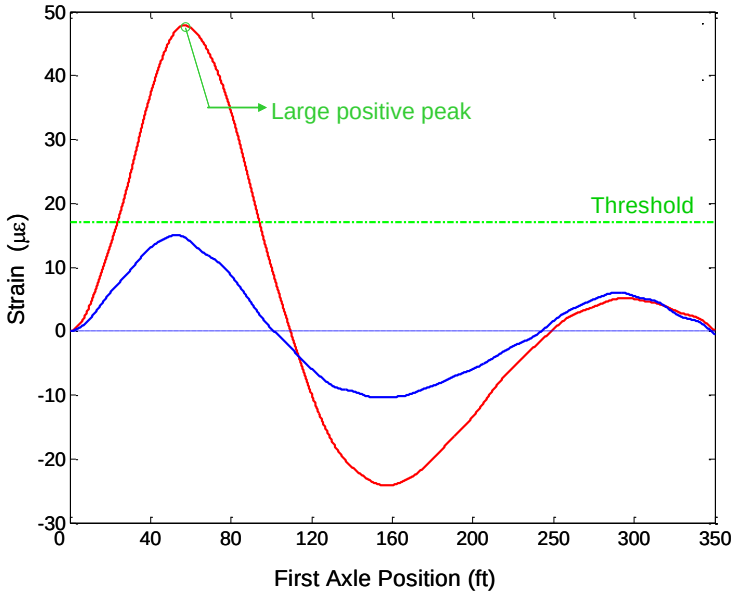

Figure 1.11 Truck Event Girder Bottom Strains (Lu 2008)

After verification by FE analysis and control tests, eight fiber optic sensors (four sensors per transverse line in two different longitudinal locations) were installed on the deck bottom for integration into the long-term structural monitoring system. A good correlation existed between the strain peaks and truck axles but in some cases the truck axles were more difficult to detect than those of the controlled load test. In these cases, a double checking algorithm is used to improve the axle detection capacity. By using the data from these sensors, other truck parameters including speed and axle spacing can be determined. It was found that the direct weight of each truck could not be calculated, however the trucks could be sorted into two categories: heavy or light. In the work completed by Lu, only data from right-lane five-axle

www.manaraa.com

heavy trucks were used in the damage detection algorithm.

Over time a number of issues with the deck bottom sensors have displayed themselves, including apparently incorrect or obscure data readings probably due to temperature fluctuations or poor bonding of the sensor. An investigation into different methods of attaching the deck bottom sensors was completed in the current study to address these issues.

The primary focus of the new damage detection algorithm developed by Lu (Lu 2008) is to detect relatively small local damage in highway bridges. The algorithm utilizes event based extreme live load strains as the input data and statistical control chart philosophies as the damage detection tool (Lu 2008). The maximum and minimum strains produced by one truck event were used to calculate an event-based strain range (for each sensor). The strain ranges from sensor pairs are used to predict each other with linear prediction models. For a system with n sensors, n^2 prediction models can be created. Study showed that residuals defined to be the difference between the predicted data from linear prediction models and the collected strain data, were more sensitive to damage than the peak strain itself. The models are then used to calculate an n x n residual matrix for each truck event. The residual matrix is further simplified into an n-degree vector (i.e., damage indicator). Multiple matrix simplification methods were compared after which the so called combined summation method (which is completed by subtracting the column summation of the residual matrix from the row summation of the residual matrix) was selected. The residuals were also standardized before the column and row summation calculation.

Once the damage indicator is obtained, one control chart for each sensor is constructed. A target false alarm rate was chosen as 0.3% following typical non-destructive evaluation practice. As the residuals were assumed to be normally distributed, the corresponding upper control limit (UCL) and a lower control limit (LCL) are set at the mean plus or minus three times the standard deviation.

As new data are collected, the residual matrix is constructed, and the residuals are plotted on the previously constructed control charts. Any point outside the control limits is termed a damage

www.manaraa.com

alarm and indicate a change in the structure which likely can be attributed to damage. As each sensor is paired with a single control chart, the control chart associated with the sensor closest to the damage will display the highest number of damage alarms.

In summary, the general steps involved in the damage detection approach are (Lu 2008):

Training Procedure:

1. Create linear prediction models from training data.
2. Calculate the residual matrix for each event.
3. Convert the residual matrix into the damage indicator.
4. Create the training stage control chart from the damage indicator.
5. Plot additional training data on the constructed control chart to test for false alarms

Monitoring Procedure:

1. Calculate the residual matrix for each event using the linear prediction model created in the training stage.
2. Convert the residual matrix into the damage indicator.
3. Chart the damage indicator to determine the structural health state.

1.2 Scope and Objective of Research

This study is primarily an experimental validation of the damage detection algorithm developed by Lu (Lu 2008), secondarily an investigation into different methods of sensor attachment to concrete, and an evaluation of alternative methods of statistically manipulating the field collected data. A number of sacrificial specimens were mounted on the US 30 bridge which had been utilized in previous phases of this work with loads induced by ambient traffic. The sacrificial specimens modeled the damage sensitive locations of the test bridge and damage was induced to the sacrificial specimens in the form of cracks and simulated corrosion. Each sacrificial specimen was connected to the existing SHM system and data were collected from the undamaged and damaged sacrificial specimens. The algorithm developed by Lu was used to detect the damage in the sacrificial specimens. For the secondary objective, small steel plates as

www.manaraa.com

the medium between the sensor and concrete were mounted to the underside of a test concrete beam. Different geometries and configurations of the steel plates along with control sensors were used. The concrete beam was subject to multiple load cases to simulate actual bridge loading conditions. The results were then compared to determine if the new techniques were valid to be used in the field.

1.3 Organization of the Report

Throughout the remainder of this report, previous SHM systems and damage detection techniques are summarized in Chapter 2. Chapter 3 details the investigation into sensor attachment methods to concrete. In Chapter 4, the experimental procedure is detailed including the use of a sacrificial specimen to model the damage sensitive web-gaps on the US30 bridge. Chapter 5 shows the results from the testing of the undamaged and damaged sacrificial specimen along with the control charts which compare the differing damage states of the sacrificial specimen. Finally, in Chapter 6, the research work is summarized and conclusions are drawn as to the validity of the statistical based damage detection algorithm.

www.manaraa.com

CHAPTER 2. LITERATURE REVIEW

A literature review was previously conducted by Lu (Lu 2008) and summarized in, "A Statistical Based Damage Detection Approach for Highway Bridge Structural Health Monitoring." That review summarized many of the structural health monitoring (SHM) and damage detection systems developed and tested prior to 2008. Also, an extensive literature review was summarized in, "Damage Identification and Health Monitoring of Structural and Mechanical Systems from Changes in Their Vibration Characteristics: A Literature Review," (Doebling, et al. 1996); the Doebling review summarizes a large array of damage detection systems developed up to 1996. The literature summarized here is intended to "fill-the-gap" between 1996 and 2009. This review is divided into two primary areas: SHM systems and damage detection. An additional short literature review was completed on the topic of sensor attachment to concrete and is shown in the following chapter.

2.1 SHM Systems

2.1.1 Wire-Based SHM Components

A common type of SHM system is one that includes an array of wired gauges. These gauges can be located almost anywhere on the structure and the locations depend on the type of data needed. Validation and testing of these types systems can take place on either real world structures or in the laboratory on scale models or other similar structures. Real world application of SHM systems has occurred on bridges ranging from short span timber bridges to long-span suspension bridges. The subsequently described SHM systems were used to test full-scale field highway bridges. Wired SHM systems are generally used for long-term, high-speed monitoring as one central data collection device provides power to the connecting gauges and also collects the corresponding data.

Guan, Karbhari, and Sikorsky describe a long-term SHM system in, "Long-Term Structural Health Monitoring System for a FRP Composite Highway Bridge Structure." (Guan, Karbhari and Sikorsky 2007). These authors define long-term SHM as the practice of using an integrated system of sensors, data acquisition devices, data transmission and processing devices, and

www.manaraa.com

corresponding algorithms to continuously monitor the condition of a structure over an extended period of time (Guan, Karbhari and Sikorsky 2007). In this specific case, long-term SHM took place on a modular bridge in Riverside County, California that carries two lanes of traffic. The monitored bridge was the Kings Stormwater Channel Composite Bridge that consists of prefabricated tubular filament-wound carbon shell girders filled, on site, with lightweight structural concrete. Supported by these tubular girders are prefabricated bridge deck panels which are made of E-glass fiber reinforced polymer. The deployed SHM system consists of a combination of accelerometers, resistance strain gauges, and potentiometers. The accelerometers were set up in a 7 ft by 6 ft grid on the bottom of the deck panels. At half of the locations, two accelerometers were mounted - one oriented vertically and one oriented horizontally. The 20 strain gauges were attached to the bottom of the deck and along the tubular girders. The positions of the strain gauges were selected to monitor high strain areas. To measure maximum deflection, four string potentiometers were placed at midspan.

As the sensors collect data, they are instantaneously sent from a wireless antenna to the University of California, San Diego where the data are compiled and analyzed. Raw data, in the form of time-histories, are processed to generate results which reflect the condition of the bridge (Guan, Karbhari and Sikorsky 2007). The method of damage detection was a direct mode shape comparison. A forced vibration test was conducted on the bridge shortly after construction to obtain the undamaged condition mode shapes. After the bridge was opened to traffic, data were collected on a daily basis and the daily mode shapes were compared to those of the undamaged structure. It was found, however, that variations in temperature and boundary conditions produced greater mode shape variations than damage produced.

Olund and DeWolf (Olund and DeWolf 2007) present three SHM systems used on three types of bridges deemed critical to Connecticut's bridge infrastructure: a steel box girder bridge, a curved cast-in-place box girder bridge, and a steel multigirder bridge in, "Passive Structural Health Monitoring of Connecticut's Bridge Infrastructure,". The SHM systems used are passive systems which consist of collecting data from ambient traffic (Olund and DeWolf 2007). By using a passive SHM system, the bridges can be monitored while open to traffic and do not have to be closed to perform controlled load tests.

www.manaraa.com

The Olund and DeWolf SHM system setup (Olund and DeWolf 2007) was basically the same for all three bridges with the main difference being where the sensors were placed. The sensors on the bridge are a combination of temperature, tilt, acceleration, and strain gauges which are all connected to a central data acquisition system located at the bridge site. For each bridge, the smallest number of sensors that would still allow for the global characterization of the structure to be identified was used. A significant early concern related to the impact that temperature gradients would have on the natural frequencies and measured rotations. This issue was dealt with by recording temperature at the same time strain and tilts were recorded. Consideration was then given to the measured temperature when calculating the natural frequencies. To give greater flexibility in the data collection capabilities the software was configured with three modes: the trigger approach which collects data only if data are above or below set limits, the interval approach which collects data at set intervals throughout a certain period of time, and manual. A modem was connected to the on-site computer; this enables the collected data to be downloaded without having to travel to the bridge.

The first bridge monitored was a curved steel box-girder bridge with a composite concrete deck. That bridge consisted of three sets of three continuous spans. The SHM system had a total of 22 sensors: 8 temperature sensors, 6 tiltmeters, and 8 accelerometers (Olund and DeWolf 2007). The second bridge was a curved cast-in-place concrete post-tensioned box-girder bridge and the SHM system consisted of 14 temperature sensors, 6 tiltmeters, and 16 accelerometers. The last bridge monitored was a steel multi-girder bridge with three spans and a composite concrete deck. The monitoring system consists of 20 uniaxial strain gauges located on one of the three spans. To track the changes in the collected data, statistical benchmarks were created from the collected data. These statistical benchmarks could be used to construct statistical envelopes and confidence intervals with which the new collected data can then be compared and analyzed.

Betz, Staszewski, Thursby, and Culshaw (Betz, et al. 2006) explored the use fiber Bragg grating sensors for fatigue crack detection in metallic structures and for SHM. Fiber Bragg grating sensors were used since it has been shown that they are capable of sensing both the loads and ultrasonic waves (Betz, et al. 2006). The structural health and usage monitoring system (HUMS) was developed to improve current inspection practices, to monitor the loads applied to the

www.manaraa.com

structure, and to detect possible damage. The fiber Bragg grating sensors can also be used as an ultrasonic detector to detect Lamb waves as they propagate through the structure.

In order to verify the use of the fiber Bragg grating sensors for damage detection laboratory testing was conducted. Load was applied to a steel plate with multiple sensors attached to its surface. Damage, in the form of a full depth notch, was then introduced to the plate. As cracks formed on either side of the notch, the sensors were able to detect the cracks and the size of the crack could be estimated through further analysis.

2.1.2 Wireless-Based SHM Components

A SHM system was introduced by Chintalapudi et al (Chintalapudi, et al. 2006) in the paper, "Monitoring Civil Structures with a Wireless Sensor Network." The primary motivation behind using the wireless network was the initial cost of implementing a dense network of wired sensors on large-scale structures. The coin-sized wireless sensors consist of vibration sensors, low power radio components, significant flash storage, and a processor. The wireless sensors are relatively easy to mount and can be organized into a dense network on the structure. Because of the relatively small size of the sensors, battery life was limited to not more than a few days. To overcome this, the sensors can operate in numerous low-power settings. The wireless sensors send the collected data to on-site hardware that can pre-process the data before sending the data to a powerful data processing computer off-site.

The software system designed, implemented, and deployed (Chintalapudi, et al. 2006) typically consists of tens of sensor nodes that send information through a series of relays to a base station which was typically a high-end PC. The system can accommodate the entrance or exit of wireless sensors into the network at any time. A large problem encountered was loss of data during transfer from the sensors to the base station. This problem was overcome by having individual sensors temporarily store data. When needed, the base station can send a request for a certain time-stamped data set; the sensor can then resend the missing data to the base station.

The system was deployed on two structures: a seismic test frame and the Four Seasons building located in Los Angeles, California. The seismic test frame was a model of a 28-ft x 48-ft

www.manaraa.com

hospital ceiling which was designed to support 10,000 pounds and has functional electric lights, fire sprinklers, drop ceiling installations, and water pipes (Chintalapudi, et al. 2006). The test ceiling can be subjected to up to 10 in. of displacement. The Four Seasons building is a four-story office building that was damaged in the 1994 Northridge earthquake and subsequently abandoned. A wireless sensor network was established on both structures, forced vibration was induced, and data were collected. It was found that real structures are heavily damped and the response to a sudden impact lasted less than a second. Large amounts of data were collected and the fundamental rationale was demonstrated: flexibility and ease of deployment, and the experiments were considered successful. Current second and third-generation wireless sensor systems are in development with accompanying software.

Kim et al (Kim, et al. 2007) present the wireless health monitoring of the Golden Gate Bridge in California in the paper, "Health Monitoring of Civil Infrastructures Using Wireless Sensor Networks." The wireless sensor network used is similar to that developed by Chintalapudi et al (Chintalapudi, et al. 2006). The main difference between the two wireless sensor networks is how they are implemented on the individual structures.

The Golden Gate Bridge presents a unique test bed for a SHM system because of the potential for large wind and seismic loads. The distances between the sensors in this work was limited due to the relatively short wireless range of the sensors. In fact, the maximum separation distance of the sensors was typically limited to 100ft and in some cases to less than 50ft. There were 53 wireless sensors placed on the west side of the main span and three on the east side of the main span. Each of the sensors monitored two directions of acceleration and ambient temperature. Four lantern batteries were used to provide power at each sensor location since no other power source was readily available; renewable sources of power were considered. A total of eight sensors were placed on the south tower - one at each intersection of the cross-bracing and towers.

Another SHM system based on wireless sensor networks was presented by Yin et al (Yin, et al. 2009) in the paper, "Design and Implementation of the Structure Health Monitoring System for Bridge Based on Wireless Sensor Network." Yin et al (Yin, et al. 2009) developed a new type of node called the S-Mote that consists of a mote (or sensor), sensor board, and batteries and

www.manaraa.com

collects acceleration data. As with other sensor nodes, the S-Mote can be placed in numerous locations on the structure and connected to a base station wirelessly. Once an S-Mote receives the command to start collecting data, the acceleration data were temporarily stored in flash memory before it was transferred wirelessly to the base station. Data loss during wireless transfer was not addressed by Yin et al (Yin, et al. 2009).

The wireless sensor network developed by Yin et al (Yin, et al. 2009) was tested on the Zheng Dian viaduct bridge located near Wuhan City. Six nodes were deployed near the middle of the bridge in a linear array (Yin, et al. 2009). The S-Motes were mounted on the bridge horizontally and connected wirelessly to a base station which was connected to a computer. The data were collected at 100Hz for 1.5 hours.

A wireless sensor network was also used to monitor the Humber Bridge in the United Kingdom. Hoult et al. (Hoult, et al. 2008) developed a system to monitor the relative humidity in the anchor blocks of the Humber Bridge as described in "Wireless Structural Health Monitoring at the Humber Bridge UK." At the anchorage, the main cable was divided into individual cable strands and tied into the foundation with no protective coating (Hoult, et al. 2008). High levels of relative humidity in these areas can cause corrosion of the steel. Dehumidifiers that turn on when the relative humidity reaches a certain percentage and wired humidity gauges were located in the anchorage. The gauges can only be accessed manually.

The motes used to monitor the temperature and humidity consist of commercially available motes from Crossbow Technology, Inc. The mote is a battery-powered central processing unit with a radio transmitter and a radio receiver (Hoult, et al. 2008). As with many wireless sensor networks, power was the main issue. Four AA batteries give the motes a life of about ten months. To conserve power and maximize the battery life, a low power mode was programmed which forces the motes to transmit data every five minutes instead of continuously. The wireless sensor network can be checked to determine if the dehumidifiers are functioning properly.

A similar but slightly more complex wireless SHM system was presented in the paper, "Distributed Structural Health Monitoring System Based on Smart Wireless Sensor and Multi-Agent Technology," by Yuan et al. (Yuan, et al. 2005). This SHM system was a distributed

www.manaraa.com

parallel concept based on the smart wireless sensor network and multi-agent system (Yuan, et al. 2005). The multi-agent concept was implemented to manage the information coming from the sensors located on a large structural network. The system consists of different types of agents including: sensing agents that monitor the structure, signal processing agents that process the data from the sensing agents, fusion agents that take the data from the signal processing agents and fuse it together to form a logical sequence of information, and other agents. The collections of agents divide up the larger task of data processing into smaller manageable pieces that can be combined into a network specific to a unique structure.

Another feature about the Yuan et al. (Yuan, et al. 2005) SHM system was that each of the sensors was connected to mini-hubs that have micro-processors that communicate wirelessly to a larger hub. The mini-hubs collect the data from the attached sensors, combine the data, and then communicate these data to an estimation agent. By having the smaller platforms, the data arrives at the fusion agent in a smaller number of larger packets, rather than a large number of small packets. This increases efficiency and reduces the amount of power needed. The sensors themselves can either be piezoelectric or fiber optic; the platforms can be modified to attach to either type of sensor. After evaluation of the entire system, the sensor platform needed improvement due to speed and memory limitations. Also, testing was limited to small scale applications; testing on large scale structures would need to be completed to verify the usefulness of the distributed parallel SHM system.

2.2 Damage Detection

Almost all SHM systems are said to have a damage detection process. Damage detection ranges from the analysis of direct readings to complex algorithms that analyze dynamic characteristics to detect structural damage. All of these detection systems have one main aspect in common; they use measured data from the bridge and try to detect damage.

2.2.1 Damage Detection by Dynamic Response

Damage detection by dynamic response is usually accomplished by exposing the structure to a dynamic load and recording data as the structure responds. In many cases, this data set is

www.manaraa.com

compared to a data set from the original undamaged structure; this comparison of data sets is completed in differing ways, a few of which are described below.

A method of structural damage detection is called the Local Damage Factor (LDF) and it was reportedly able to detect the location and severity of damage. LDF takes two random vibration signals, one from the local structure and the other from the entire structure, and finds the correlation between them through a process known as auto-correlation. From these correlations, the auto-spectral densities are found using a Fourier transform. The auto-spectral densities are used to find the generalized coherence function which in turn indicates the severity of the nonlinearity between the local structure and the entire structure. Damage in the structure usually reduces the stiffness of the local structure where the damage occurs, and it purportedly increases the nonlinear severity between the local structure and the entire structure (Wang, Ren and Qiao 2006). From the coherence function, the LDF can be found; a change, or damage, in the structure will change the LDF.

A modified LDF (MLDF) was subsequently introduced that does not need the data and dynamic characteristics of the undamaged structure. This method was beneficial because in many cases the undamaged structure is not attainable and undamaged data cannot be recorded.

In the case of Wang, Ren, and Qiao (Wang, Ren and Qiao 2006), LDF and MLDF were evaluated with a 3-D steel frame to determine if damage could be detected using both methods. Baseline data were collected and a crack was then introduced into one of the frame legs. The authors report that both methods effectively determined the severity and location of the damage in this case and provide a simple and straightforward approach to local damage detection (Wang, Ren and Qiao 2006).

A damage detection technique is presented by Ng and Veidt (Ng and Veidt 2009) which uses Lamb waves to locate and estimate the severity of the damage. The Lamb-wave technique uses an array of piezoelectric transducers that transmit and receive an excitation frequency that can then be analyzed. The structure can then be reconstructed using superposition.

Numerical studies were conducted to investigate the Lamb wave technique. The studies utilized

www.manaraa.com

finite element models to predict the Lamb wave propagation through the material and the simulated damage detection. A simple laboratory test of a carbon-fiber-reinforced composite plate was conducted. In this test transducers were located at four corners around the simulated damage area. The composite laminate was excited using Lamb-waves and data collected using the transducers. The data were then compared to data from finite element models. Through the numerical and experimental studies, the Lamb wave based technique for damage detection has been verified to detect and locate different stages of damage in composite laminate structures.

A method of damage detection presented by Guan, Karbhari, and Sikorsky (Guan, Karbhari and Sikorsky 2007) compares the mode shape curvatures of the undamaged and damaged structure. It has been found that mode shape curvature was more sensitive to local changes of stiffness and was shown to be particularly suitable for damage localization in beam-like structures (Guan, Karbhari and Sikorsky 2007). The mode shape curvature of the undamaged structure was considered the "baseline" and all other mode shape curvatures computed from the potentially damaged structure were compared to this "baseline." The general trends of the differing mode shape curvatures were found to be similar but that they were differed in distinct places leading to the classification and location of the damage.

In the paper titled, "Nondestructive Crack Detection Algorithm for Full-Scale Bridges," Kim and Stubbs (Kim and Stubbs 2003)present a method to determine crack location, size, and shape. These descriptors of the crack are determined by the change in modal characteristics (e.g., natural frequencies and mode shapes) of the structure. A data set was collected for the undamaged structure and then compared to data from the damaged structure. Specifically changes in modal shapes and natural frequencies are used to identify the presence of damage. The crack detection algorithm can then use the collected data to locate and determine the qualities of the damage.

In order to experimentally verify the crack detection algorithm, a full-scale test bridge was located and initial modal tests were performed to obtain a set of baseline undamaged data. Once initial data collection was complete, four levels of damage were introduced to the bridge by means of torch cutting flanges and webs certain distances. The first damage case damaged a central portion of the web, the second the lower half of the web, the third the lower half of the

www.manaraa.com

web plus the lower flange tips and the fourth the entire bottom half the I-beam cross-section. After each level of damage was established, modal tests were performed and data were collected to compare to the undamaged data set.

The data collected were analyzed using the crack detection algorithm and the algorithm was found to reasonably predict the size and location of the damage. False alarms were triggered during some parts of the analysis but the authors are working on further refining the nondestructive crack detection algorithm.

Galvanetto, Surace, and Tassotti (Galvanetto, Surace and Tassotti 2008) present a new structural damage detection method based on proper orthogonal decomposition in the paper, "Structural Damage Detection Based on Proper Orthogonal Decomposition: Experimental Verification." This damage detection technique uses proper orthogonal modes (POM) and the variance between the orthogonal modes of an undamaged structure and a damaged structure to detect the level of damage the structure. This damage detection approach does not require the creation of a mathematical model.

The first step was to collect data and construct a POM for the undamaged structure. This was accomplished by placing many accelerometers on the structure and recording data. The data are then be used to create the POM. This undamaged POM will be used to compare to all of the additional POM's created from the potentially damaged structure.

To verify the proper orthogonal decomposition damage detection method and to ensure its accuracy, a cantilever beam (20 x 20 x 520 mm) was constructed and accelerometers were attached to the undamaged structure. A shaker was used in two different locations and vibrated at three different frequencies to obtain undamaged structure data. Saw cuts were then introduced into the cantilever at increasing depths and the structure was shaken two different locations and at three different frequencies. The first saw cut was 1 x 20 x 0.5 mm and the second cut was 1 x 20 x 2 mm. From the collected data, POM's were created and it was found that the damage was accurately located.

Another approach to structural damage detection was presented in the paper, "Vibration Based

www.manaraa.com

Damage Detection in a Uniform Strength Beam Using Genetic Algorithm," by Panigrahi, Chakraverty, and Mishra (Panigrahi, Chakraverty and Mishra 2009). In this damage detection procedure, a Genetic Algorithm (GA) was used to solve an optimization procedure specified by a residual force vector (Panigrahi, Chakraverty and Mishra 2009). After the objective function has been solved, it could then be related back to the physical properties of the structure. These physical properties are directly related to the structural stiffness. The underlying approach assumes that the stiffness of a structure decreases when there is damage to the structure. Two cases were investigated in the validation of the damage detection algorithm: the first being a uniform strength beam with a slope function integrated into the width of the beam (0.08 x 0.01 m to 0 x 0.01 m with a length of 0.8 m), and the second being a uniform strength beam with a slope function integrated into the width and depth of the beam (0.08 x 0.015 m to 0 x 0 m with a length of 0.8 m). Data were collected from the undamaged states of the beams along with different stages of damage. Throughout this process, the modes of the damaged structures were found to be lower than those of the undamaged structure. For both cases, the Genetic Algorithm identified damage for both uniform strength beams.

In the paper, "Experimental Validation of Structural Health Monitoring for Flexible Bridge Structures," Caicedo and Dyke (Caicedo and Dyke 2005) present health monitoring system specifically validated on a model of a cable-stayed bridge that uses changes in a structure's dynamic characteristics (e.g., natural frequencies, mode shapes) to detect and locate damage. There are five steps to implementation of the technique: development of an identification model, sensor placement, data acquisition, modal identification, and parameter identification (Caicedo and Dyke 2005). Data are obtained from both the undamaged and potentially damaged structure to make a direct comparison between the two.

The identification model was created using finite element software and the model must be complex enough to accurately model the behavior of the structure but not too complex as to have very large quantities of data. The primary purpose for creating the model was to find the critical locations to place the accelerometers. Once the locations are identified, accelerometers are then placed on the bridge and data acquisition can begin. The dynamic excitation of the bridge can either be known or unknown (the eigensystem realization algorithm can calculate the natural

www.manaraa.com

frequencies and mode shapes with either). The differences in the natural frequencies and mode shapes was what determined if there is damage and where the damage was located on the structure.

Numerous experimental tests were conducted on the cable-stayed bridge model. The model has a total length of 2 m and a width of 19 cm with the h-shaped tower being 50 cm tall, 29 cm wide at the base, and 18.41 cm wide at the top. A total of sixty cables were used to support the deck, with connections at 1.27 cm increments (Caicedo and Dyke 2005). A finite element model was constructed and accelerometers were placed on the test model to coincide with critical locations identified on the finite element model. The undamaged structure was dynamically excited and data were collected and analyzed. Damage was introduced into the structure by randomly choosing a small deck section and replacing it with a smaller 'damaged' element. The damaged structure was also dynamically excited and data were collected. By comparing the natural frequencies and mode shapes of the undamaged and damaged structures using the algorithm stated above, the damage could be detected and located.

2.2.2 Damage Detection Without Undamaged Structure

A unique feature about a few damage detection systems is the fact that the undamaged structure is not needed to detect future damage of the structure. Each method has a different way of accomplishing this but in general a theoretical model is constructed and data collected from the bridge are compared to the model in some fashion. Summarized below are two such approaches.

In a paper by Kim and Melham (Kim and Melhem 2004) titled "Damage Detection of Structures by Wavelet Analysis," a relatively new method was presented for damage detection and SHM that includes the utilization of dynamic characteristics of the structure that does not need an analysis of the structure in order to detect and locate damage on the structure. Typical modal based methods encounter various difficulties including obtaining correct material properties and the need to measure vibration responses of structures before damage occurs. These difficulties are reportedly able to be eliminated by using wavelet analysis.

Wavelet analysis is a mathematical and signal processing tool that takes raw vibration data and

www.manaraa.com

analyzes the decomposition and irregularities of the signal. It is a time-frequency analysis that provides more detailed information about non-stationary signals which traditional Fourier analysis miss (Kim and Melhem 2004). Through this, the damage can be detected and reported to the agency or department monitoring the structure in the case of structural health monitoring systems.

Saadat et al (Saadat, et al. 2004) present an intelligent parameter varying technique (IPV) for damage detection in structures that behave non-linearly under seismic conditions in the paper, "Structural Health Monitoring and Damage Detection Using an Intelligent Parameter Varying (IPV) Technique." The IPV technique combines features of non-parametric and parametric simplified structural models to recognize the non-linear behavior portions of the response during seismic loading and uses this to identify areas on or within the structure where damage may be located. Rather than comparing this non-linear behavior of the damaged structure to the behavior of the non-damaged structure, the IPV technique identifies structural forces that mathematically return the structure back to its original shape, called restoring forces, to detect the differing levels of damage. Case studies and simulations were investigated to determine if the IPV technique recognizes the structural restoring forces of the damaged structure which can be related to damage that had taken place.

2.2.3 Statistical Based Damage Detection

Another general damage detection approach is one that only uses statistics to analyze data collected from the bridge. Worden and Manson present a study on a statistical approach to damage detection in their paper, "Damage Detection Using Outlier Analysis." Outlier analysis detects when a machine or structure deviates from the normal condition responses; the analysis detects when data points occur outside of the normal behavior range. The outliers can arise on either side of the data set signaling the performance of the machine or structure is out of the ordinary.

For more complicated sets of data, a discordancy test called Mahalanobis squared distance was used to analyze the outliers. The Mahalanobis squared distance approach, which is a function for calculating distances between two seemingly related points, was used in case studies presented in

www.manaraa.com

the paper and was successfully demonstrated on numerous large data sets. As with most data analyses, assumptions were made to simplify the outlier analysis damage detection procedure.

www.manaraa.com

CHAPTER 3. INVESTIGATION OF SENSOR ATTACHMENT

3.1 Introduction

In order for the SHM system to detect the trucks crossing the US30 bridge and obtain the peak strain values vital to damage detection, sensors need to be adhered to the underside of the concrete deck. The porous nature and moisture content of the concrete, ambient temperature fluctuations, and the cyclic strain range of the sensor all contribute to the difficult nature of attaching sensors to concrete. By controlling one or more of these variables, the effectiveness of the sensor attachment can be improved. Previous research summarized in the following section investigating the sensor attachment has not been entirely satisfactory. Commercially available products were also investigated but showed similar ineffective results as the previous research.

In this chapter, a brief investigation to develop effective methods of attaching fiber-optic sensors to concrete surfaces was completed. Methods previously implemented and researched are summarized in Section 3.2, the experimental method for the investigation is discussed in Section 3.3, and the results are shown in Section 3.4. Finally, in Section 3.5, the research is summarized, conclusions are drawn as to the effectiveness of the attachment method, and future work is recommended.

3.2 Literature Review

This brief literature review investigates different techniques to accurately measure strain on a concrete surface for field applications over long time periods. Numerous techniques exist with options such as the basic use of sensors and epoxy to the complex systems of externally mounted sensors bonded to the concrete using bolts. However, only a few of the selected techniques were reviewed with specific interest placed on the applicability to fiber-optic sensors.

In, “A Gauge for Measuring Long-Term Cyclic Strains on Concrete Surfaces,” Salah el Din and Lovegrove propose mounting sensors on a bent metal strip, or frame, to measure strains on a concrete surface. The metal strip and sensors are shown in Figure 3.1. The function of the metal strip is to transform the axial strain on the surface of the test material to a bending strain in the middle part of the frame (Salah el Din and Lovegrove 1981).

www.manaraa.com

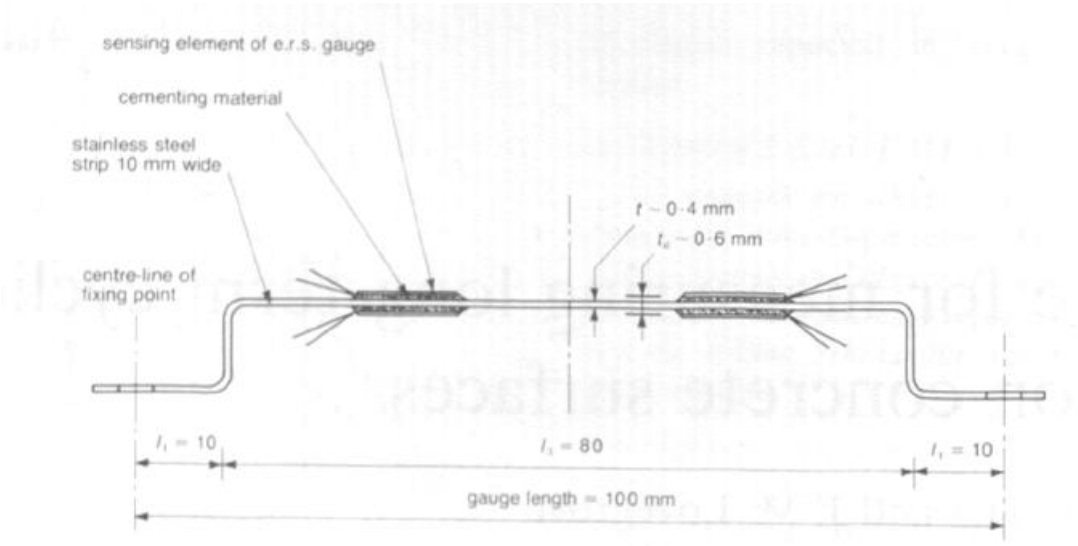

Figure 3.1 Dimensions and Construction of the Gauge (Salah el Din and Lovegrove 1981)

The goal is to reduce the post-yield strain from the test material to reasonable strains in the frame the sensors can sustain over long periods of time. From testing, it was found that the sensors on the frame reduce the concrete strain by a factor of about twenty-five, which may lead to inaccuracies when the original strain in the material is needed. Because of the drastic strain reduction, the possible inaccuracies, and considering post-yield strains are not needed in the US30 bridge project, the metal frame was not chosen as a sensor attachment option for further investigation.

Doornink (Doornink 2006) used Loctite H4500 epoxy and a tensioning device attached to the concrete and placed over the sensor to hold the sensors in place while installing the carbon-fiber-enclosed fiber optic strain gauges in, "Damage Detection in Bridges through Fiber Optic Structural Health Monitoring." The device placed a constant force on the sensors and epoxy to ensure a solid bond. Silicone was spread over the sensors for protection from the weather. Installation of the sensors on the steel members of the US30 bridge took place in October, 2005 and the sensors were recording accurate strain reading as of May, 2010. The preparation of the bonding surfaces along with the constant force provided during bonding helped ensure the longevity of the sensor bond. The preparation of the bonding surfaces along with the constant

www.manaraa.com

force provided during bonding helped to ensure the longevity of the sensor bond.

In, "A Statistical Based Damage Detection Approach for Highway Bridge Structural Health Monitoring," by Lu (Lu 2008), Loctite H4500 was also used to bond the deck bottom sensors to the underside of the US30 bridge deck. The device and silicone used by Doornink (Doornink 2006) were not used in the installation of the deck bottom sensors. A number of the deck bottom sensors have been replaced since the original installation due to ineffective bond. The weather, temperature variations, and the rough, uneven surface of concrete may be the cause of the bond failure between the carbon-fiber package and the concrete. The following chapter investigates differing methods of installing the deck bottom sensors to the concrete.

3.3 Experimental Procedure

The main goal of the sensor attachment testing was to find a way to easily and reliably attach a sensor to the underside of the concrete deck of the US30 bridge and achieve acceptable epoxy bonding. In the sensor attachment completed in previous research, the epoxy bond between the sensor and concrete was found to be largely variable. The weather conditions, amount of force placed on the curing epoxy, and the amount of time the force was applied affected the quality of the epoxy bond between the sensor and concrete. By properly controlling these variables the epoxy bond will increase in quality.

To control the variables affecting the epoxy bond, the sensor attachment was completed in a controlled environment by attaching the sensors to small steel plates and curing the epoxy in a laboratory setting. Various plate dimensions and orientations and the types of epoxy were investigated. The steel plates were attached to the underside of a half section of a prestressed concrete beam that had been previously tested to failure with screws, epoxy, or a combination of screws and epoxy.

The concrete beam had been previously tested to failure and had large cracks through the top and bottom flanges. To eliminate the large cracks, the beam was cut in half and one of the halves was used as the test concrete surface. Because the width of the beam flange limited the testing to a single variable comparison (i.e., comparing two different types of epoxy or comparing epoxy

www.manaraa.com

and screws) multiple testing locations longitudinally along the bottom of the beam were used. Multiple tests were completed and are described in the paragraphs below.

3.3.1 Tests 1 and 2

In Tests 1 and 2, combinations of two types of epoxy, two plate geometries, and screws were chosen to be directly compared. Bridge Diagnostics Inc. (BDI) strain gauges were used as the monitoring sensors in all tests. In each test group, three BDI gauges were used; two applied to steel plates and the third attached directly to the concrete surface and used as a control by which the other two sensors were compared. All BDI gauges were applied to their surfaces using Loctite 410 epoxy with Loctite 7452 accelerant as per the recommendations of Bridge Diagnostics Inc.

Two different types of epoxy were chosen to be compared in Tests 1 and 2. They were chosen based on performance on past projects and recommended uses for the epoxies provided by the manufacturers, Loctite and Sika. The epoxies used were Loctite H4500 and Sikadur 32.

The first plate, called the 7 in. rectangular plate, was 7 in. by 1.75 in. with a thickness of 0.05 in. The thickness was chosen to eliminate plate buckling which can be caused by the difference between the thermal coefficients of steel and concrete. The plate was designed to fit the BDI gauge and is shown in Figure 3.2. The 7 in. rectangular plate was attached to the concrete by placing concrete screws through the holes in the plate also shown in Figure 3.2, by spreading epoxy along the entire width of the plate, or by using both screws and epoxy.

The second plate, called the tabbed plate, was designed to have a shorter gauge length than the rectangular plate in order to record localized peaks in the strain data. The 7 in. rectangular plate had a gauge length of 6 in. and the strain values are averaged over the gauge length. As the gauge length increases, the average peak strain will decrease and by decreasing the gauge length, the peak strain values for a truck event may be more accurately measured. The dimensions of the tabbed plate were 5 in. by 4 in. with a thickness of 0.05 in. and a gauge length of 3.5 in. This gauge length more closely represents the gauge length of the BDI gauges and is shown in Figure 3.3.

www.manaraa.com

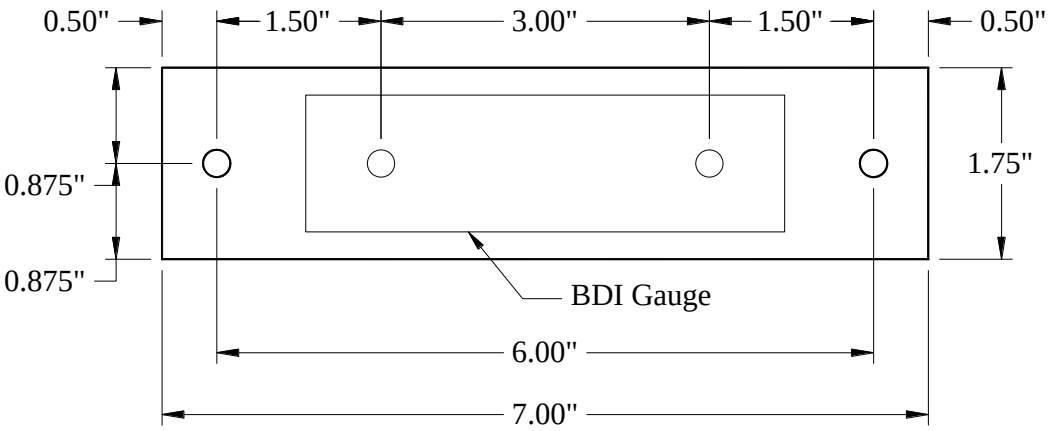

Figure 3.2 7 in. Rectangular Plate

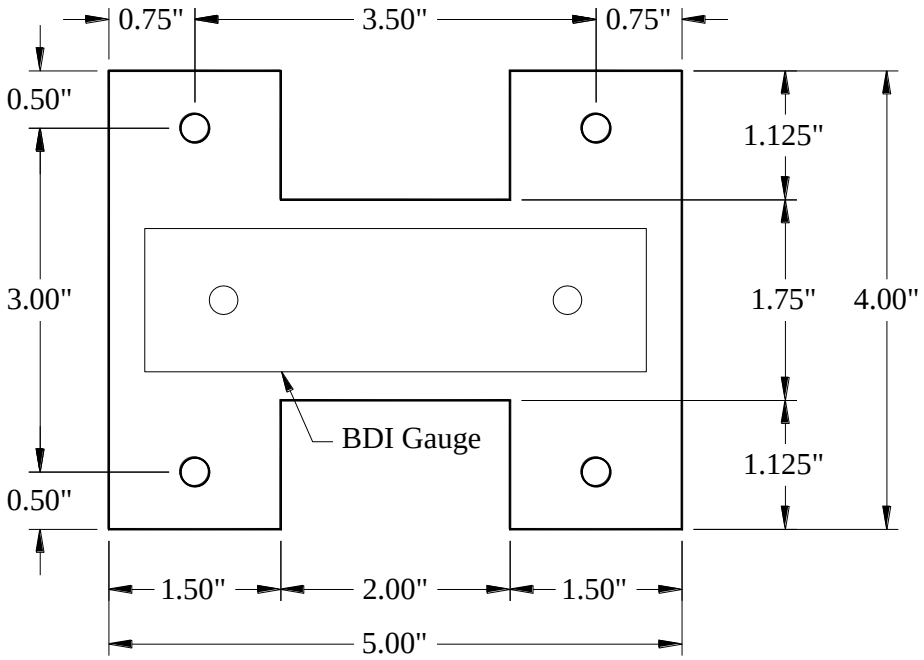

Figure 3.3 Tabbed Plate

The steel plates were aligned on the bottom of the beam such that a single variable (i.e., plate geometry, type of epoxy, use of screws) was compared. To compare all of the above stated variables, four test groups were used and are listed in Table 3.1. The alignment of each test group on the beam and the loading configuration are shown in Figure 3.4.

www.manaraa.com

Table 3.1 Tests 1 and 2 Test Groups and Associated Eight Connection Combinations

Test Group		Variables
	1	7 in. Rectangular, No Screws, Sikadur 32
I	A	Control
	2	7 in. Rectangular, No Screws, Loctite H4500
	3	Screws, No Epoxy, 7 in. Rectangular
II	B	Control
	4	Screws, No Epoxy, Tabbed
	5	7 in. Rectangular, Screws, Sikadur 32
III	C	Control
	6	7 in. Rectangular, Screws, Loctite H4500
	7	Tabbed, Screws, Sikadur 32
IV	D	Control
	8	Tabbed, Screws, Loctite H4500

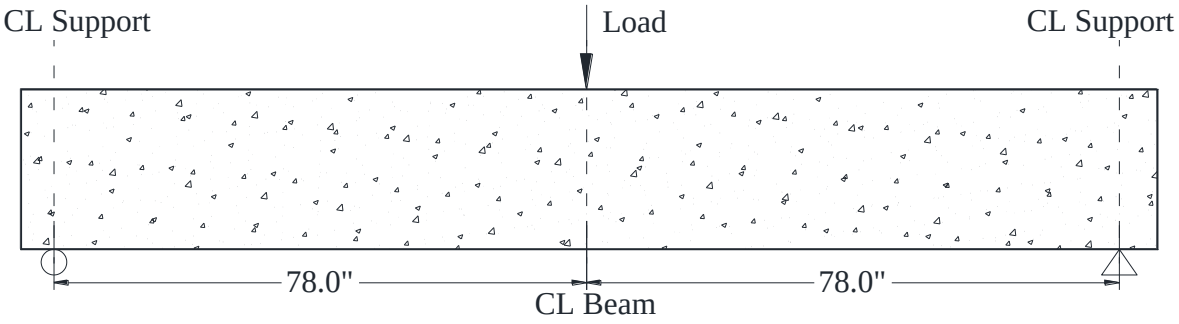

a. Side View

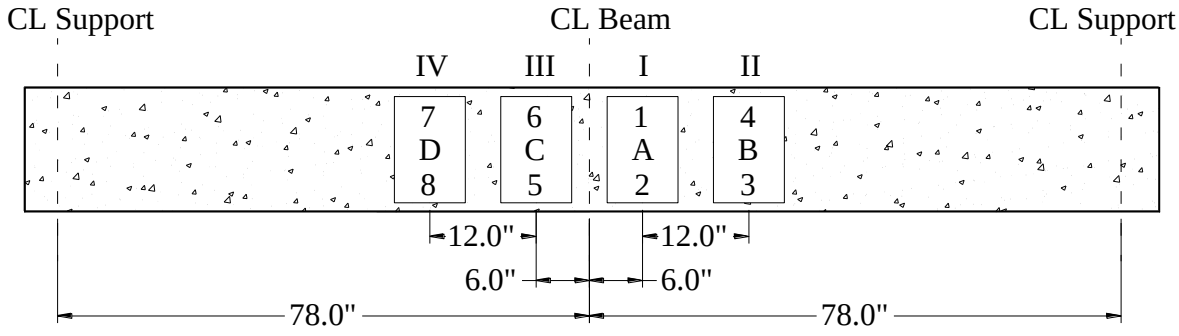

b. Bottom View

Figure 3.4 Beam Setup and Test Group Alignment

www.manaraa.com

To test the static and dynamic strain transferring capabilities of the combinations, multiple loadings were completed within Tests 1 and 2. Loads were applied slowly at midspan of the beam to simulate static loading. Maximum loads were applied and released quickly down to the specified load multiple times which creates peaks in the strain data to simulate cyclic loading similar to the peaks caused by ambient traffic. Finally, a sustained static test during which a constant load was applied over a period of 10 minutes was completed to evaluate the viscoelastic behavior of the epoxy. Table 3.2 shows the test loadings. To confirm the results from Test 1, the loadings within Test 2 were the same as Test 1.

Table 3.2 Test Loadings

Loading	Type	Applied Load (lbs.)
St-X	Static	0-20,000
St-Y	Static	0-25,000
St-Z	Static	0-30,000
C-X	Cyclic	15,000-20,000
C-Y	Cyclic	20,000-25,000
C-Z	Cyclic	0-10,000
Su-X	Sustained	0-25,000

3.3.2 Test 3

After the completion and data analysis of Tests 1 and 2, another test, called Test 3, was completed. Based on Tests 1 and 2, the Loctite H4500 epoxy produced more accurate results and was chosen to be the only epoxy used in Test 3. Screws and epoxy were also chosen to be used in all test combinations. The only variable to be compared was the geometry of the plates. All other features of Tests 1 and 2 were kept the same for Test 3 including the use of BDI gauges, the layout of the test groups along the bottom of the beam, and the use of a control gauge. In Test 3, two additional plate geometries were introduced: a square plate and a 10 in. long rectangular plate (see Figure 3.5 and Figure 3.6).

The square plate had the same outer dimensions of the tabbed plate and had a thickness of 0.05 in. The shape was chosen to determine if the narrow central section of the tabbed plate had any beneficial effects on the accuracy of the strain transfer from the concrete to the BDI gauge. The

www.manaraa.com

10 in. rectangular plate was a longer version of the 7 in. rectangular plate and was designed to investigate the effects gauge length has on the cyclic strain peak magnitude and location.

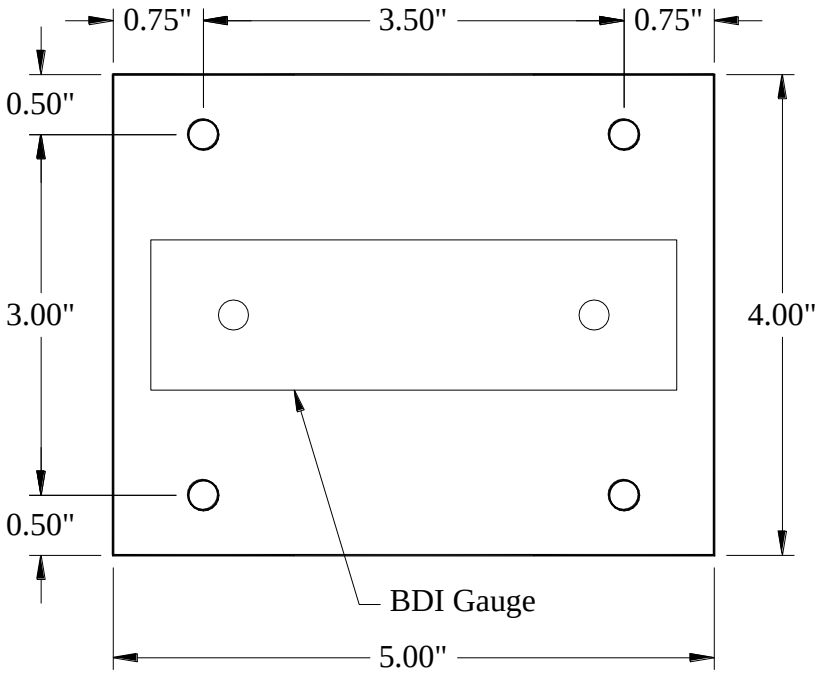

Figure 3.5 Square Plate

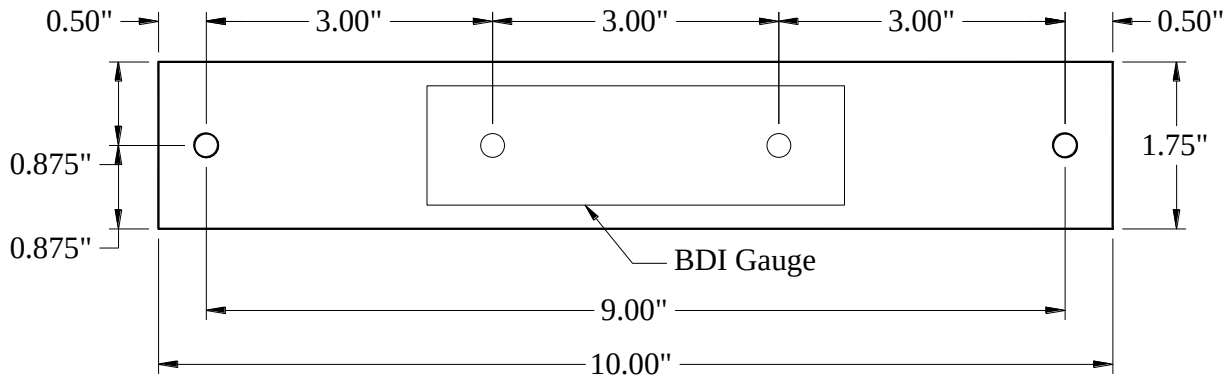

Figure 3.6 10 in. Rectangular Plate

To compare the new plate geometries, test groups were established and are shown in Table 3.3. The steel plates in Test 3 were aligned similarly to Tests 1 and 2 and the alignment of the test groups is shown in Figure 3.4. The loading procedure for Test 3 also followed the previously

www.manaraa.com

outlined procedure for consistency between the tests. The static, cyclic, and sustained loadings are shown in Table 3.2.

Table 3.3 Test 3 Test Groups and Associated Eight Connection Combinations

Test Group		Variables
	1	Tabbed
I	A	Control
	2	Square
	3	Square
II	B	Control
	4	7 in. Rectangular
	5	Tabbed
III	C	Control
	6	7 in. Rectangular
	7	7 in. Rectangular
IV	D	Control
	8	10 in. Rectangular

3.4 Experimental Results

Data from all tests and loadings were collected and plotted to directly compare the relative performance between test groups relative to the control results. Testing and analysis took place throughout the summer of 2009. Results from Tests 1 and 2 and Test 3 are shown and discussed in the following section.

3.4.1 Tests 1 and 2

Loading St-Y was representative of the static loadings (i.e., loadings St-X, St-Y, and St-Z) and therefore only those results are shown (see Figure 3.7). The results of all of the test groups were well above the set maximum allowable percentage of error of five percent, except for the combination of a tabbed plate attached to the concrete with screws (Test Group IV, Combination 8) and Loctite H4500 epoxy. Test Group IV, Combination 8 performed within acceptable error

www.manaraa.com

limits in the static test, as shown in Figure 3.7d.

Another source of poor bond performance was the use of Sikadur 32 epoxy (see Figure 3.7a, Figure 3.7c, and Figure 3.7d). Note that when the load was removed from the beam, the strain remained negative and "drifted" back to zero indicating visco-elastic behavior. Other poor bond behavior was displayed when the plates were attached to the concrete using only screws, causing negative strain values during loading as shown in Figure 3.7b. A small offset of the holes between the plate and concrete could have applied a compressive force that may have pre-compressed the plate. When the beam was loaded, a tension force was applied to the plate overcoming the pre-compression which may have caused the negative strain readings.

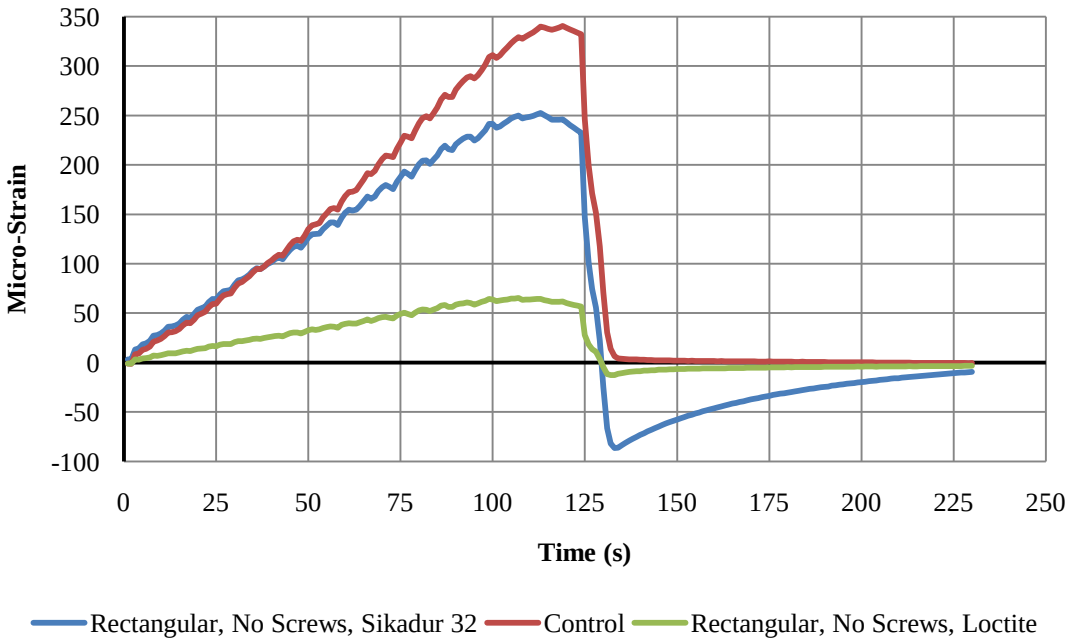

a. Test Group I: Combinations 1, A, and 2

Figure 3.7 Tests 1 and 2 Loading St-Y Results

www.manaraa.com

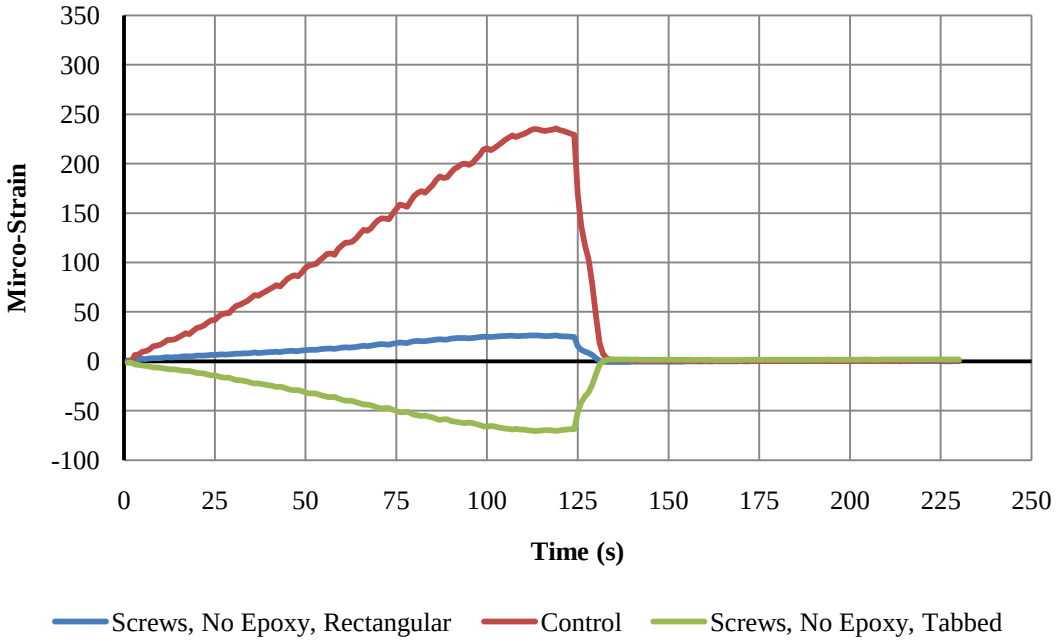

b. Test Group II: Combinations 3, B, and 4

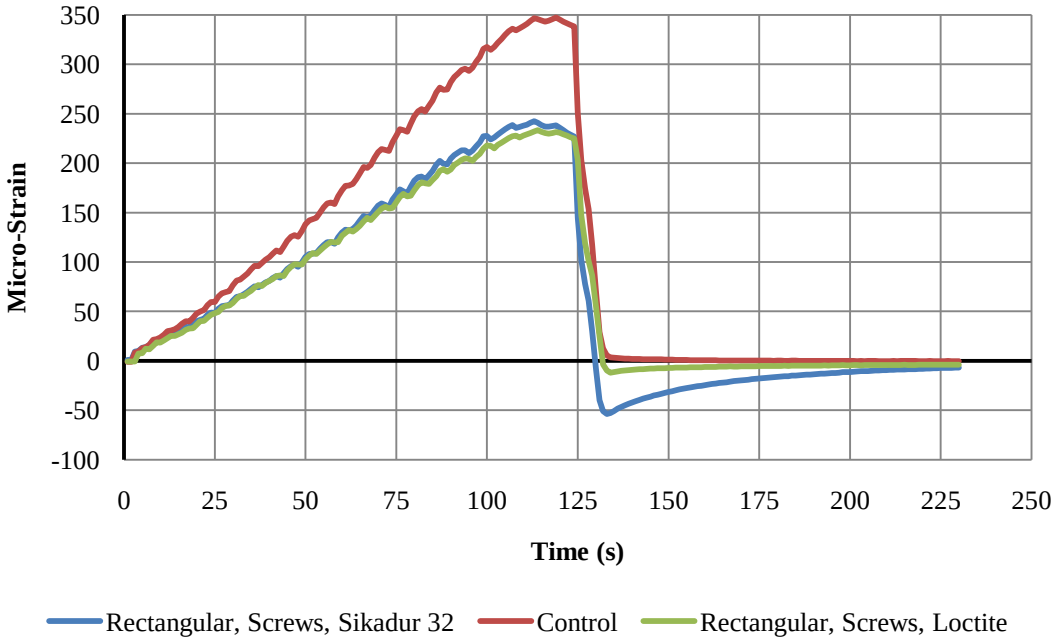

c. Test Group III: Combinations 5, C, and 6

Figure 3.7 continued Tests 1 and 2 Loading St-Y Results

www.manaraa.com

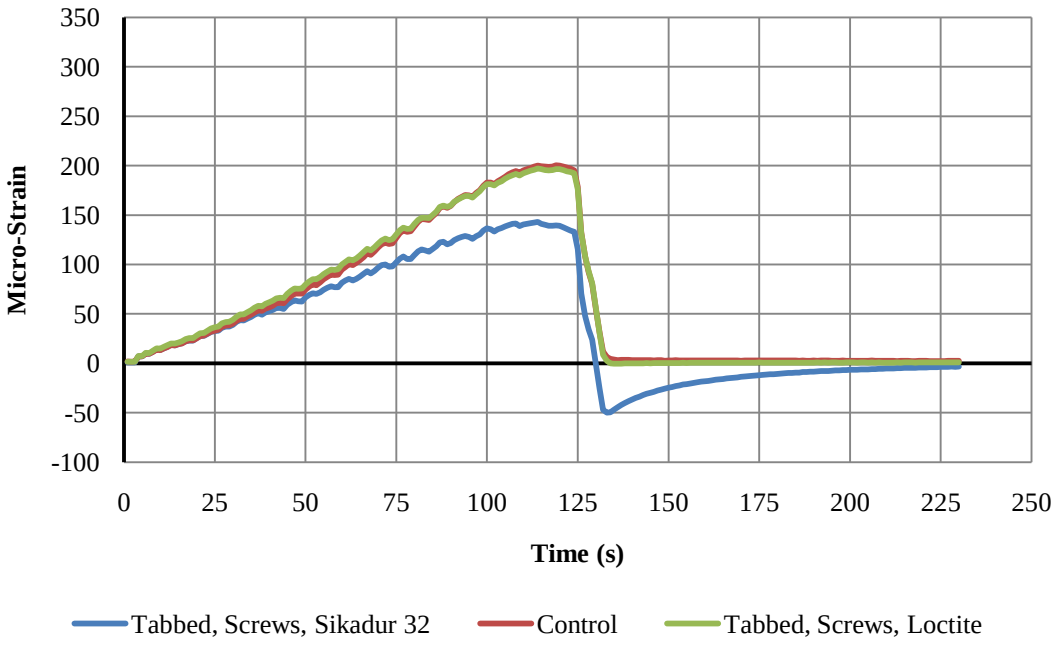

d. Test Group IV: Combinations 7, D, and 8

Figure 3.7 continued Tests 1 and 2 Loading St-Y Results

Loading C-Y was representative of the cyclic loadings (i.e., loadings C-X, C-yY, and C-Z) and the results are shown in Figure 3.8. The cyclic loading results are similar to the static loading results previously discussed because similar types of poor structural performance occur in both results: the viscoelastic behavior after load removal associated with using Sikadur 32 is shown in Figure 3.8a, Figure 3.8c, and Figure 3.8d. The negative strain values under loading for the combinations attached by screws only are shown in Figure 3.8b. The tabbed plate attached to the concrete by screws and Loctite H4500 epoxy again closely matched the control values and is shown in Figure 3.8d. The results of the remaining combinations again have a very poor structural performance as compared to the control for each test group.

www.manaraa.com

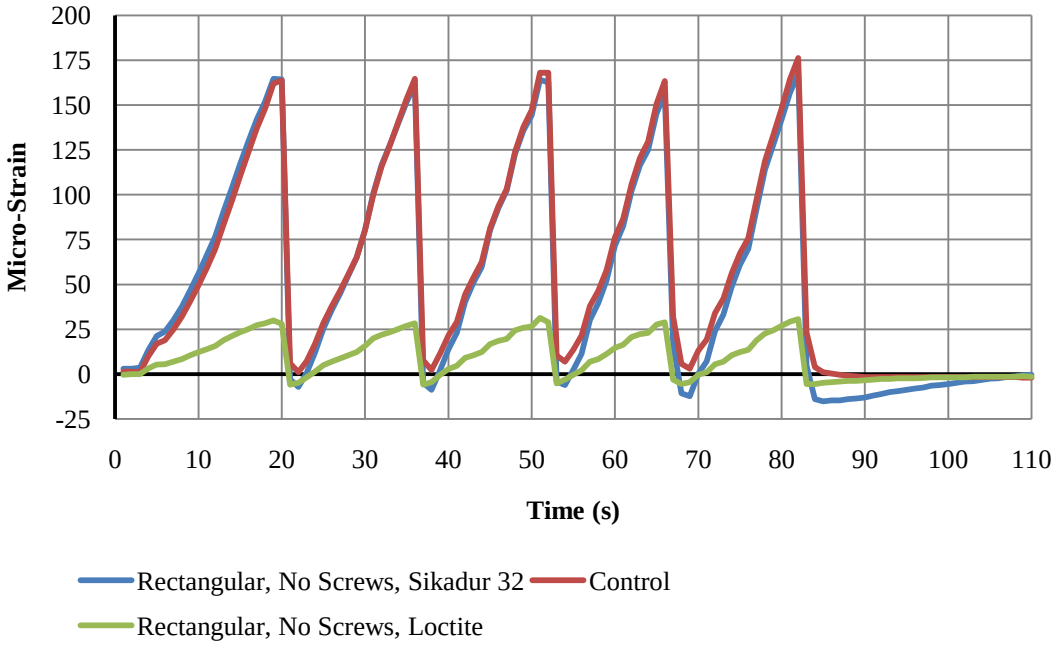

a. Test Group I: Combinations 1, A, and 2

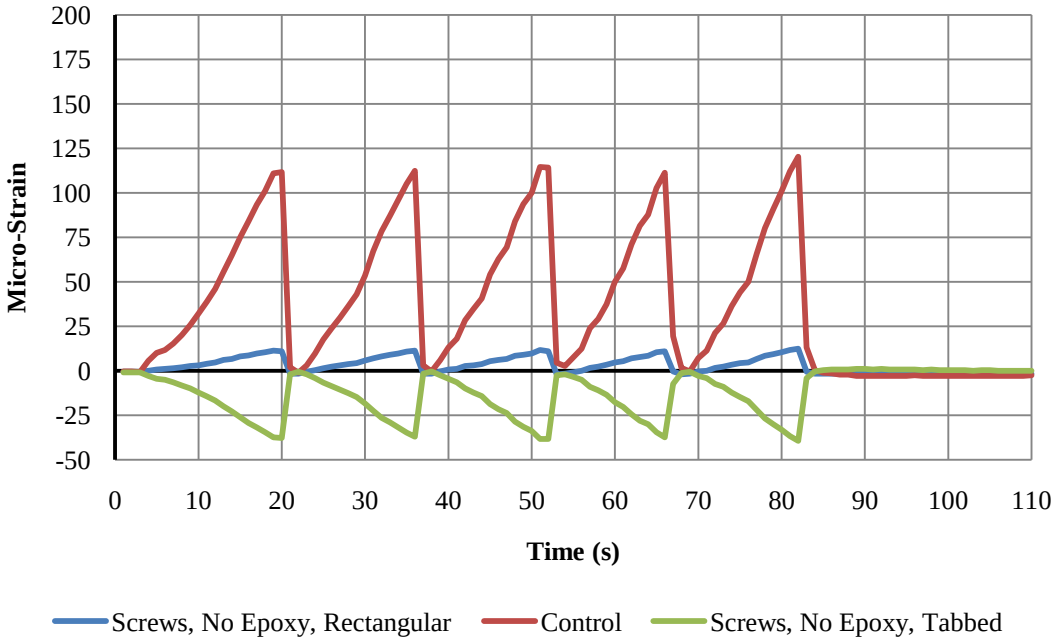

b. Test Group II: Combinations 3, B, and 4

Figure 3.8 Tests 1 and 2 Loading C-Y Results

www.manaraa.com

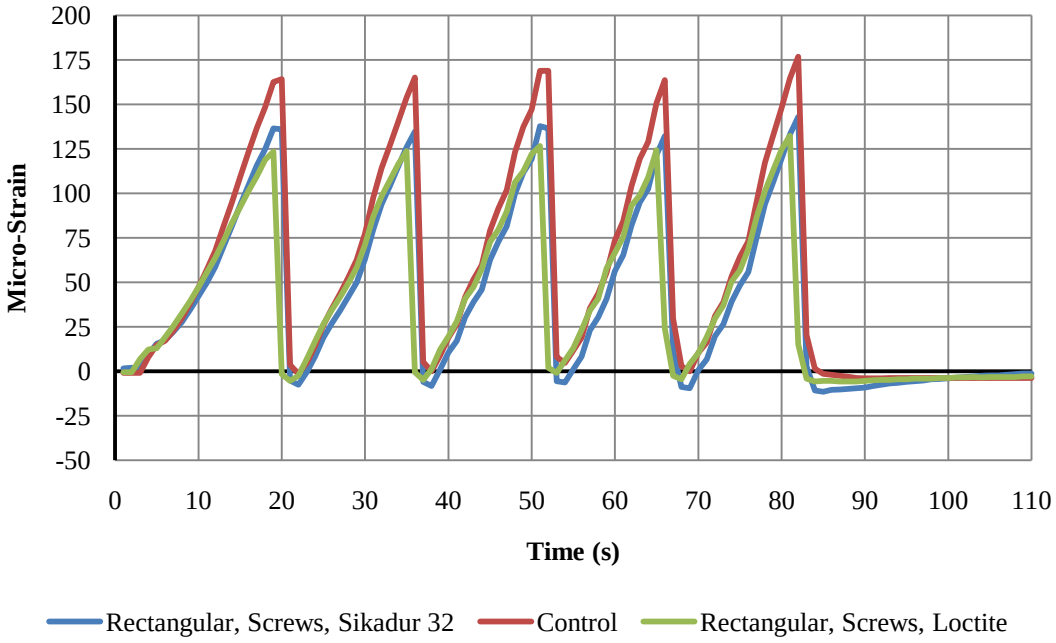

c. Test Group III: Combinations 5, C, and 6

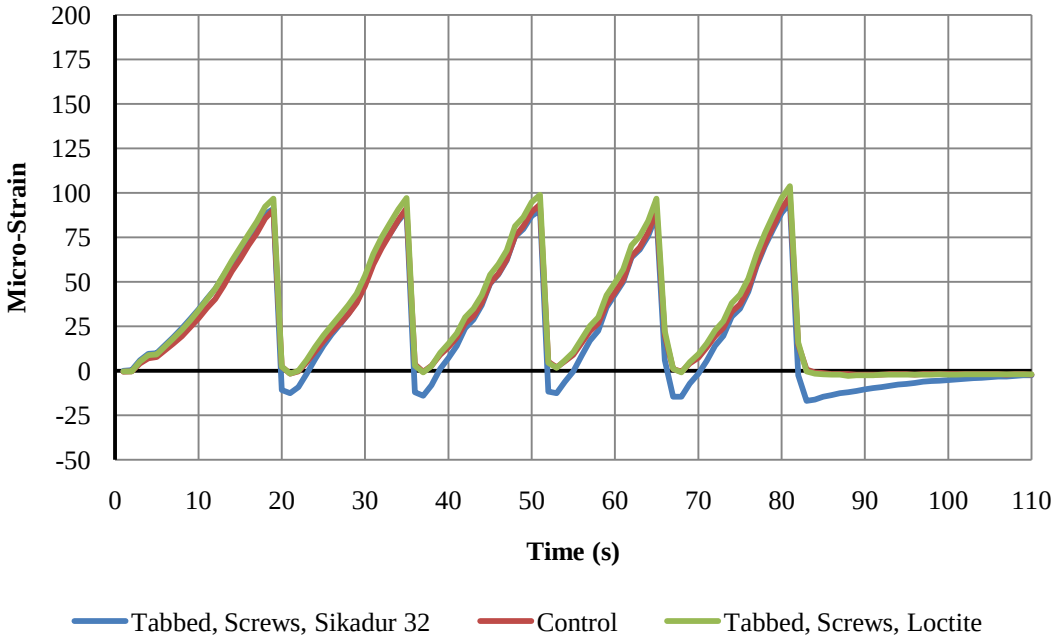

d. Test Group IV: Combinations 7, D, and 8

Figure 3.8 continued Tests 1 and 2 Loading C-Y Result

A sustained loading was completed for Tests 1 and 2 and the results are shown in Figure 3.9. Figure 3.9b indicates negative strain values during loading for the combinations without epoxy

www.manaraa.com

(Test Group II, Combinations 3 and 4), correlating to the results of the static and cyclic loadings shown previously in Figure 3.7 and Figure 3.8. Figure 3.9a, Figure 3.9c, and Figure 3.9d show that the viscoelastic behavior of the combinations with Sikadur 32 epoxy (Test Group I, Combination 1; Test Group III; Combination 5; Test Group IV, Combination 7) was more pronounced perhaps since the load is sustained over a longer amount of time. In the combinations where only epoxy was used to attach the plate to the concrete (Test Group I, Combinations 1 and 2 in Figure 3.9a), the strain loss was about 50% of the initial strain. The combinations with Loctite H4500 (Test Group I, Combination 2; Test Group III, Combination 6; Test Group IV, Combination 8) show a relatively small decrease in strain as shown in Figure 3.9a, Figure 3.9c, and Figure 3.9d.

Based upon the results of Tests 1 and 2, the use of Sikadur 32 alone and screws alone in the combinations was eliminated from further testing due to large errors. The combination of screws and Loctite H4500 epoxy produced the best results, were easier to install, and therefore were used in Test 3.

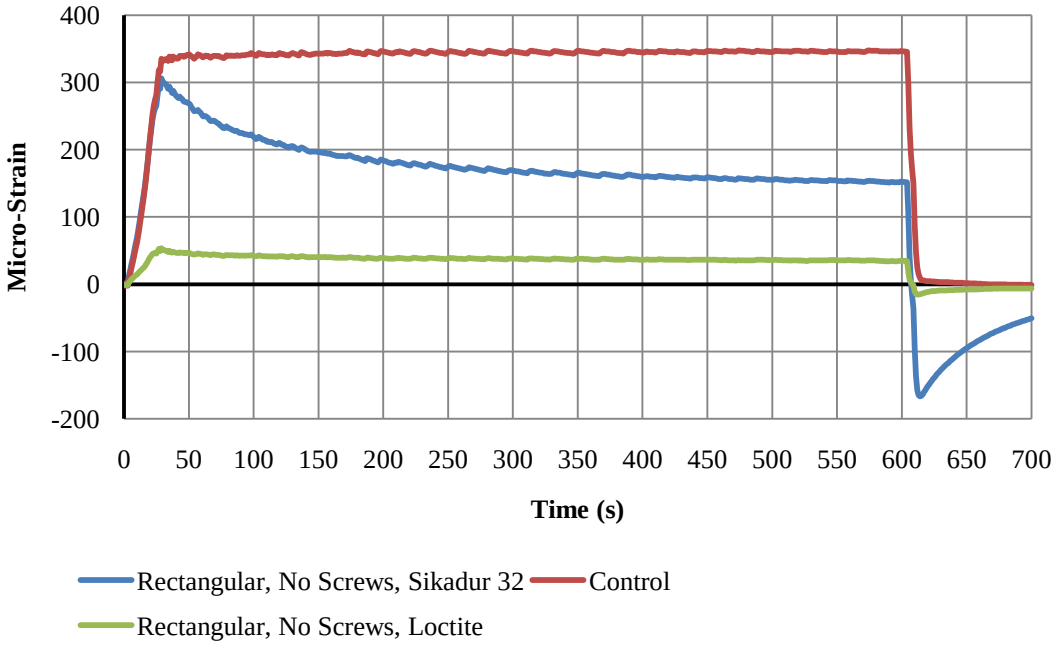

a. Test Group I: Combinations 1, A, and 2

Figure 3.9 Tests 1 and 2 Loading Su-X Results

www.manaraa.com

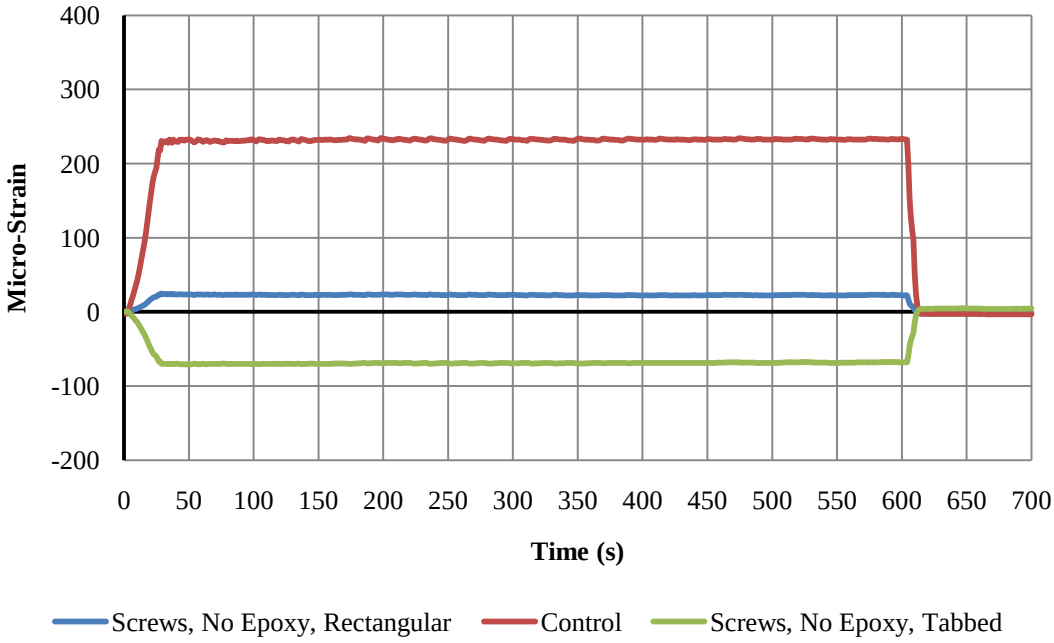

b. Test Group II: Combinations 3, B, and 4

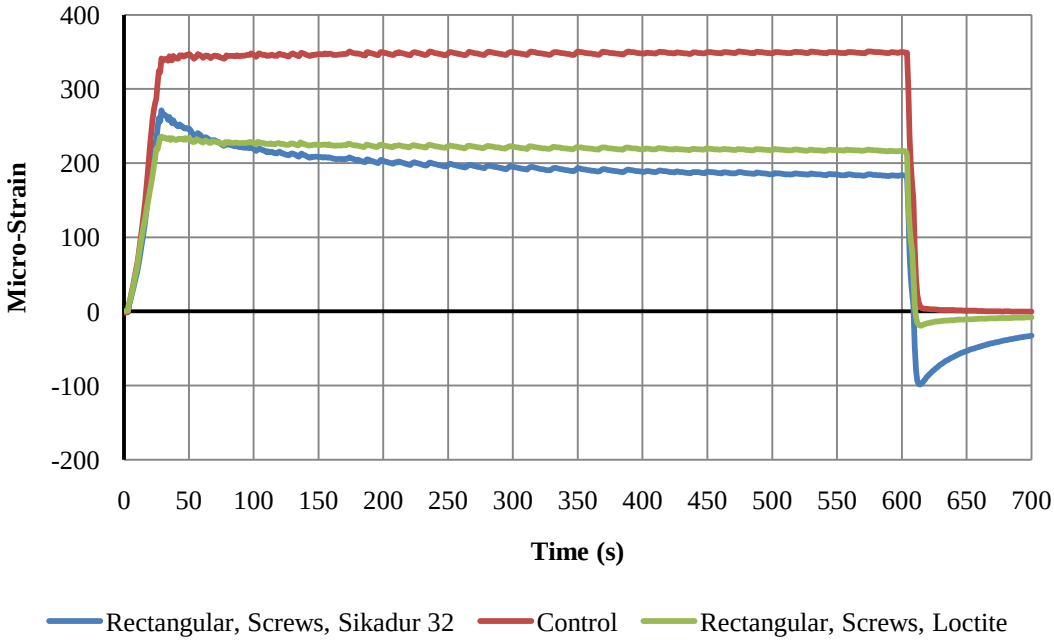

c. Test Group III: Combinations 5, C, and 6

Figure 3.9 continued Tests 1 and 2 Loading Su-X Results

www.manaraa.com

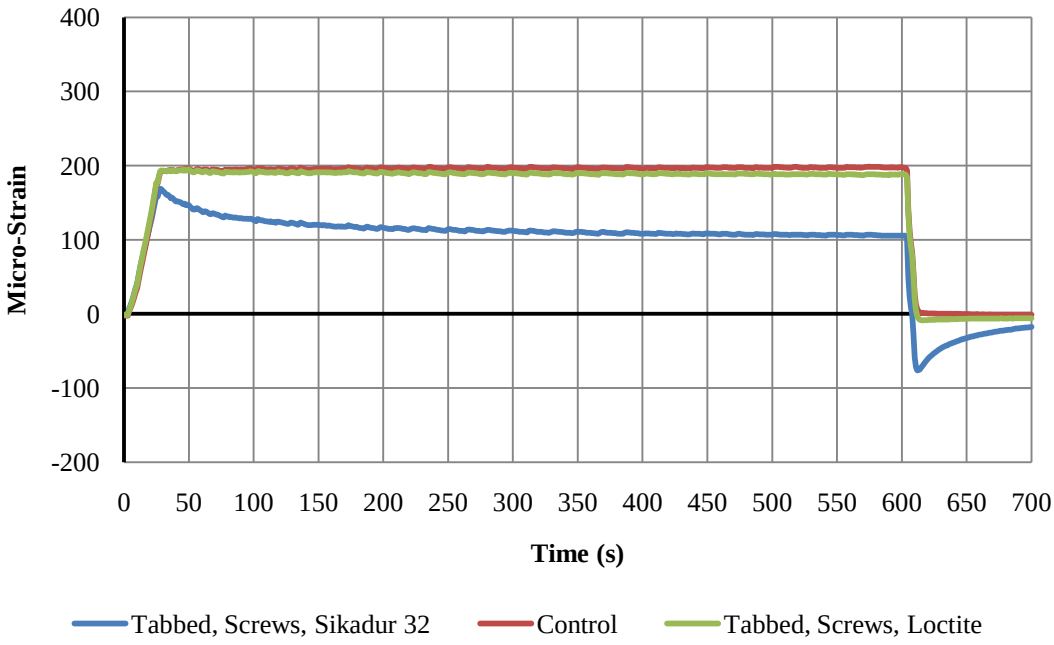

d. Test Group IV: Combinations 7, D, and 8

Figure 3.9 continued Tests 1 and 2 Loading Su-X Results

3.4.2 Test 3

In Test 3, new plate geometries were introduced and only one connection variation was used (screws with Loctite H4500) to attach all the combinations to the concrete. The results for loading St-Y only, which was representative of all results for static loading, are shown in Figure 3.10. The strain values from the combinations again do not correlate with the strain values from each control gauge. The tabbed plate attached by screws and Loctite H4500 epoxy that closely matched the control in Tests 1 and 2 (Test Group IV, Combination 8) did not match the control in Test 3 (Test Group I, Combination 1; Test Group III, Combination5) suggesting that the results for this combination were erroneous in Tests 1 and 2 (see Figure 3.10a and Figure 3.10c) and did not provide reliable and usable data. The strain values for the 10 in. rectangular plate combination (Figure 3.10d, Test Group IV, Combination 8) were higher than those from the control gauge.

Multiple cyclic loadings were completed in Test 3; loading C-Y appeared to be representative of the cyclic loadings for all data. The results for loading C-Y are shown in Figure 3.11 and follow the same patterns as the results from the static loadings. One main inconsistency was in the

www.manaraa.com

results of the tabbed plates (Test Group I, Combination 1 and Test Group III, Combination 5). In Figure 3.11c, the strain values from the tabbed plate closely follows the values from the control while in Figure 3.11a the strain values from the tabbed plate did not closely follow the control. Improper loading or installation may be the cause of this discrepancy and each plate was evaluated further in the sustained loading results.

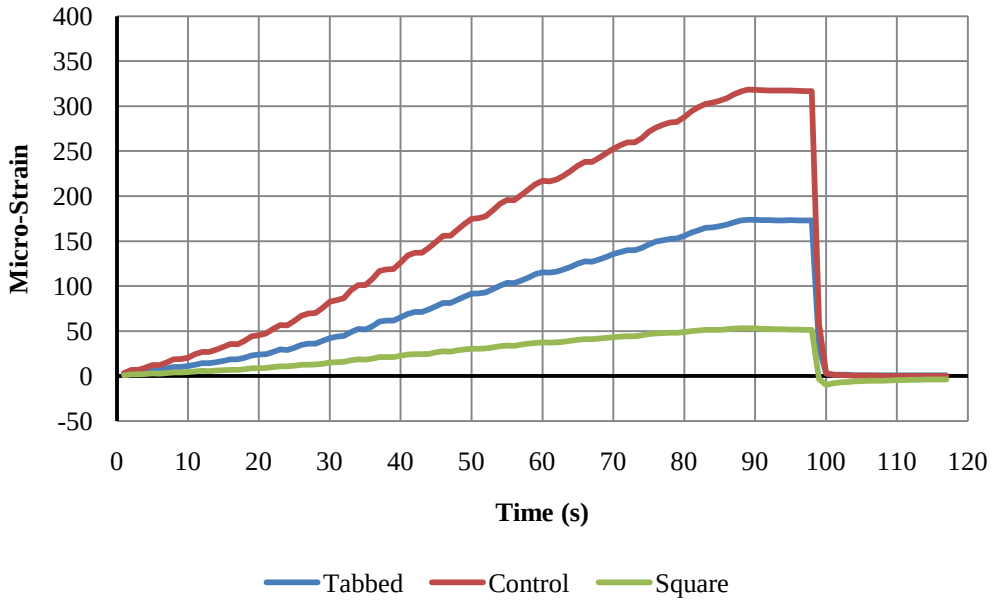

a. Test Group I: Combinations 1, A, and 2

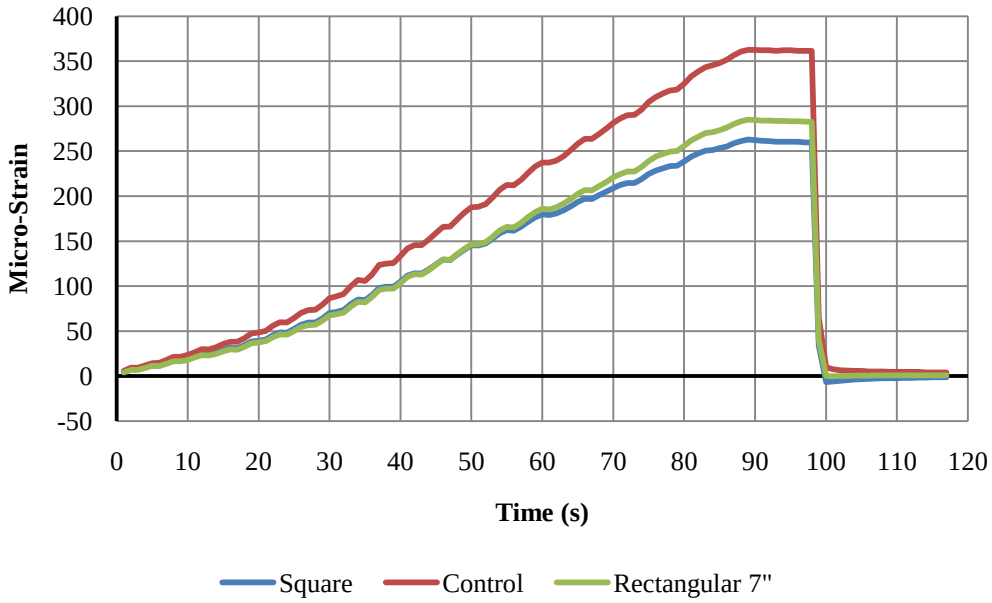

b. Test Group II: Combinations 3, B, and 4

Figure 3.10 Test 3 Loading St-Y Results

www.manaraa.com

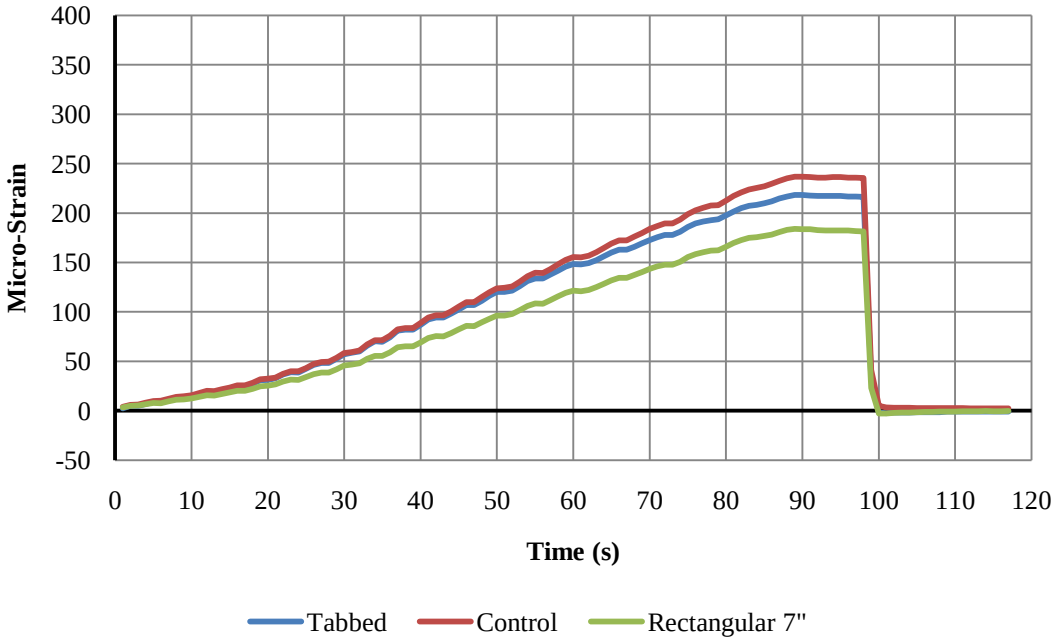

c. Test Group III: Combinations 5, C, and 6

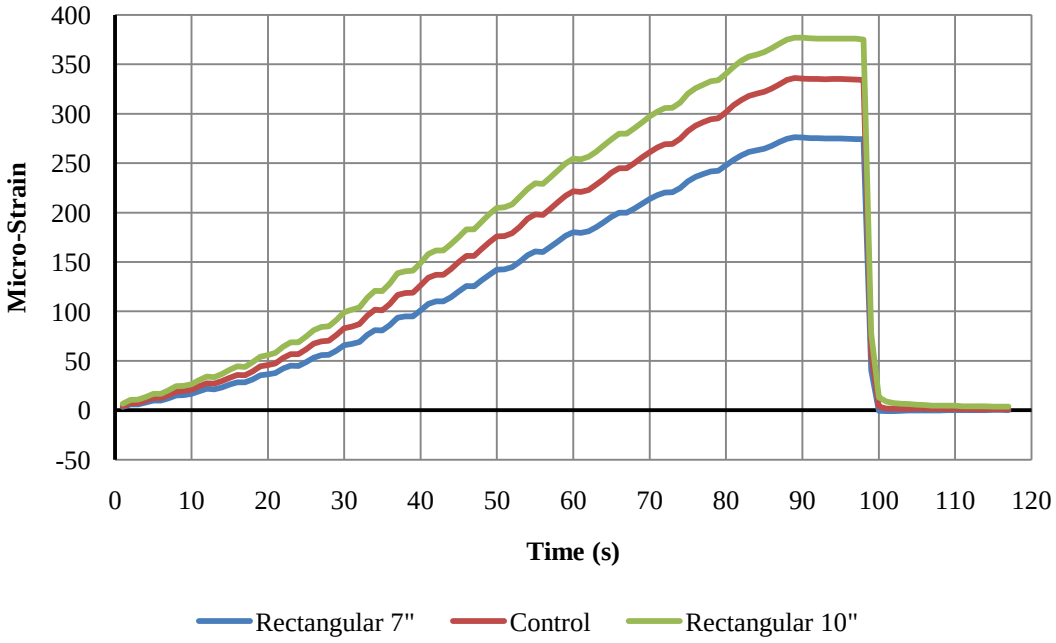

d. Test Group IV: Combinations 7, D, and 8

Figure 3.10 continued Test 3 Loading St-Y Results

www.manaraa.com

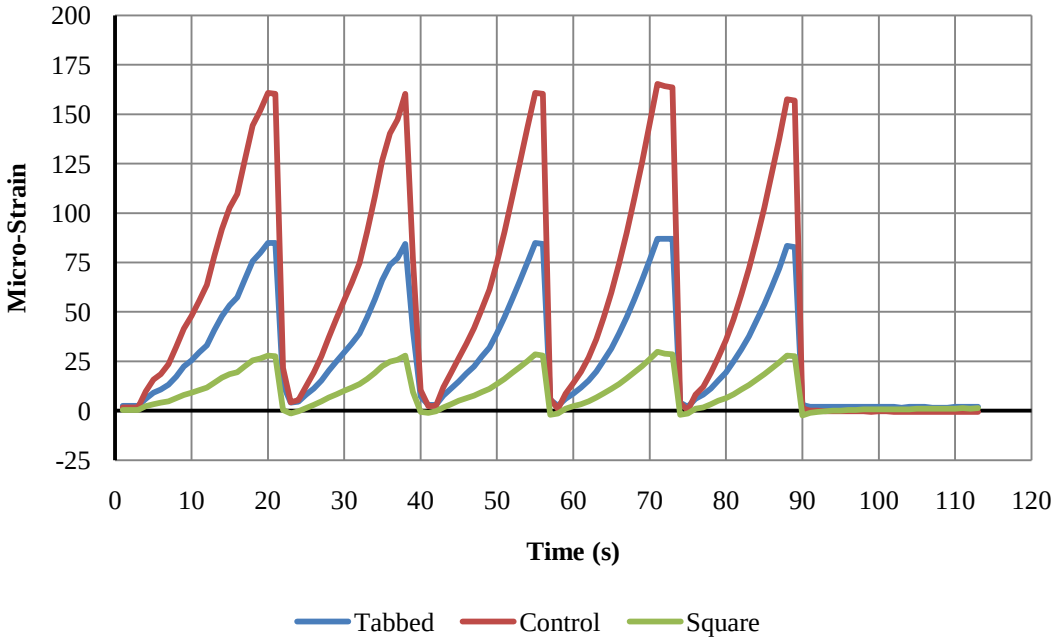

a. Test Group I: Combinations 1, A, and 2

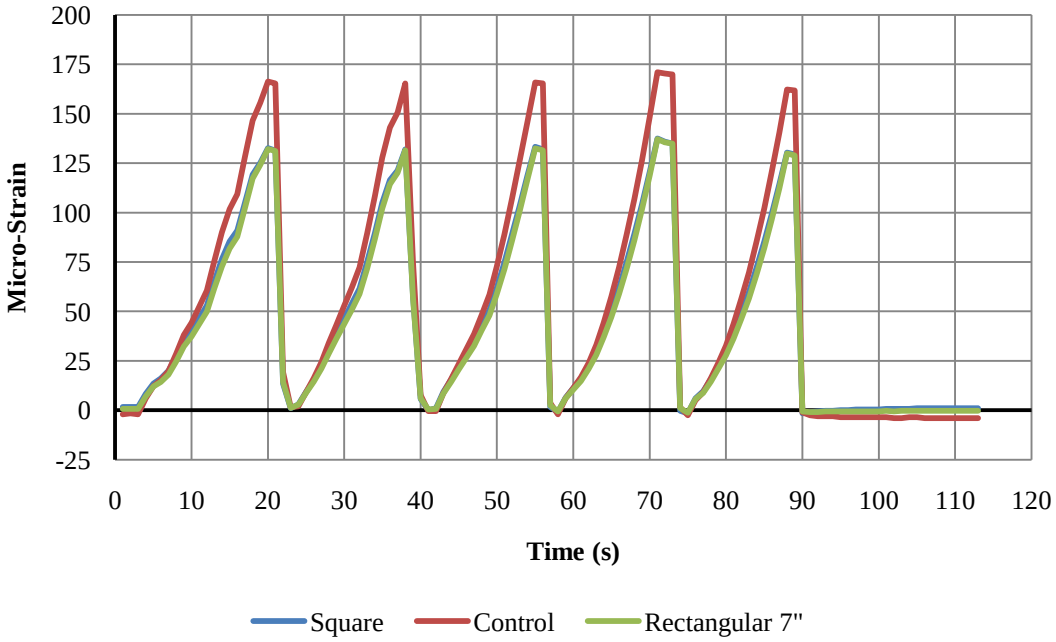

b. Test Group II: Combinations 3, B, and 4

Figure 3.11 Test 3 Loading C-Y Results

www.manaraa.com

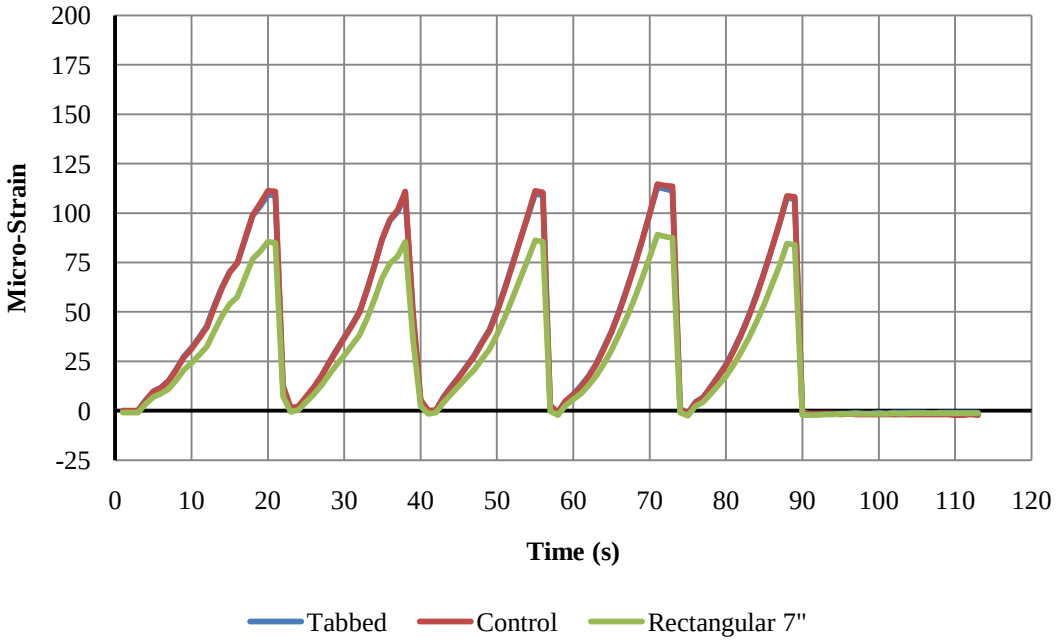

c. Test Group III: Combinations 5, C, and 6

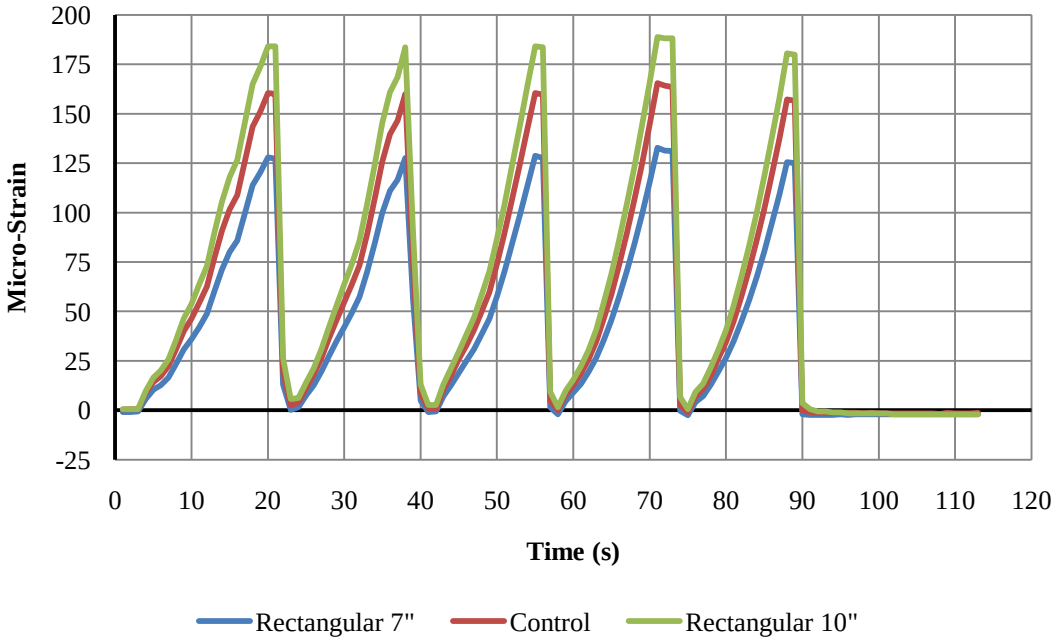

d. Test Group IV: Combinations 7, D, and 8

Figure 3.11 Test 3 Loading C-Y Results continued

A final sustained loading was completed in Test 3 and the results are shown in Figure 3.12. The sustained loading results were consistent with the static loading results; the strain readings from the combinations are below the control readings except for the readings from the 10 in.

www.manaraa.com

rectangular plate (Test Group IV, Combination 8) as shown in Figure 3.12d. The strain readings of all the combinations also mostly remain constant across the time indicating minimal viscoelastic behavior of the Loctite H4500 epoxy.

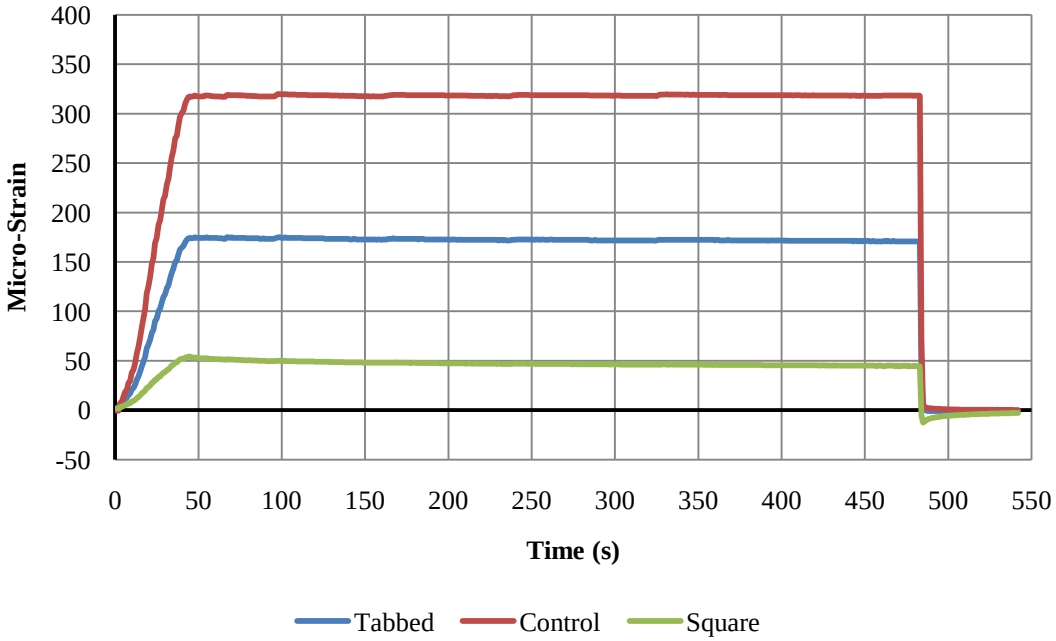

a. Test Group I: Combinations 1, A, and 2

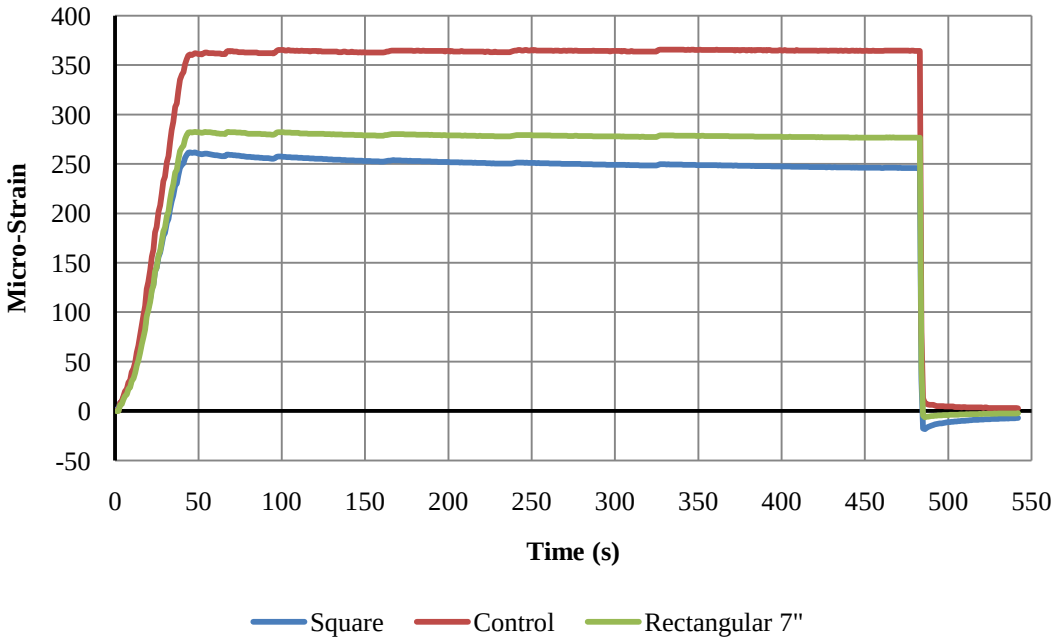

b. Test Group II: Combinations 3, B, and 4

Figure 3.12 Test 3 Loading Su-X Results

www.manaraa.com

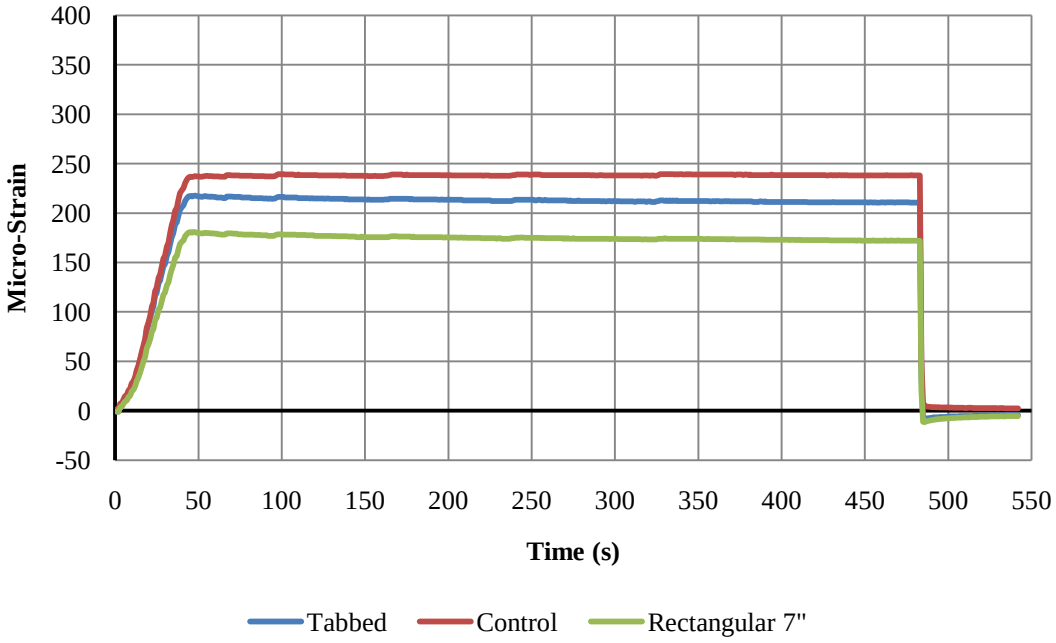

c. Test Group III: Combinations 5, C, and 6

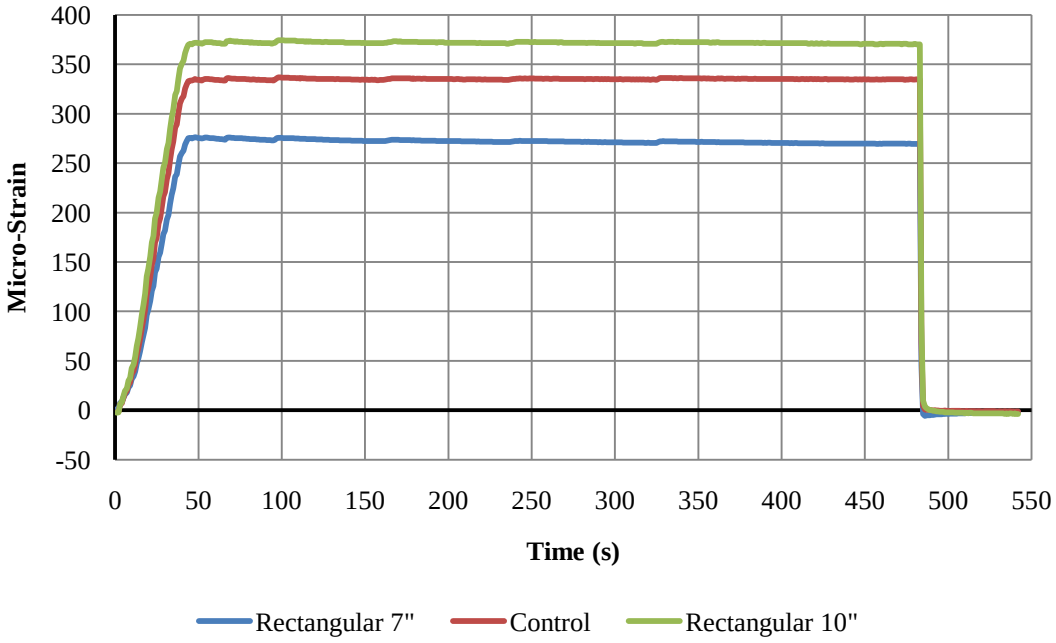

d. Test Group IV: Combinations 7, D, and 8

Figure 3.12 Test 3 Loading Su-X Results continued

www.manaraa.com

3.5 Summary and Conclusions

3.5.1 Summary

In previous research, multiple techniques of sensor attachment to concrete were investigated. All of these techniques either could not be integrated into the existing structural health monitoring system or were used previously and problems arose. An investigation into differing sensor attachment techniques was completed.

The main goal of the sensor attachment testing was to find a way to easily attach a sensor to the underside of the concrete deck of the US30 bridge and achieve acceptable epoxy bonding. Bonding the sensor to a thin steel plate with epoxy and attaching the plate to the concrete deck with epoxy, screws, or a combination of epoxy and screws was investigated. Testing in a laboratory was completed to determine which steel plate geometry should be used. A prestressed concrete I-beam was used as the test concrete surface. Within each test group were two combinations of connection variables and a control gauge. Multiple tests with multiple loadings were conducted to compare all of the connection variables.

In Tests 1 and 2, the 7 in. rectangular and tabbed plate geometries were tested. Loctite H4500 epoxy, Sikadur 32 epoxy, and screws as the means of attachment to the concrete were also tested. Within Tests 1 and 2 multiple static and cyclic loadings and a sustained loading were completed to determine the effects of differing loadings on the test combinations. From the results of these loadings, Sikadur 32 epoxy was eliminated from further testing because of the unacceptable viscoelastic behavior observed after unloading. Using screws without epoxy to attach the plates was also eliminated from further testing because of the negative strain observed during loading. Almost all of the results showed unacceptable errors between the control and the combinations revealing that the strain was not adequately transferred from the concrete to the gauge. The combination of screws and Loctite H4500 epoxy produced the best results in Tests 1 and 2 and were used in Test 3.

In Test 3, two additional plate geometries were evaluated: a square plate and a 10 in. rectangular plate. The loadings in Tests 1 and 2 were also completed in Test 3 for consistency across all

www.manaraa.com

three tests. All combinations were bonded to the concrete with Loctite H4500 epoxy and screws. Large errors between the combinations and the control were again present in the results; none of the combinations were within the acceptable limits of error and therefore could not be used to accurately measure strains on US30 bridge.

3.5.2 Conclusions

Upon review of this research on a technique to attach sensors to concrete, the following conclusions can be made:

1. When used the Sikadur 32 epoxy caused adverse viscoelastic behavior. The performance was particularly bad for loading sustained over a long period of time.

2. The use of both screws and Loctite H4500 epoxy to attach the steel plate to concrete reduces the percentage of error of the strain readings and is easier to install compared to other attachment combinations. In this specific case, when screws without epoxy were used the strain readings were inconsistent and were negative.

3. The results showed that no combination of the investigated plate geometry, epoxy, and screws produced accurate and verifiable strain readings that closely matched those of the adjacent control gauge.

www.manaraa.com

CHAPTER 4. EXPERIMENTAL PROCEDURE

This chapter describes the processes and tools used to experimentally validate the damage detection algorithm developed by Lu (Lu 2008) in, "A Statistical Based Damage Detection Approach for Highway Bridge Structural Health Monitoring." A description of the dimensions and instrumentation of the demonstration bridge, an introduction and purpose of the sacrificial specimen, and an explanation of the types of damaged induced to the sacrificial specimen is included in the following sections.

4.1 Demonstration Bridge

For the experimental validation, a two-girder fracture-critical demonstration bridge that was previously instrumented with fiber optic sensors was utilized. The demonstration bridge has numerous fatigue sensitive locations which were closely monitored and, ultimately, the need for the SHM system. The following sections provide general information, describe the fatigue sensitive locations on the bridge, and describe the instrumentation on the demonstration bridge.

4.1.1 General Information

As with related work preceding that described herein, the bridge used in this project was the Eastbound US Highway 30 (US30) Bridge crossing the South Skunk River near Ames, IA (Figure 4.1). The US30 Bridge has three spans with two equal outer spans (97.5 ft) and a longer middle span (125 ft), a width of 30 ft, and a skew of 20 degrees. The superstructure consists of two continuous welded steel plate girders, 19 floor beams, and two stringers that support a 7.25 in. thick cast-in-place concrete deck. The bridge supports are pinned at the west pier and are roller-type supports at the east pier and at each of the abutments. The abutments are stub reinforced concrete and the piers are monolithic concrete (Lu 2008). The general bridge framing plan along with general member dimensions can be seen in Figure 4.2.

4.1.2 Fatigue Sensitive Details: Girder Web-Gap

In previous research by Wipf et al, several fatigue sensitive locations of the US30 Bridge were

www.manaraa.com

instrumented with fiber optic strain gauges. These locations are generally located at the connection between the floor beams and the web of the welded plate girders as shown in Figure 4.3a. During initial construction of the bridge, the connection plate welded to the web of the plate girder extended to directly under, but not welded to, the top flange of the plate girder. As vehicles cross the bridge the deflection of each of the girders differs due to the skew of the bridge; this causes a rotation of the floor beam which is especially pronounced near the piers (Lu 2008). Due to its large stiffness, the composite concrete deck restrains rotation of the plate girder top flange. Therefore, as the floor beam rotates, double curvature bending of the plate girder web (between the top flange and the top of the floor beam connection plate) occurs. This phenomenon can schematically be seen in Figure 4.3b. This double curvature creates high levels of stress and has been linked to the formation of fatigue cracks. Cutting back the floor beam connection plate, as illustrated in Figure 4.3c, allows the double curvature to act over a longer length (Figure 4.3d). This reduces the stress concentration/levels and, therefore, reduces the susceptibility to fatigue cracking. Although this repair reduces the fatigue damage it does not completely eliminate it. In some cases fatigue cracks have continued to develop in these regions. Autonomous detection of crack formation in these areas was the precipitous for this and preceding work.

a. Side View **b. Bottom View**

Figure 4.1 Photographs of the US30 South Skunk Bridge (Lu, 2008)

www.manaraa.com

المنارة للاستشارات

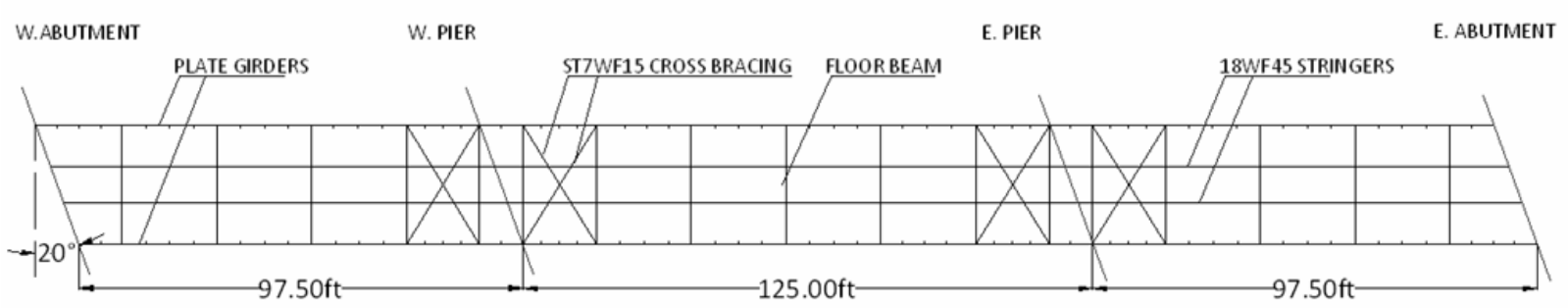

a. Plan view

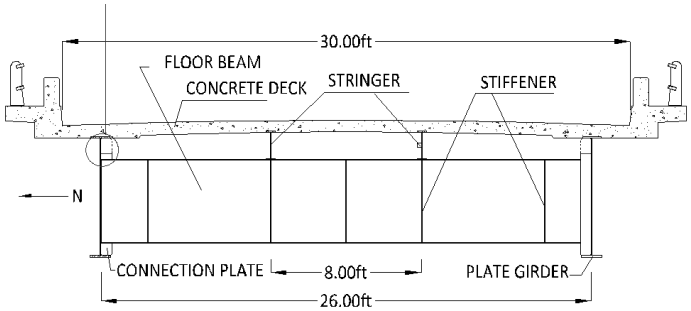

b. Typical cross section

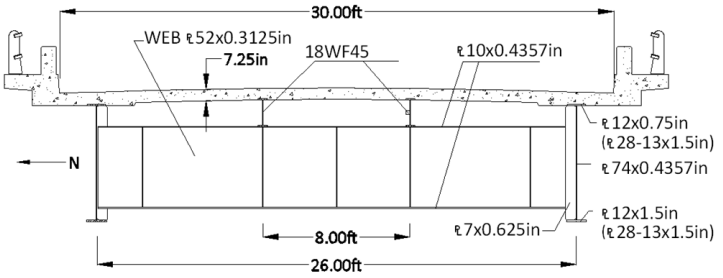

c. Sizes of structural components

Figure 4.2 Plan view and Sectional views of US30 Bridge (Lu, 2008)

www.manaraa.com

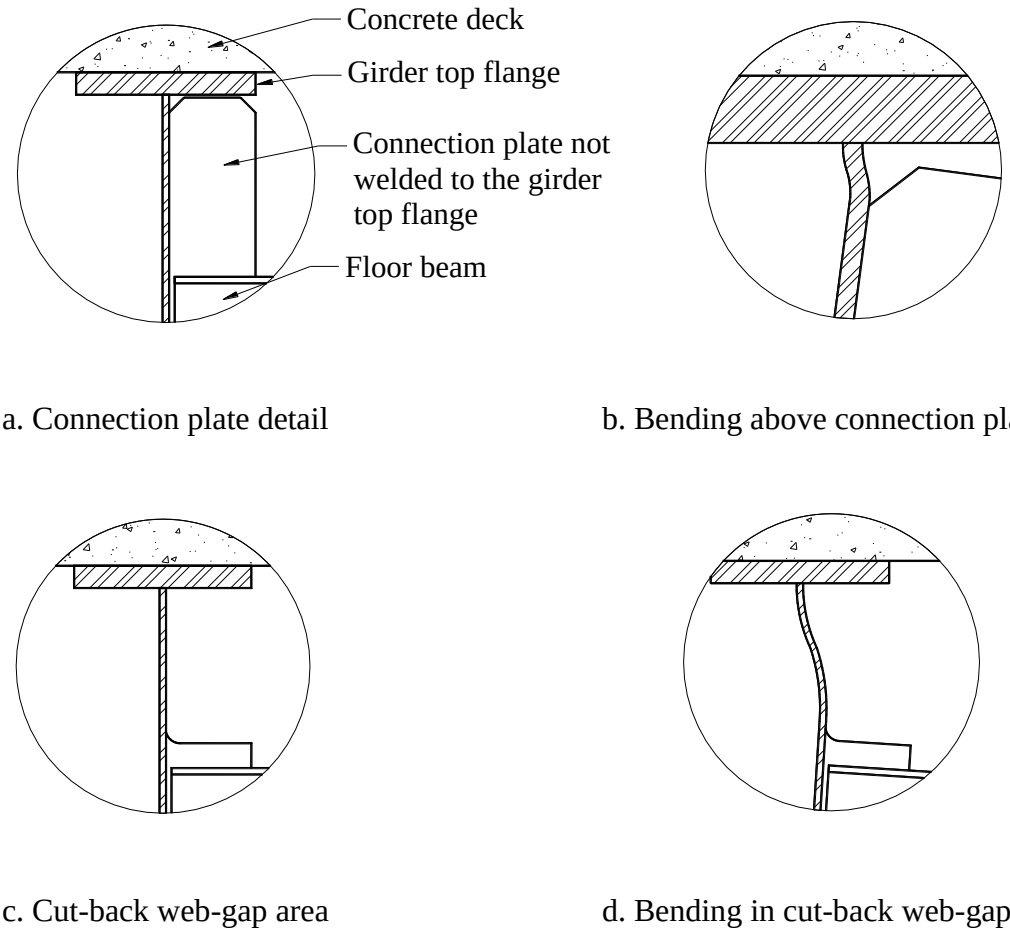

a. Connection plate detail

b. Bending above connection plate

c. Cut-back web-gap area

d. Bending in cut-back web-gap area

Figure 4.3 Web-Gap Details and Out-of-Plane Bending Behavior (Lu, 2008)

4.1.3 Instrumentation

During previous work a total of 48 fiber-optic strain gauges were installed on the previously mentioned US30 bridge. Numerous fiber optic strain gauges were placed in the web cut-back regions to monitor the strain caused by live loads. Figure 4.4 shows the location of the 5-sensor array at C-NG-CB (description below) which is geometrically similar to all web gaps. Note that the sensor numbers shown in Figure 4.4 will be used elsewhere in this report.

Sensors were also placed at numerous other locations on the US30 bridge. These sensors were distributed across six cross-sections (Figure 4.5) and are aligned in two orientations: vertical or horizontal. Sensors were installed on the bottom flanges of the two plate girders, the bottom

www.manaraa.com

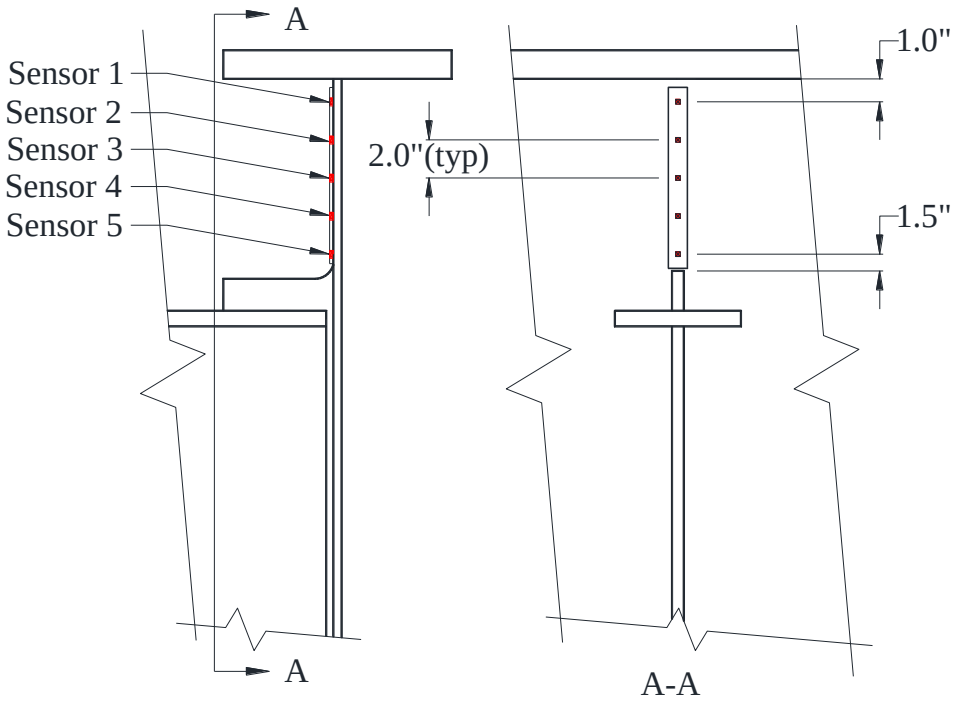

Figure 4.4 Typical Instrumented Web-Gap

flanges of multiple floor beams, the bottom flanges and webs of the stringers, and on the deck bottom. The distribution of the sensors across the different cross-sections (Sections A through F and Lines 1 and 2) is summarized in Figure 4.6. A naming convention for the sensors based on their location and orientation was inherited from previous work with descriptions shown in Table 4.1. For example, a sensor designated B-NG-BF-H means the sensor is at section B, on the north girder, on the bottom flange, and in the horizontal orientation. More information on the complete monitoring system can be found in, "Damage Detection in Bridges through Fiber Optic Structural Health Monitoring," (Doornink 2006) and, "A Statistical Based Damage Detection Approach for Highway Bridge Structural Health Monitoring," (Lu 2008).

www.manaraa.com

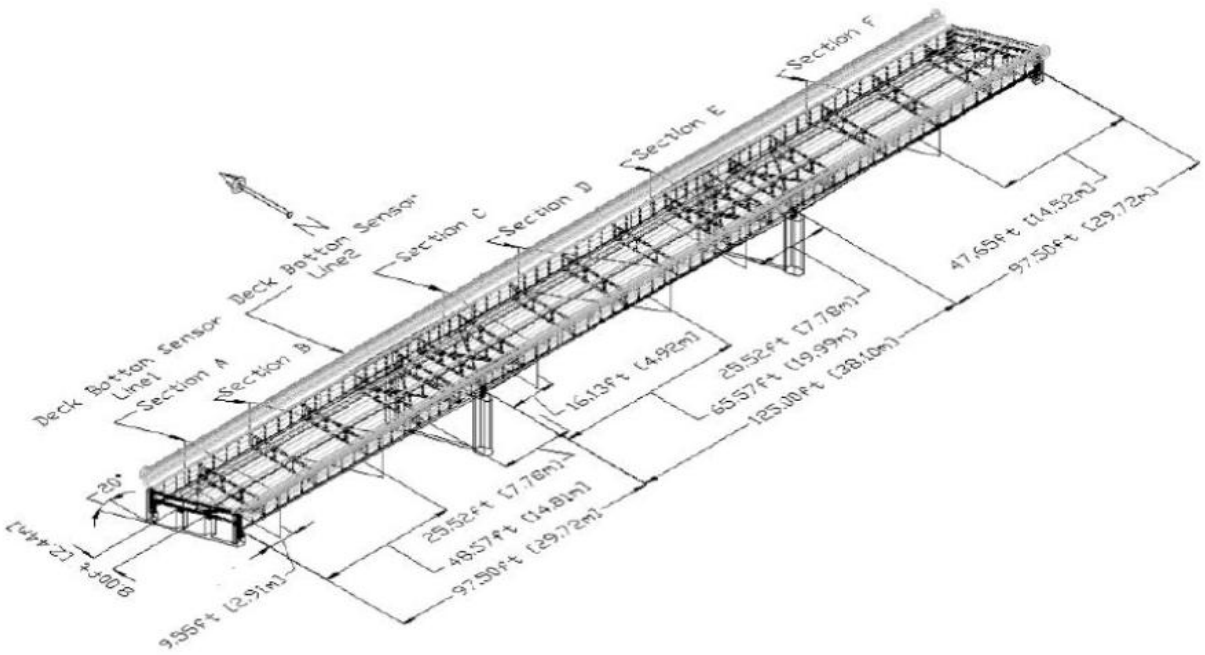

Figure 4.5 Cross Sections of US30 Bridge and Sensor Longitudinal Locations (Lu 2008)

4.2 Sacrificial Specimen

As the goal of this work was to validate the damage detection algorithms developed in previous work and in light of the fact that the Iowa DOT prohibited the introduction of damage into a public bridge, a sacrificial specimen was designed, installed at the US30 bridge, and forced to accumulate damage. The design and configuration of the sacrificial specimen focused on simulating the double curvature bending occurring within the web-gap regions.

4.2.1 Sacrificial Specimen Description

The sacrificial specimen details are shown in Figure 4.7 and a photograph is shown in Figure 4.8. To encourage similar strain levels and behaviors, the sacrificial specimen plate thicknesses and welds were designed to match those found on the US30 bridge. The sacrificial specimen consists of two web-gaps connected by a steel plate (simulating the floor-beam connection plate). In this configuration each of the two web gaps undergoes double curvature bending similar to the actual bridge (see Figure 4.9).

www.manaraa.com

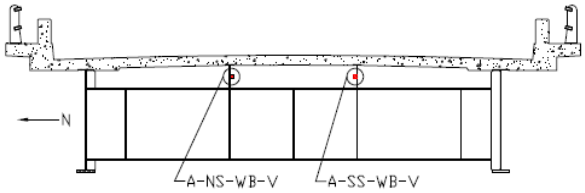

a. Cross section A

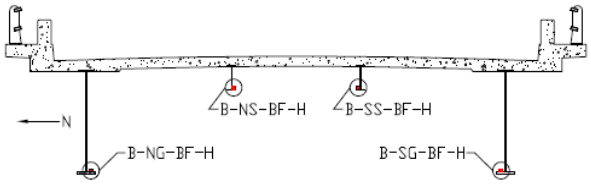

b. Cross section B

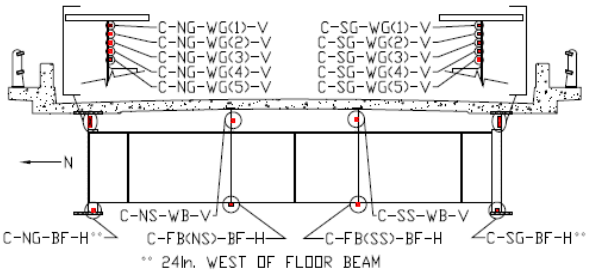

c. Cross section C

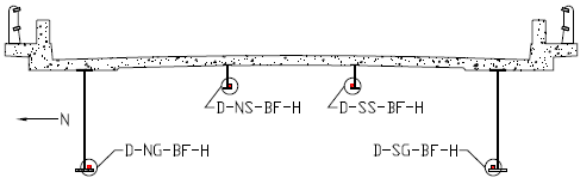

d. Cross section D

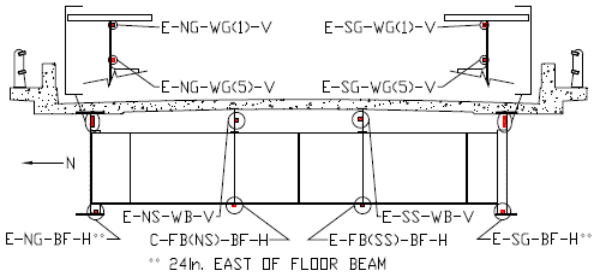

e. Cross section E

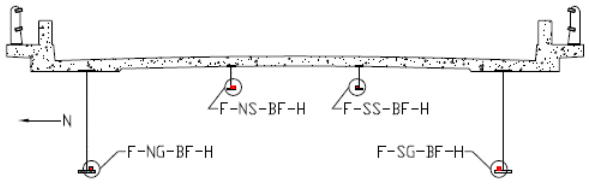

f. Cross section F

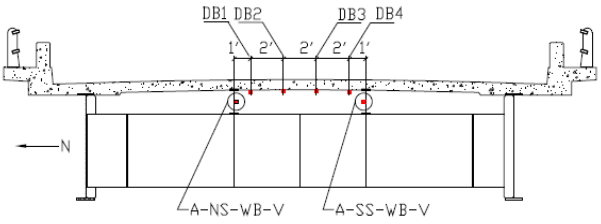

e. Line of deck-bottom sensors at Section A

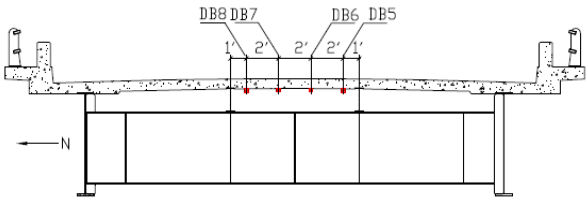

f. Line of deck-bottom sensors above fifth floor beam

Figure 4.6 Sensors Located at the Bridge Frame System (Lu 2008)

www.manaraa.com

Table 4.1 Naming convention for sensor installed on the US30 bridge (Lu 2008)

Member	Description	**Part**	Description	**Orientation**	Description
NG/SG	North Girder/ South Girder	BF	Bottom flange	H	Horizontal
NG/SS	North Stringer/ South Stringer	CB	Cut-back region	V	Vertical
FB	Floor Beam	WB	Web		
DB	Deck Bottom				

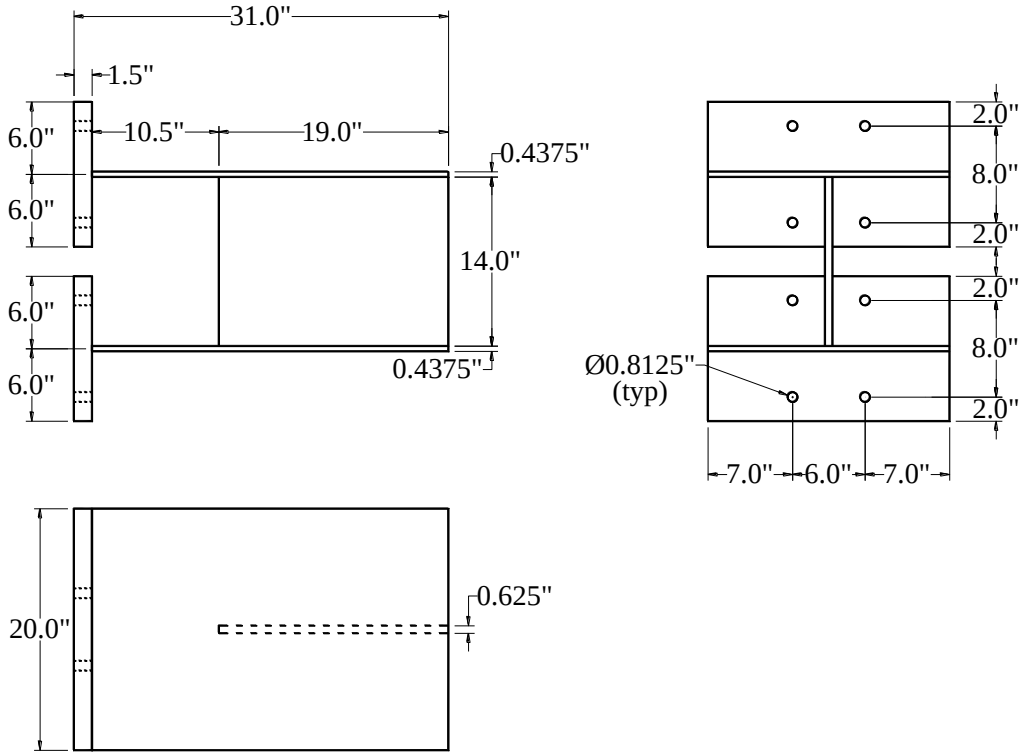

Figure 4.7 Sacrificial Specimen Geometric Details

A finite element model (FEM) of the sacrificial specimen was constructed before fabrication to study the behavior. The FEM is shown in Figure 4.10 and the strain contour plot from a point load placed at the end of the sacrificial specimen can be seen in Figure 4.11. The high strain locations from the FEM of the sacrificial specimen (e.g. the dark blue and yellow areas in Figure 4.11) coincide with the expected high strain locations caused by double curvature bending. A simpler beam-type analysis also confirmed the general behavior. In total two sacrificial

www.manaraa.com

specimens were fabricated and tested.

Figure 4.8 Photo of Sacrificial Specimen

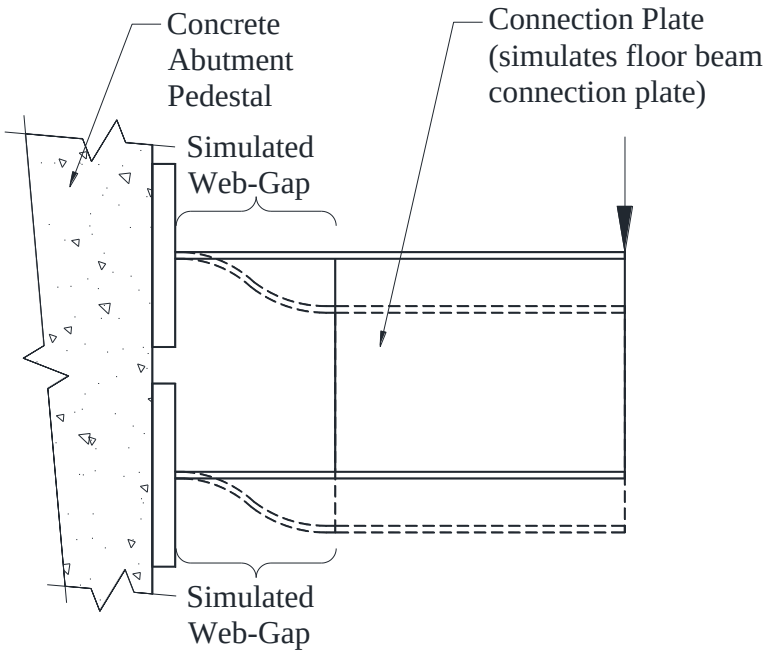

Figure 4.9 Double Curvature Bending of Sacrificial Specimen

www.manaraa.com

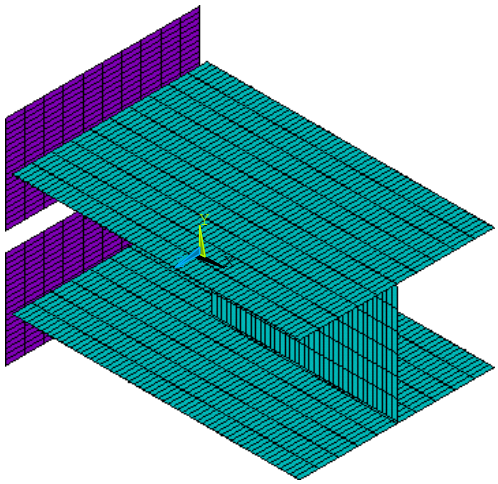

Figure 4.10 Finite Element Model of Sacrificial Specimen

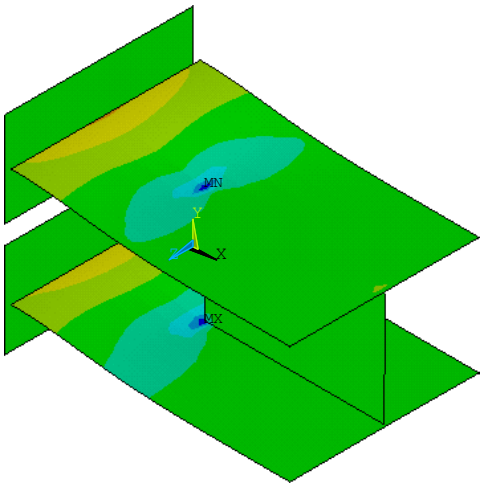

Figure 4.11 Strain Contour Plot of Sacrificial Specimen

4.2.1.1 Sacrificial Specimen 1

Sacrificial Specimen 1 was fabricated with a small EDM notch through the thickness of the top plate (i.e., the plate directly connected to the steel strut) near an anticipated high strain area (Figure 4.11) as illustrated in Figure 4.12. Sacrificial Specimen 1 modeled two web-gap areas connected by together by a simulated connection plate which in turn helps to transform the ambient traffic loads into double curvature bending of the simulated web-gaps. When subjected to high strains and a large number of cycles, a crack was expected to initiate at the EDM notch. Different damage levels were introduced in sacrificial Specimen 1 and are discussed in later

www.manaraa.com

paragraphs.

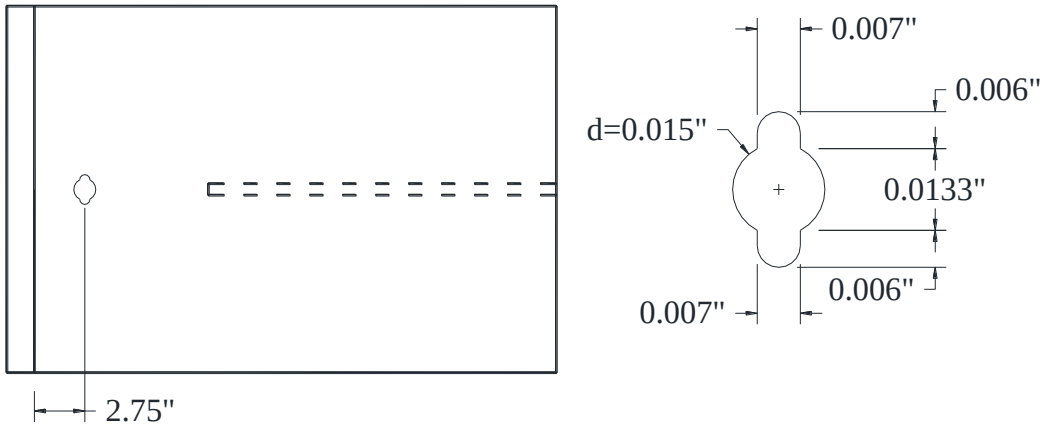

Figure 4.12 Dimensions and Location of Notch

4.2.1.2 Sacrificial Specimen 2

Sacrificial Specimen 2 was constructed as shown in Figure 4.7 and instrumented as shown in

Figure 4.13. The EDM notch through the thickness of the top plate was not fabricated on sacrificial Specimen 2 due to the cracking that did not occur through the EDM notch in sacrificial Specimen 1 as expected. When the location of the EDM notch was determined on sacrificial Specimen 1, the second high strain location was not considered as a possibility for a crack location.

4.2.2 Sacrificial Specimen Instrumentation

An array of four fiber optic sensors arranged in-line was installed in one web-gap of each sacrificial specimen as shown in
Figure 4.13. Carbon fiber reinforced polymer was used to hold the sensors in place and to attach the sensors to the steel. A grating length (i.e., sensor length) of each of the sensors was chosen as 5 mm to ensure the accurate recording of peak strains. The array was chosen to closely match the sensor arrays placed on the web-gaps of the US30 bridge (Figure 4.4). The area of steel on which the sensors were attached using Loctite H4500 epoxy was sanded down and pressure was applied to ensure proper bonding of the carbon fiber package and the accuracy of the strain

www.manaraa.com

readings. This process was completed for all sacrificial specimens.

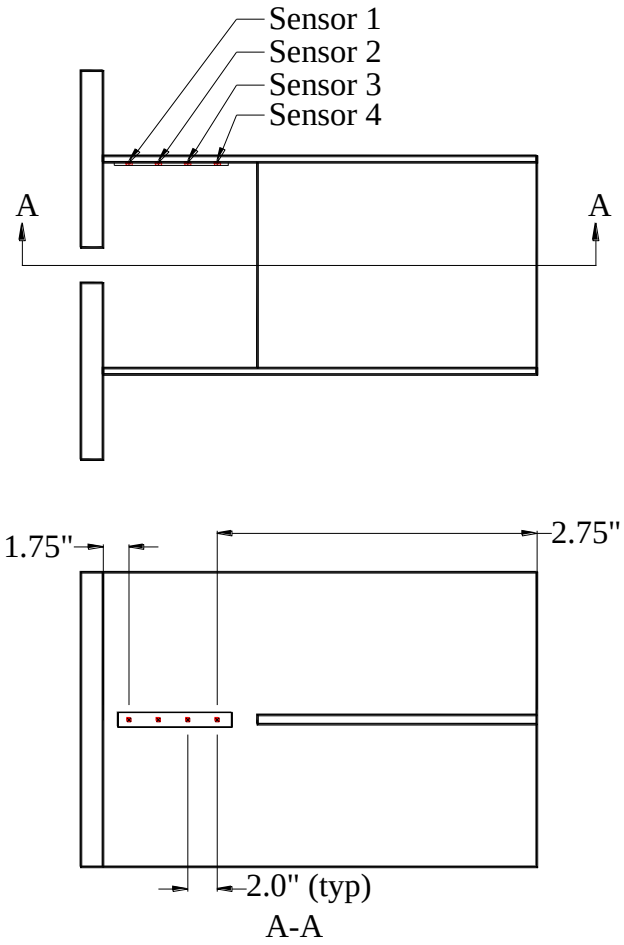

Figure 4.13 Sacrificial Specimen with Sensor Array Details

4.2.3 Sacrificial Specimen Installation

Each sacrificial specimen was installed in a horizontal orientation with the plates simulating the girder top flanges secured to a west abutment pedestal using anchor bolts as shown in Figure 4.14. A steel strut attached to the sacrificial specimen and a stringer transfers load from the bridge to the sacrificial specimen.

Typical strain vs. time curves for both the bridge and sacrificial specimen web-gaps shown are shown in Figure 4.15. These data were produced by a single, five-axle truck driving across the bridge. Note that the strains for the sacrificial specimen web gap were collected using a four-

www.manaraa.com

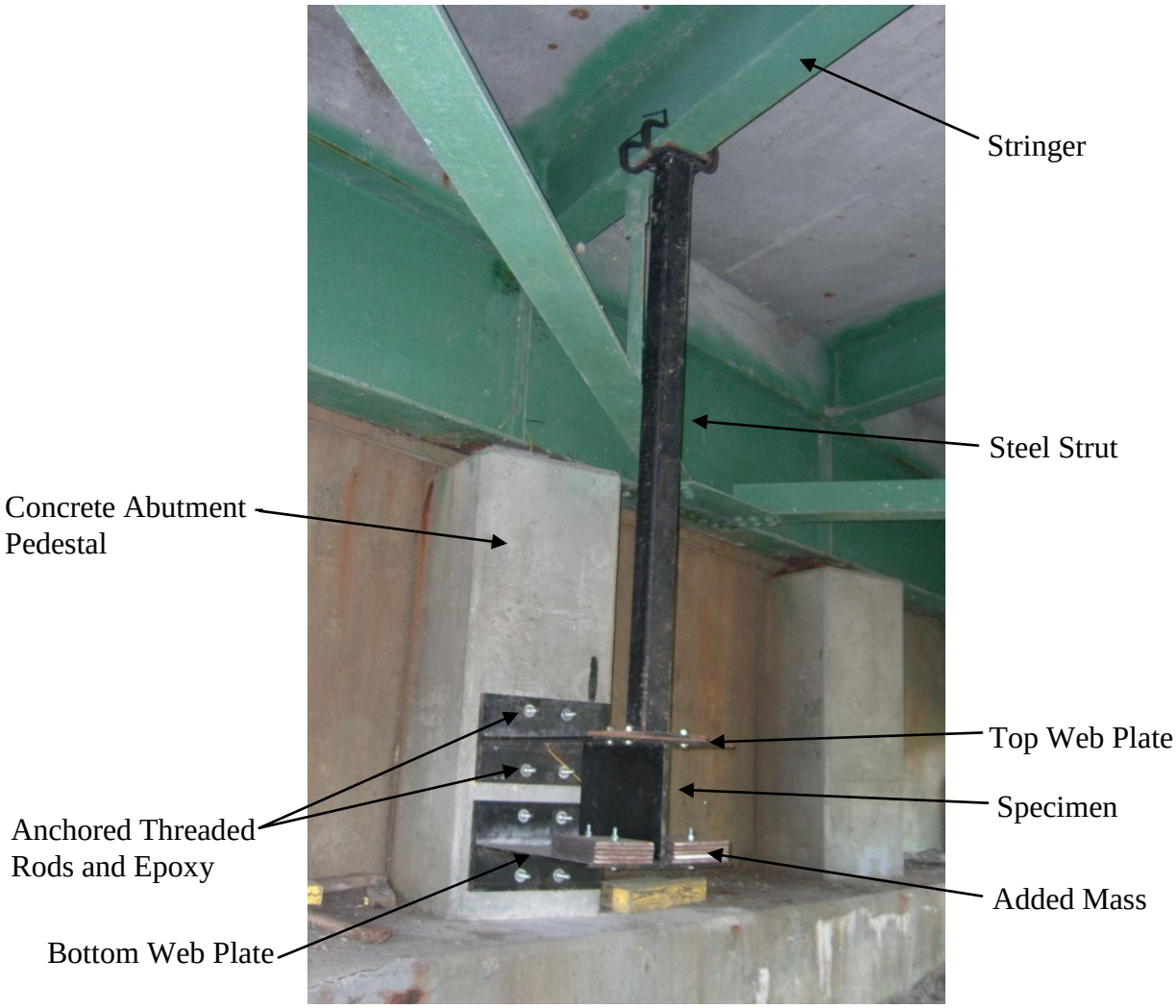

Figure 4.14 Photograph of Typical Installed Sacrificial Specimen

sensor array whereas strains in the bridge web gap were collected using a five-sensor array. As a result the gauges are not measuring strain at exactly the same location in the web gap. As can be seen in Figure 4.15 the shape of the strain curve from the sacrificial specimen generally matches the shape of the strain curve from the US30 bridge. However, the strain range in the sacrificial specimen was consistently observed to be less than that in the bridge. The results of this lead to two conclusions. First, the sacrificial specimen was unlikely to develop a fatigue crack in a "reasonable" time period. Second, it was felt that if damage could be detected in this lower strain range environment the sensitivity in the bridge should be even higher. Further, the strain distribution in the web-gap at a single point in time was evaluated and is shown in Figure 4.16.

www.manaraa.com

The distribution in the sacrificial specimen again matches the shape of that from the US30 bridge. The approximate linear strain variation from negative to positive shows that double curvature bending occurs in both web-gaps.

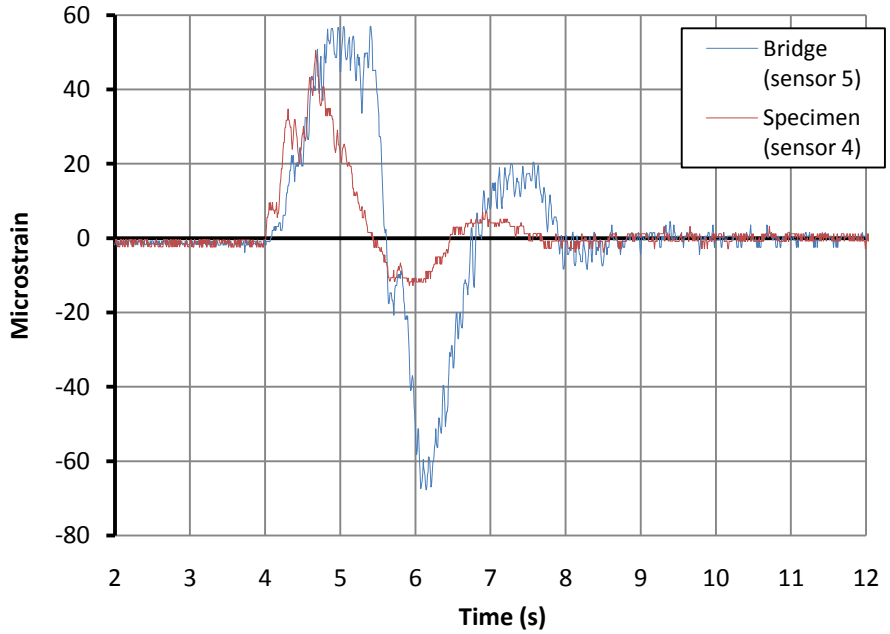

Figure 4.15 Strain Response in Web-Gaps Due to Typical 5-Axle Truck

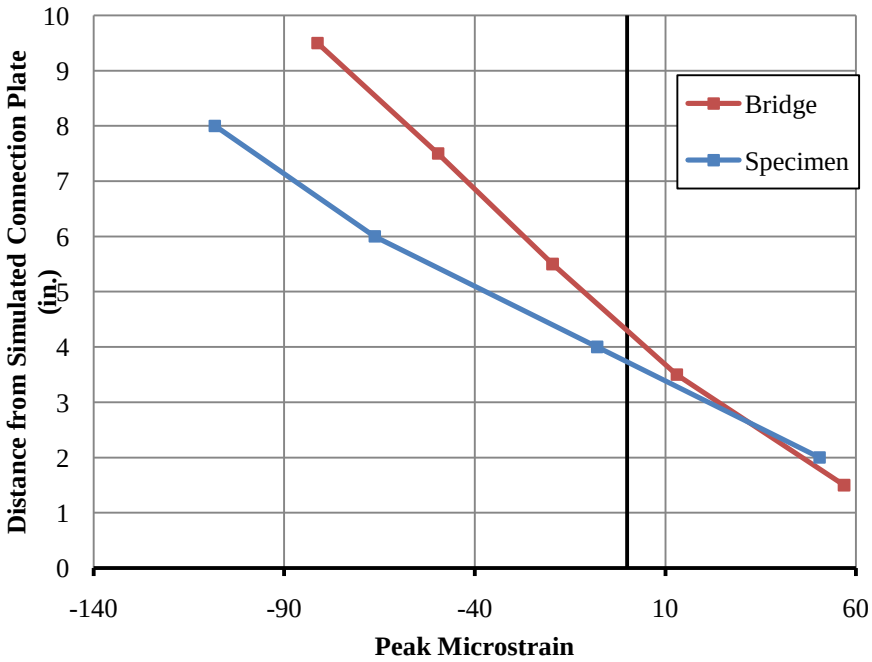

Figure 4.16 Distribution of Strain in Web-Gaps Due to Typical 5-Axle Truck

www.manaraa.com

4.3 Data Collection and Analysis

In order for the damage detection algorithm to detect damaged, data from both the undamaged and damaged structure must be collected. For this experimental verification of the algorithm, damage must be introduced to the sacrificial specimen and not to the US30 bridge. This section details the data collection and the data analysis process.

4.3.1 Data Collection

Baseline data for each undamaged sacrificial specimen and bridge (i.e., training data) were collected for approximately one month. The process for collecting and processing the training data is described in detail in, "A Statistical Based Damage Detection Approach for Highway Bridge Structural Health Monitoring" (Lu 2008) and was summarized in Section 1.1. After training data were collected, the sacrificial specimen was damaged by either creating a fatigue crack or by simulating thickness loss caused by corrosion

4.3.2 . Data Analysis

Once the training data collection is complete, the process of creating prediction models begins. Prediction models plot a best fit line through peak strain values of all combinations of sensor pairs. Additional data are plotted on the prediction models and the vertical distance from the data to the best fit line is calculated and called the residual. The residuals are compiled for each sensor pair in matrices and simplified so each sensor has one vector. These vectors are then used to create control charts, as previously described. The control charts have upper control limits (UCL) and lower control limits (LCL) set by adding and subtracting three times the standard deviation of the data to/from the mean, respectively. In all cases, points outside the control limits are possible indicators of damage. The control charts must be visually analyzed in order to determine the location and severity of the occurring damage.

4.4 Damage Creation Protocols

The first type of damage induced was fatigue cracking. Accelerated fatigue damage was created by subjecting the sacrificial specimen to many cycles of loading using the rotary shaker shown in

www.manaraa.com

Figure 4.17. The rotary shaker is a motor with eccentric weights which rotate at a user specified frequency up to 100 Hz. The rotary shaker may be "dialed in" to the resonant frequency of the attached object to create very large strain values and number of cycles. To accumulate damage quickly, the shaker was bolted to the free end of the sacrificial specimen and then operated near the natural frequency of the sacrificial specimen. This induced high levels of strain at the high rate needed to create fatigue cracks in a relatively short time. Mass was added to the sacrificial specimen as shown in Figure 4.14 to reduce the resonant frequency to within the operable range of the shaker. In general, the rotary shaker was operated in the range of 60 Hz to 70 Hz.

The second type of damage investigated was thickness loss that might result from corrosion. This damage was simulated by removing steel in a discrete area with a hand-held rotary grinder.

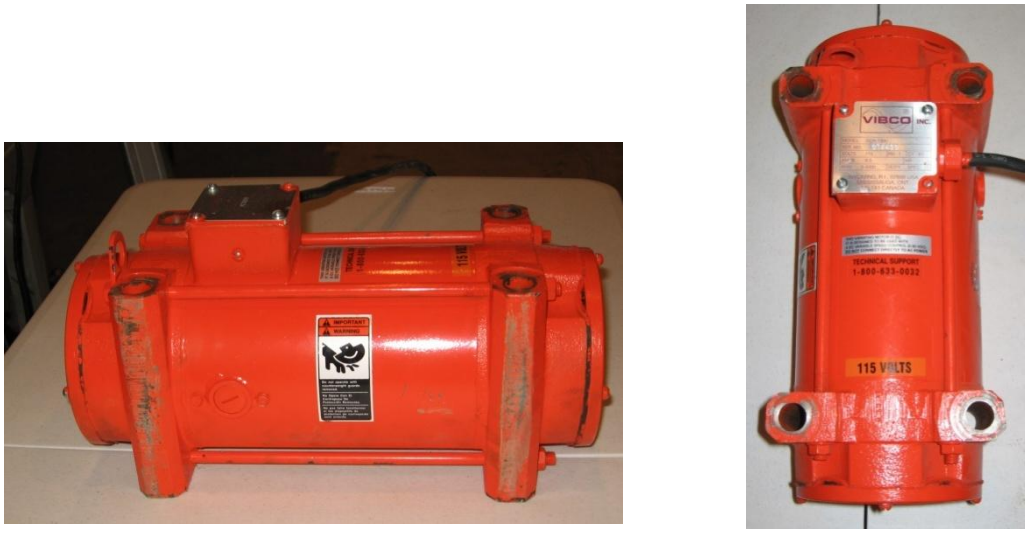

a. Side View b. Top View

Figure 4.17 Photograph of Rotary Shaker

www.manaraa.com

CHAPTER 5. EXPERIMENTAL RESULTS

In this chapter results and discussions related to the training and post-damaged evaluation are presented. A brief statistical analysis of the data for Specimen 2 is also presented and discussed.

5.1 Sacrificial Specimen 1

Sacrificial Specimen 1 was installed at the US30 bridge as shown in Figure 4.14 and undamaged data, called training data, were collected from May 10, 2009 to June 3, 2009. The SHM system being validated in this work only uses heavy, right-lane, 5-axle trucks and among the 5,105 right-lane 5-axle trucks, 2,009 are classified as heavy trucks.

5.1.1 Training prior to Damage

Select control charts for the sensors on the undamaged sacrificial Specimen 1 and for other sensors on the US30 bridge are shown in Figure 5.1. The control charts from other sensor throughout the bridge are generally representative of the remaining bridge sensors. The control charts for sensors B-NG-BF-H and D-SG-BF-H are shown in Figure 5.1e and Figure 5.1f, respectively, and are representative of all girder bottom-flange sensors on the bridge. The control charts for sensors B-SS-BF-H and D-NS-BF-H are shown in Figure 5.1g and Figure 5.1h, respectively, and are representative of all stringer bottom-flange sensors on the bridge. The control charts for sensors C-SG-CB(1)-V, C-SG-CB(5)-V, E-SG-CB(1)-V, and E-SG-CB(5) are shown in Figure 5.1i, j, k, and l, respectively, and are representative of all sensors in the cut-back areas of the bridge. These sensors will be used throughout the remaining sections to provide a means with which to compare the control charts mounted on the specimens. R-sum values (i.e., the difference between predicted and actual strain values, also called residuals) are plotted on the control charts versus Truck Group number. Recall that in this work a truck group size of ten was used. The upper and lower dash-dot lines in Figure 5.1 and all similar figures are called upper control limit (UCL) and lower control limit (LCL), respectively. As described previously the UCL and LCL are the average of the training truck groups plus or minus, respectively, three standard deviations of the training data. The fundamental assumption, then, is that points above the UCL or below the LCL are considered a damage indicator. To test the control limits, 400

www.manaraa.com

heavy truck events were withheld from the training data and used as testing data. The resulting data are similarly shown in Figure 5.1. As can be seen, nearly all points lie between the LCL and UCL indicating that the LCL and UCL have been properly set.

5.1.2 Post-Damage: Damage Detection

After a cumulative time of approximately one hour of vibrating sacrificial Specimen 1 at resonance (as discussed previously) a large crack was observed near the simulated connection plate of the web-gap of both top and bottom web plates. The top and bottom cracked web plates can be seen in Figure 5.2. The cracks were not detected earlier because they did not occur through the fabricated EDM notch and formed quickly. The top plate crack was approximately 7 in. long and the bottom plate crack was approximately 6.5 in. long.

Data were collected from the damaged sacrificial Specimen 1 from August 25, 2009 to September 4, 2009. A total of 2,415 right lane 5-axle trucks were detected, and among them; 860 of the 2,415 were classified as heavy trucks. R-sum values for each sensor were calculated (using a truck group size of ten) and then plotted on the previously constructed control charts (see Figure 5.3).

www.manaraa.com

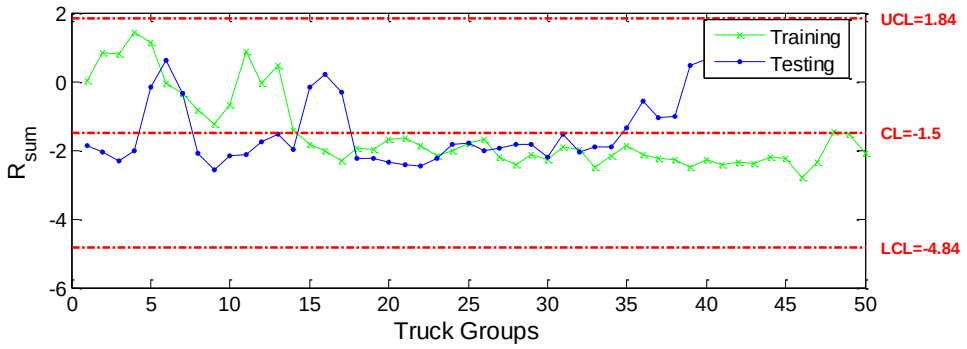

a. Sensor 1

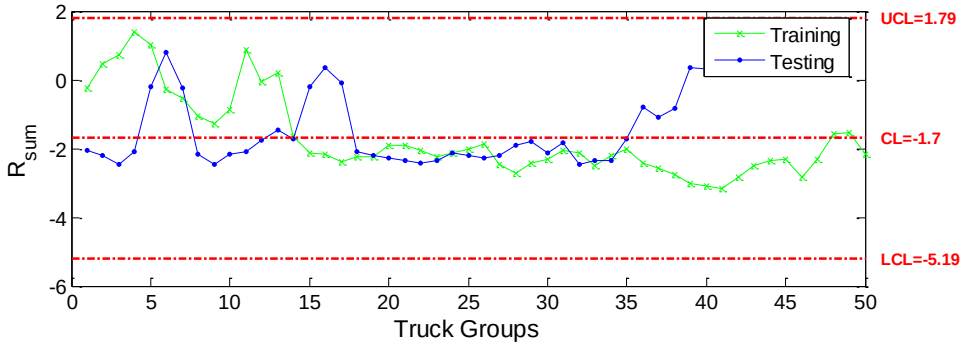

b. Sensor 2

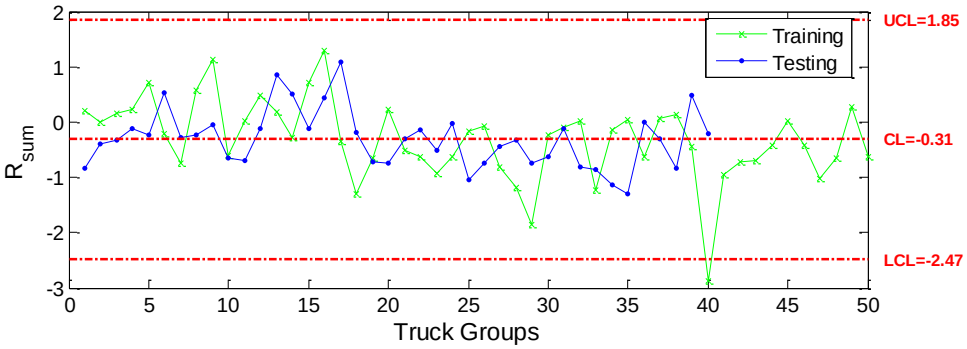

c. Sensor 3

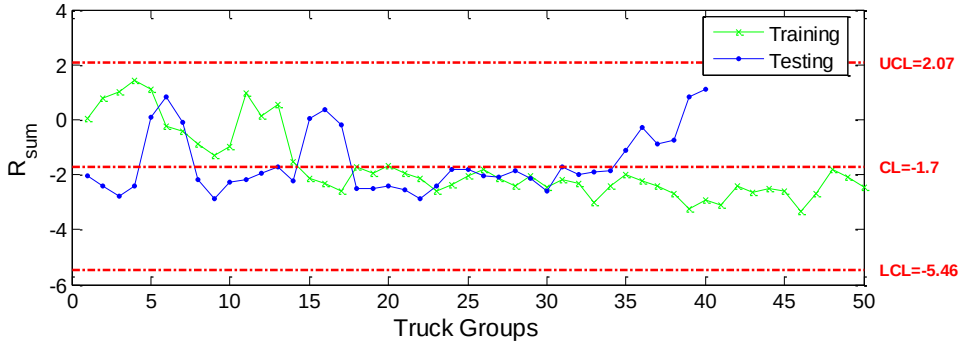

d. Sensor 4

Figure 5.1 Undamaged Sacrificial Specimen 1 Control Charts

www.manaraa.com

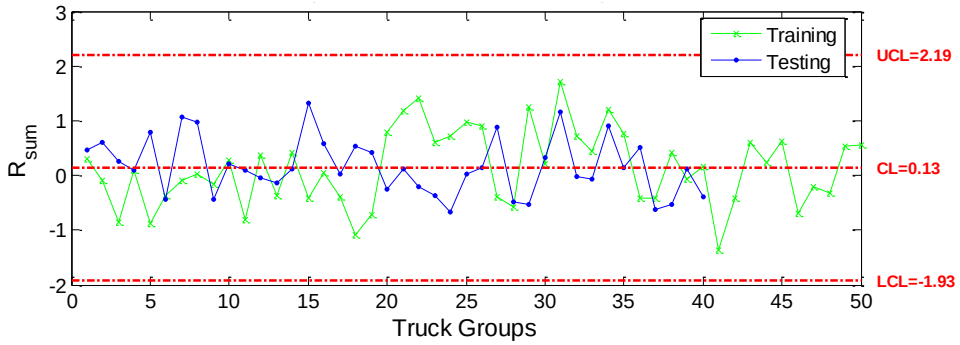

e. B-HG-BF-H

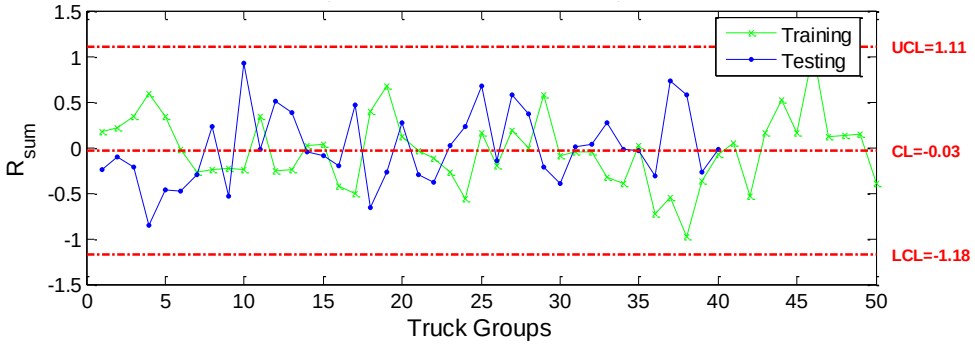

f. D-SG-BF-H

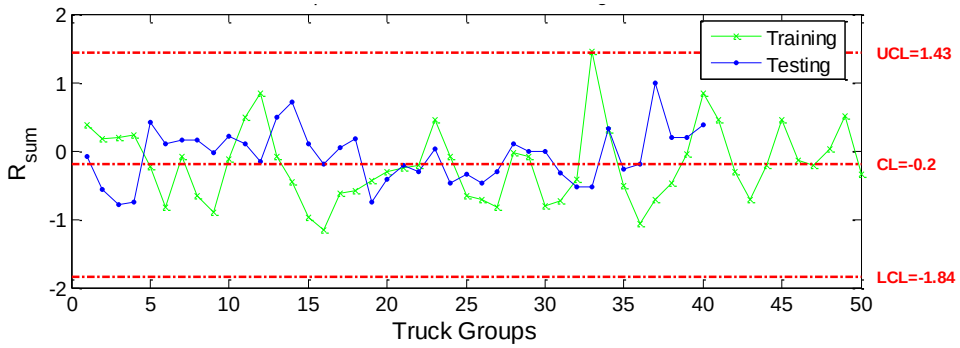

g. B-SS-BF-H

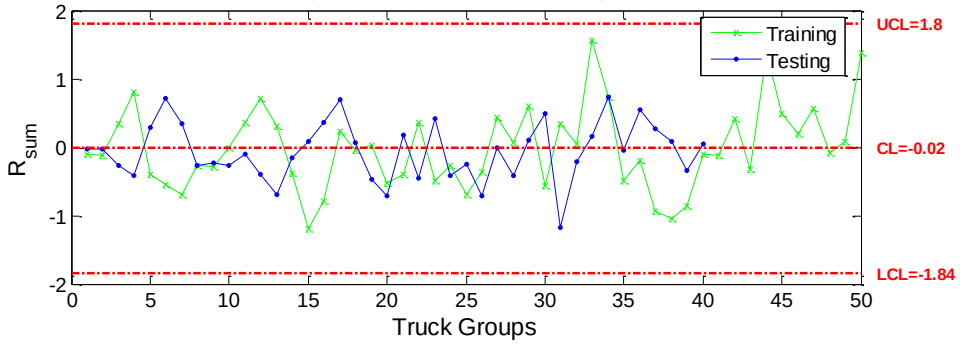

h. D-NS-BF-H

Figure 5.1 continued Undamaged Sacrificial Specimen 1 Control Charts

www.manaraa.com

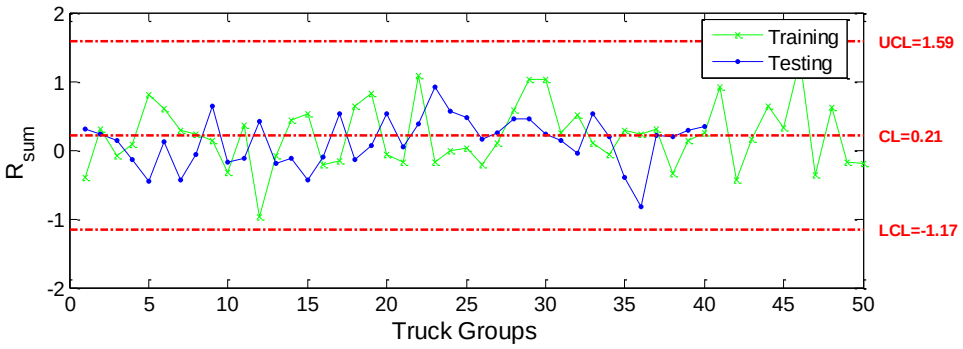

i. C-SG-CB(1)-V

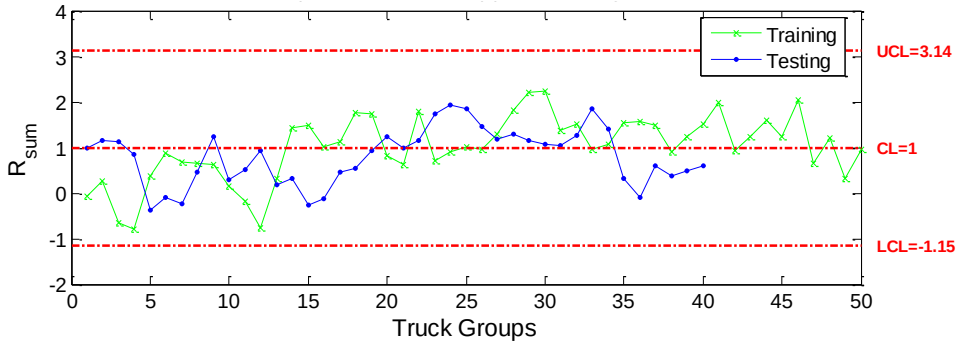

j. C-SG-CB(5)-V

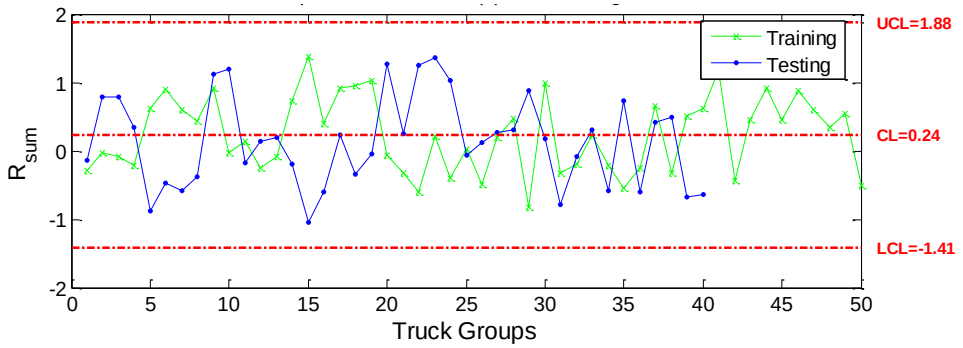

k. E-SG-CG(1)-V

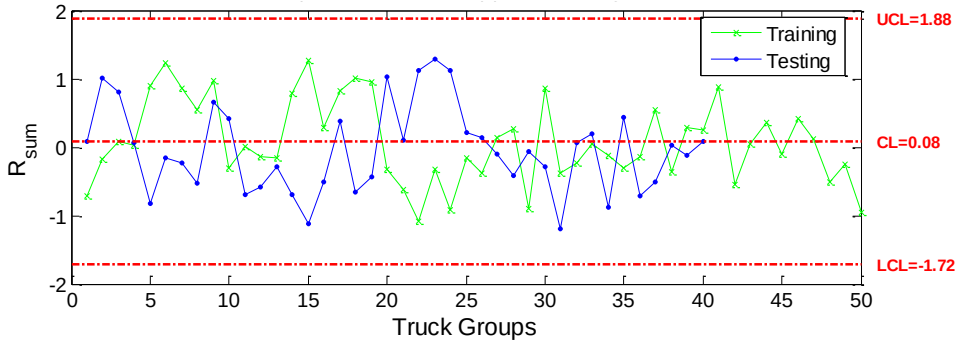

l. E-SG-CB(5)-V

Figure 5.1 continued Undamaged Sacrificial Specimen 1 Control Charts

www.manaraa.com

a. Top web plate cracking

b. Close-up of top web plate cracking

c. Bottom web plate cracking

d. Underside of bottom web plate cracking

Figure 5.2 Photographs of Sacrificial Specimen 1 Cracking

The control limits in each of the charts shown in Figure 5.3 match the control limits shown on the corresponding charts in Figure 5.1. For sensors two, three, and four, all of the R-sum values are outside the control limits indicating damage has been detected. Since the damage is located closest to sensor 4, it was expected that a large amount of points would be outside the control limits; indeed in Figure d all point are outside the control limits. Sensor's 2 and 3 shown in Figure b and c, respectively, also have every point outside the control limits. This fact may be an

www.manaraa.com

indication that the damage that occurred near sensor 4 was quite severe (i.e., the further away damage is detected from the source the more severe the damage).

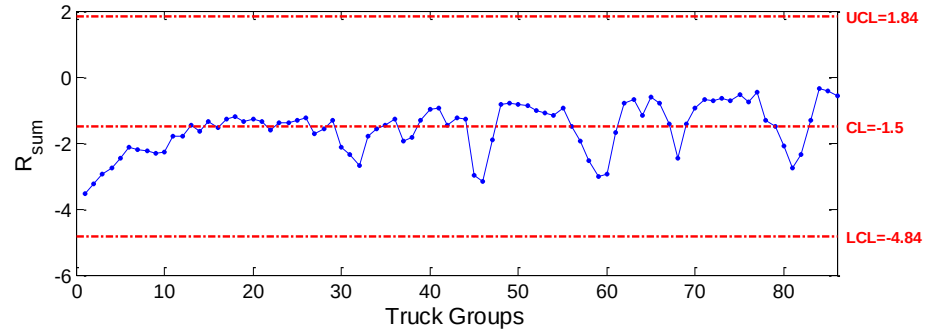

a. Sensor 1

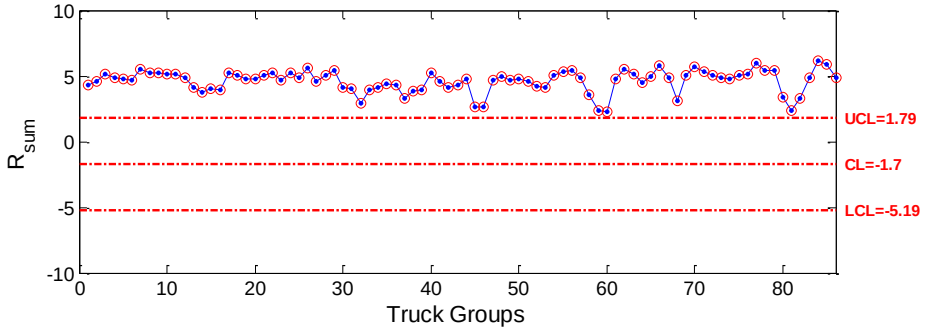

b. Sensor 2

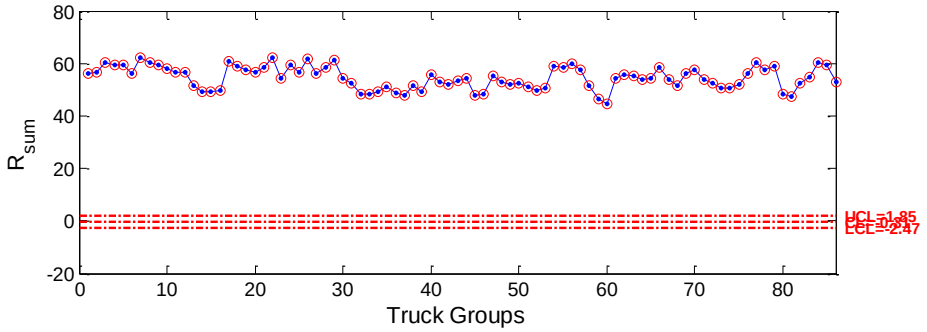

c. Sensor 3

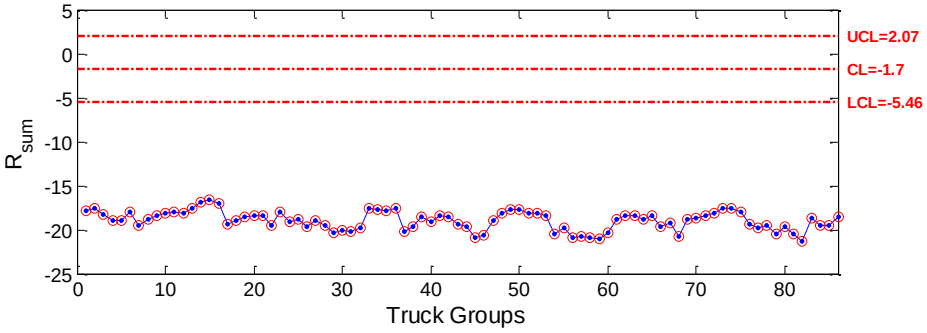

d. Sensor 4

Figure 5.3 Post-Damage Sacrificial Specimen 1 Control Charts

www.manaraa.com

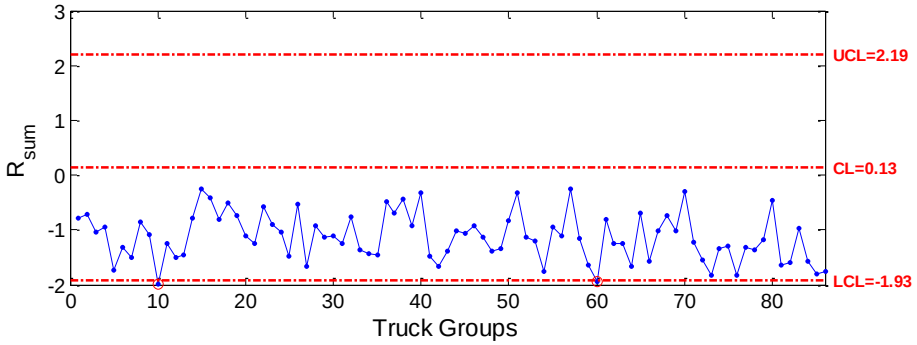

e. B-NG-BF-H

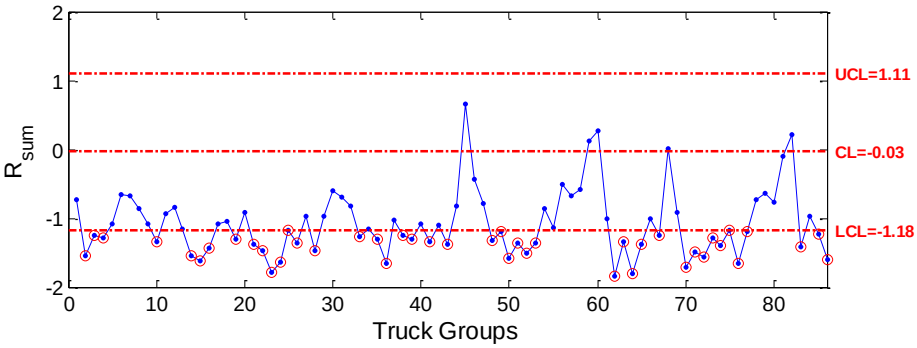

f. D-SG-BF-H

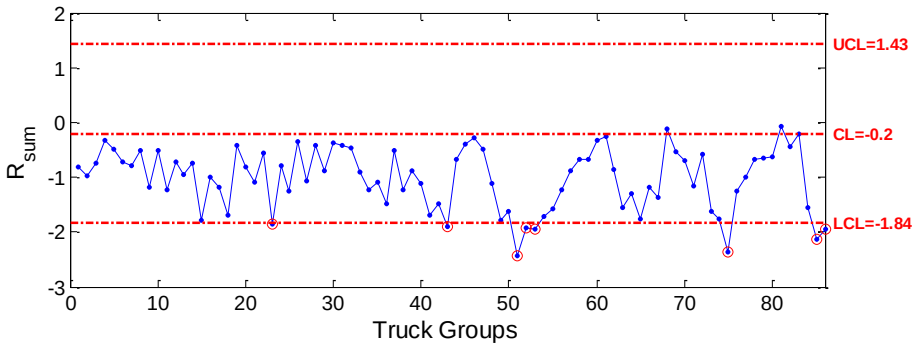

g. B-SS-BF-H

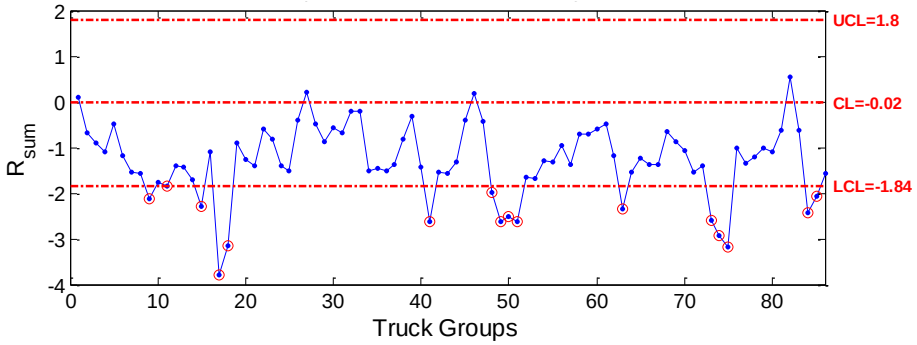

h. D-NS-BF-H

Figure 5.3 continued Post-Damage Sacrificial Specimen 1 Control Charts

www.manaraa.com

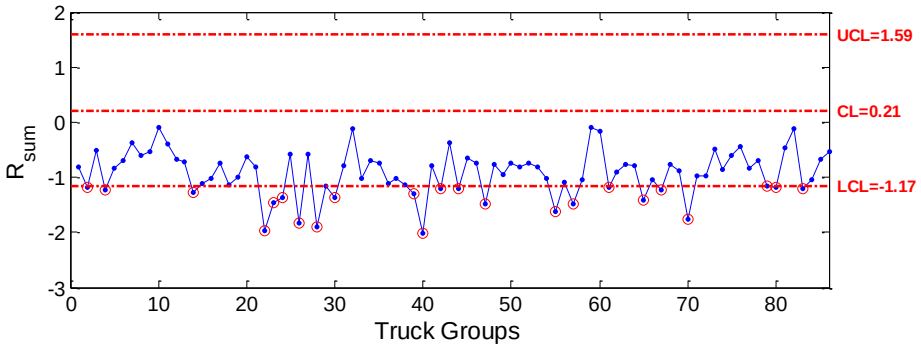

i. C-SG-CB(1)-V

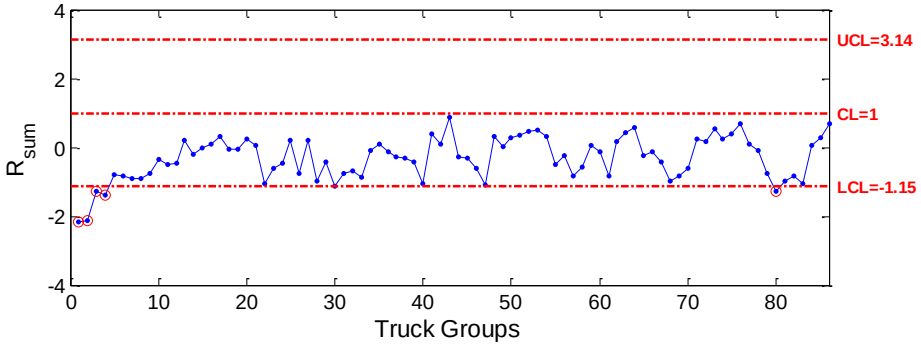

j. C-SG-CB(5)-V

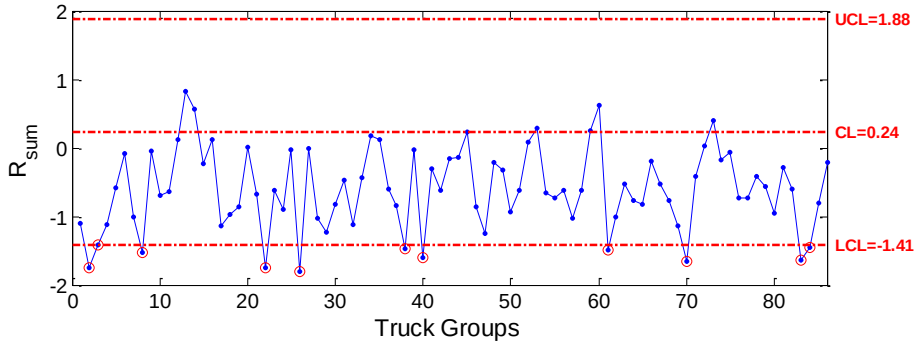

k. E-SG-CB(1)-V

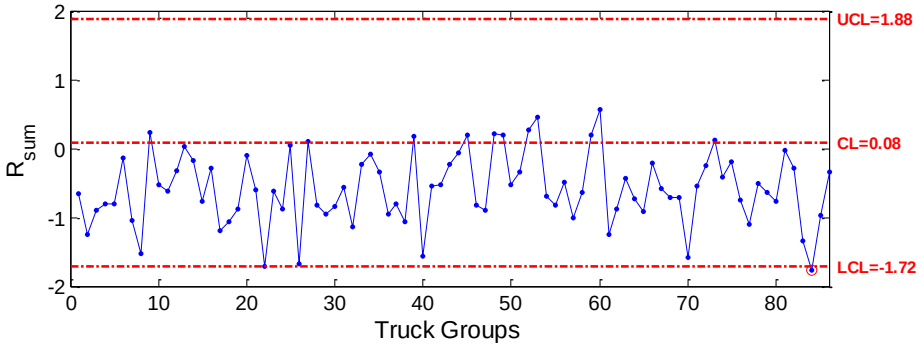

l. E-SG-CB(5)-V

Figure 5.3 continued Post-Damage Sacrificial Specimen 1 Control Charts

www.manaraa.com

In the control charts for the sensors not on Specimen 1 in Figure 5.3e through Figure 5.3l all have at least one point outside the control limits and four (Figure 5.3f, h, i, and k) have a large percentage of points (greater than 10%) outside the control limits. Although this may be an indication of damage near these sensor locations, it was determined through analysis of the data that the control chart results for other sensors on the bridge are influenced by the large indications of damage from the sensors on Specimen 1. Specifically during the row and column-sum calculations needed to create a single control charts for each sensor, the largely skewed values from the sensors on Specimen 1 contribute a larger percentage to the column and row-sum values compared to the values contributed by the other sensors. The contribution of the large values may shift a large percentage of R-sum values outside the control limits as can be seen in Figure 5.3f, h, i, and k. Therefore it was concluded that there was no damage at these locations but rather the R-sum values were skewed due to the contribution of the large R-sum values from the sensor on Specimen 1.

A possible damage severity indicator is the distance the damaged points are away from the average of the training data. For example, in Figure d the R-sum average of the damaged data is roughly negative seventeen, a large distance away from the training data R-sum average of approximately negative two. This large difference in the average also occurs in Figure c and is to be expected.

5.2 Specimen 2

Sacrificial Specimen 2 was installed at the US30 bridge and training data were collected from December 11, 2009 to January 31, 2010. From the collected training data, 3,653 heavy right lane five-axle trucks were detected and used in the control chart construction and false alarm testing.

5.2.1 Training prior to Damage

Control charts for the collected training data from sacrificial Specimen 2 were constructed from 3,653 heavy, right lane, five-axle trucks following the same procedure outlined in Section 5.1.1 and are shown in Figure 5.4. One-thousand truck events were withheld from the training data to be used as testing data and are also shown on the control charts as the blue lines. If the control

www.manaraa.com

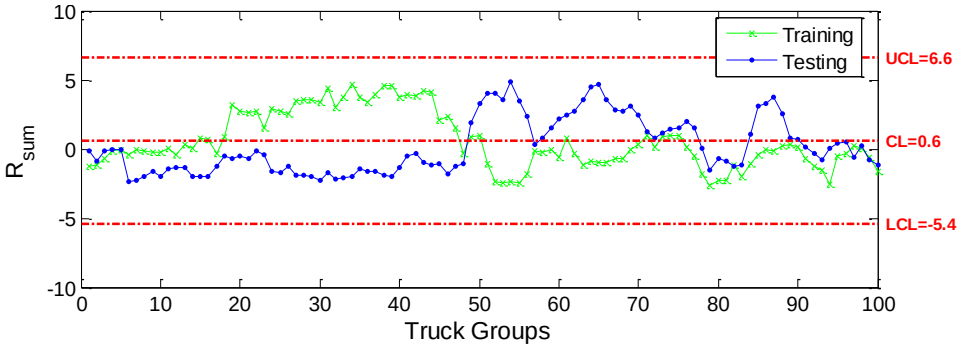

a. Sensor 1

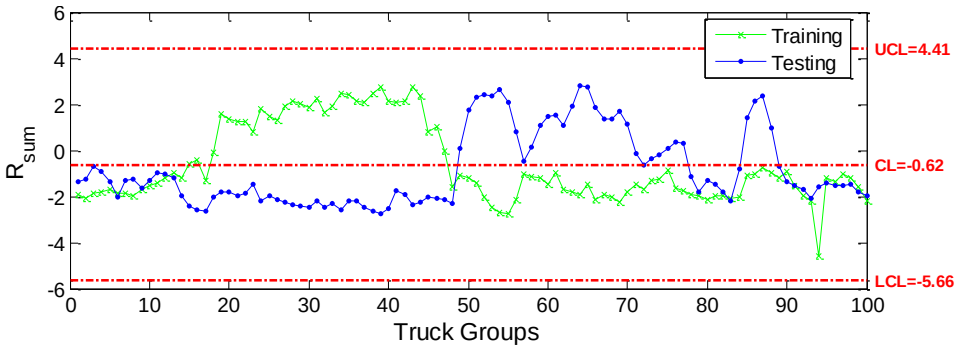

b. Sensor 2

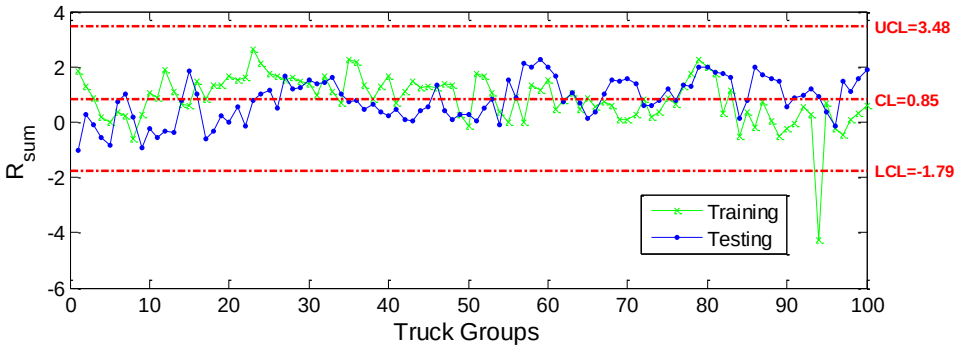

c. Sensor 3

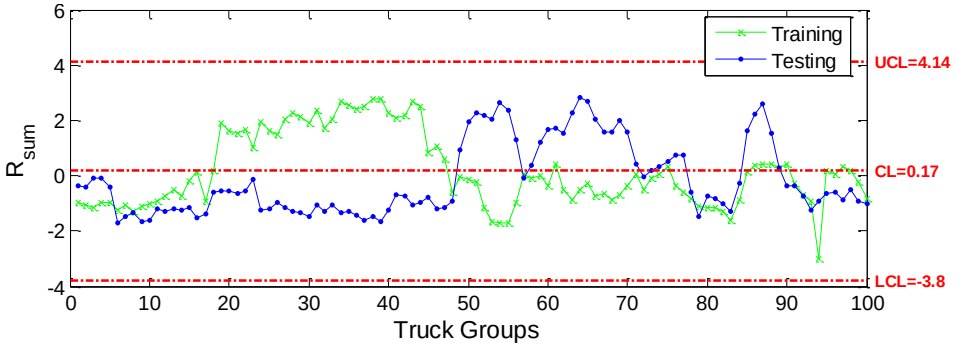

d. Sensor 4

Figure 5.4 Undamaged Sacrificial Specimen 2 Control Charts

www.manaraa.com

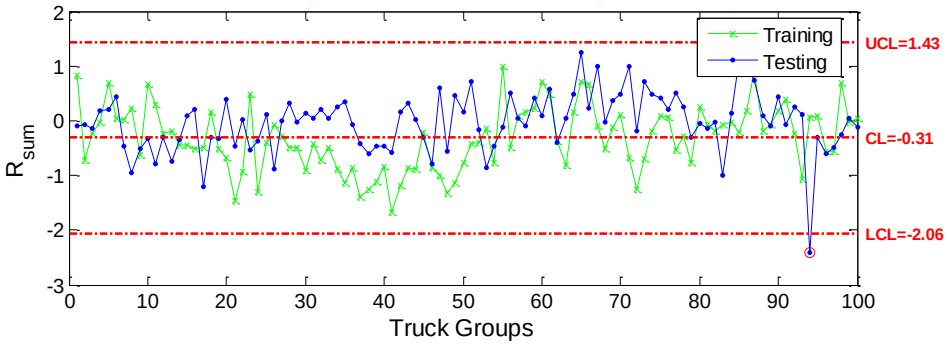

e. B-NG-BF-H

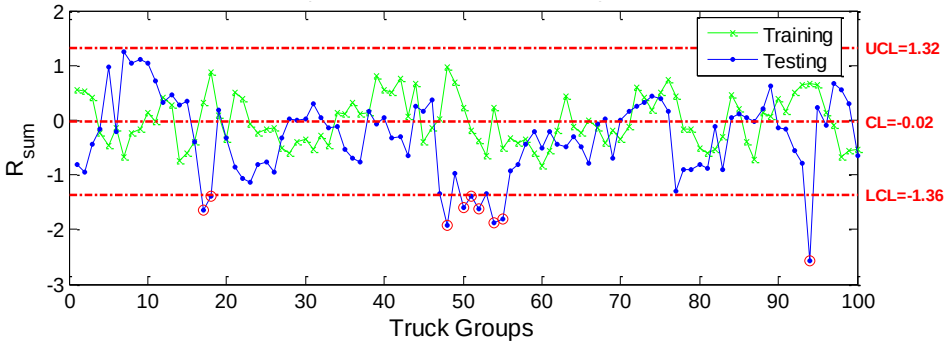

f. D-SG-BF-H

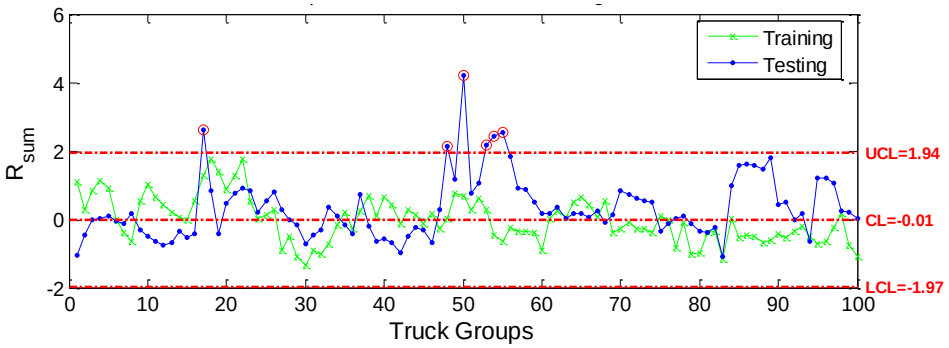

g. B-SS-BF-H

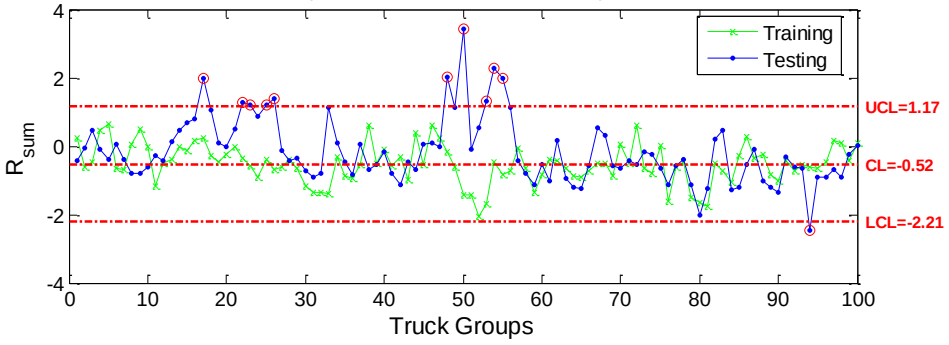

h. D-NS-BF-H

Figure 5.4 continued Undamaged Sacrificial Specimen 2 Control Charts

www.manaraa.com

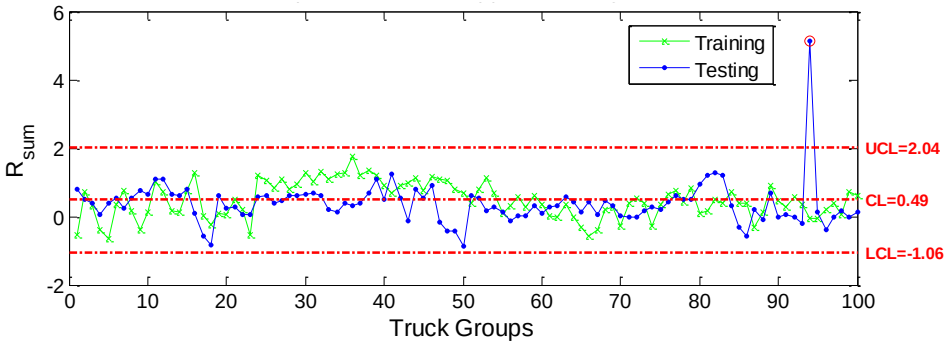

i. C-SG-CB(1)-V

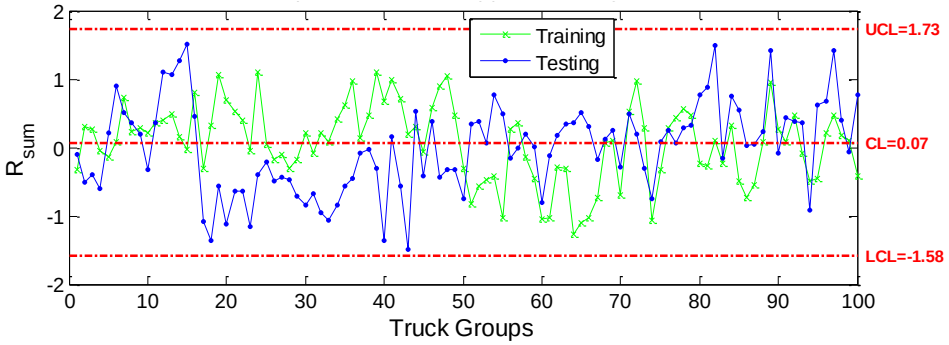

j. C-SG-CB(5)-V

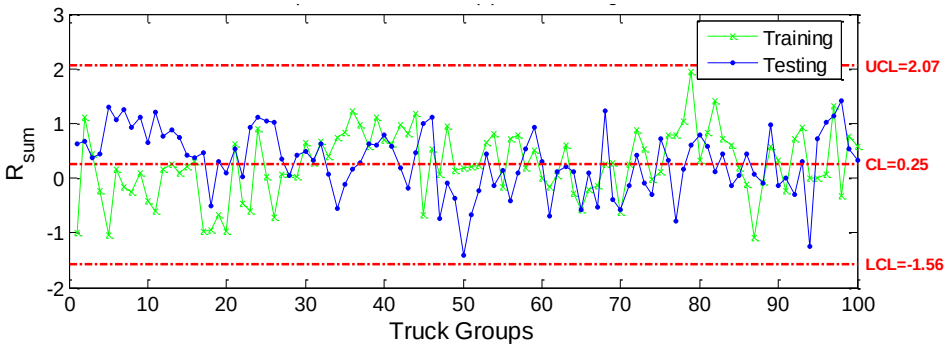

k. E-SG-CB(1)-V

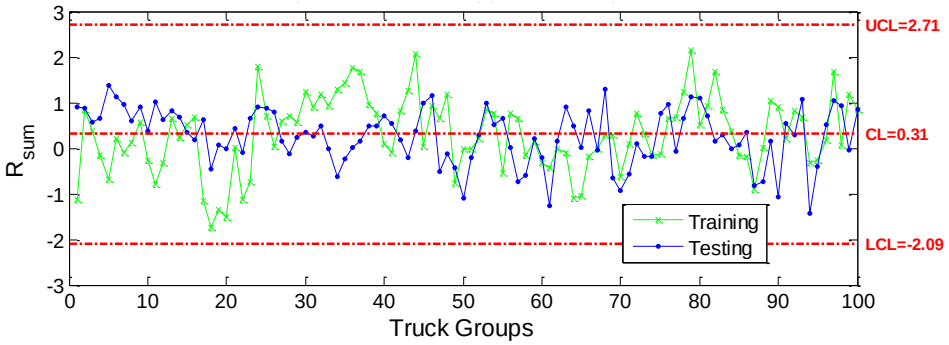

l. E-SG-CB(5)-V

Figure 5.4 continued Undamaged Sacrificial Specimen 2 Control Charts

www.manaraa.com

charts were constructed correctly very few, if any, points should fall outside the control limits for the undamaged structure (e.g., no more than 1%). As can be seen multiple points are below the LCL in Figure 5.4c, f, g, and h and may be due to natural variability in the data, an overweight or unusual truck passing over the US30 bridge, be an indicator of unknown damage, may be a false-positive, or may represent a flaw in the methodology. All of the testing data follow the average established by the training data and display the characteristics of an undamaged structure.

5.2.2 Post-Damage: Damage Detection

To study different levels of damage occurring in the web-gap area, different crack sizes were produced in specimen 2. After each propagation of the crack to a larger size,damage data were collected and control charts produced. The procedure and results pertaining to each crack size is described in the paragraphs below.

On February 16, 2010 sacrificial Specimen 2 was vibrated at an average resonant frequency of 66 Hz for approximately 18 minutes (71,000 cycles) before a crack occurred. The crack was approximately 1.25 in. long and occurred in Region 4 of the top web plate (similar to the cracking of sacrificial Specimen 1). The cracking is shown in Figure 5.5.

Data were then collected from the damaged sacrificial Specimen 2 from February 16, 2010 to February 23, 2010 and a total of 627 heavy right lane five-axle trucks were detected. The control charts for sacrificial Specimen 2 with the 1.25 in. crack are shown in Figure 5.6. The control limits for each sensor in Figure 5.6 match the control limits for each sensor in Figure 5.4. The R-sum data for Sensor Four (i.e., the sensor closest to the crack) are below the LCL thus, indicating damage detection. In Figure 5.6a, b, and c there are no R-sum data outside the control limits which is an indication that the damage that occurred closest to sensor 4 is not severe enough to cause a change in behavior at these locations. Note, however, for sensors 1, 2, and 3 the R-sum data moved slightly downward following the trend shown in Figure 5.6d. As the damage becomes more severe, it is thought that these R-sum data will continue to shift until all data points are out of the control limits.

www.manaraa.com

a. Overview of Top Web-Plate Cracking

b. Top Web-Plate Cracking

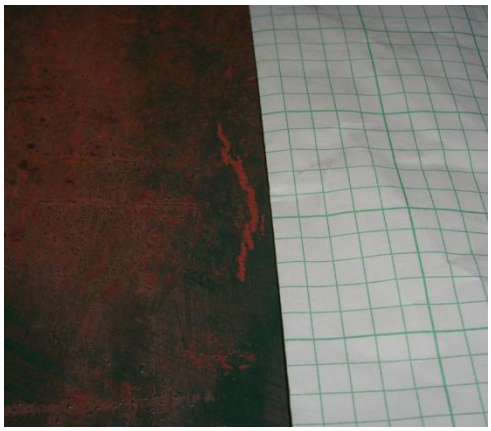

c. Close-Up of Crack

Figure 5.5 Photographs of Specimen 2 Top Web Plate Cracking of Sacrificial

Also noticeable in Figure 5.6f and Figure 5.6h are the higher percentage of R-sum values outside of the control limits. In Figure 5.6f, 14.5% of the R-sum values are outside of the control limits and in Figure 5.6h, 8.1% of the R-sum values are outside of the control limits. As discussed earlier, this may be due to the large values provided by the sensors on Specimen 2 which may shift multiple R-sum values outside the control limits even though damage may not be present at those other locations. The typical unidirectional shift in R-sum values was not observed for sensor D-SG-BF-H in Figure 5.6f. This figure shows multiple R-sum values outside both the upper and lower control limits. Even though a distinct shift in the R-sum values is not present, the cause of the R-sum values outside of the control limits may still be the inclusion of the

www.manaraa.com

larger-than-average Specimen 2 sensor residuals in the column and row-sum calculations.

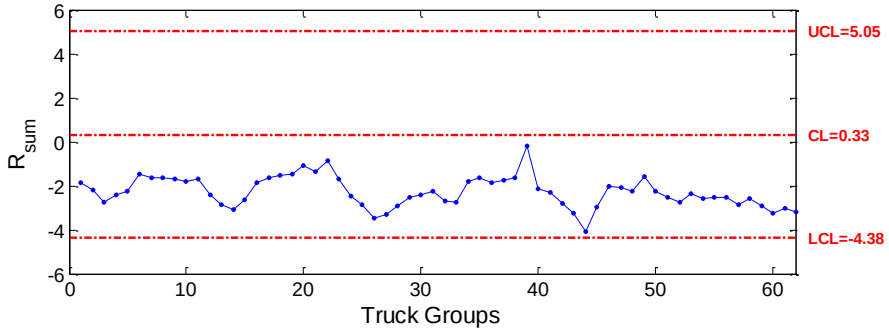

a. Sensor 1

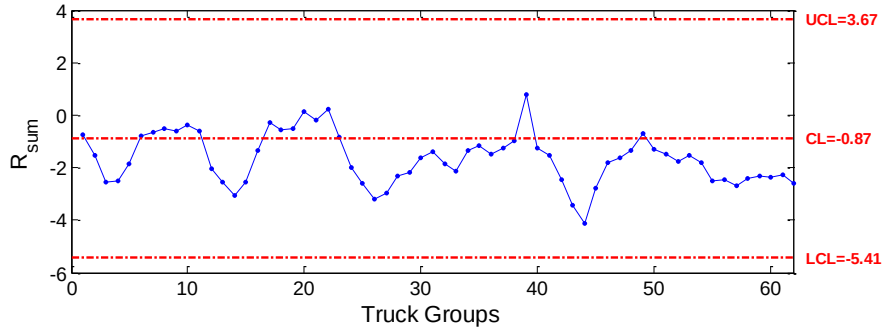

b. Sensor 2

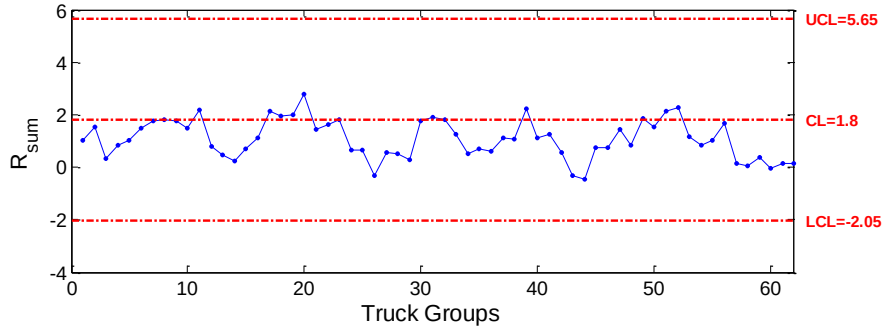

c. Sensor 3

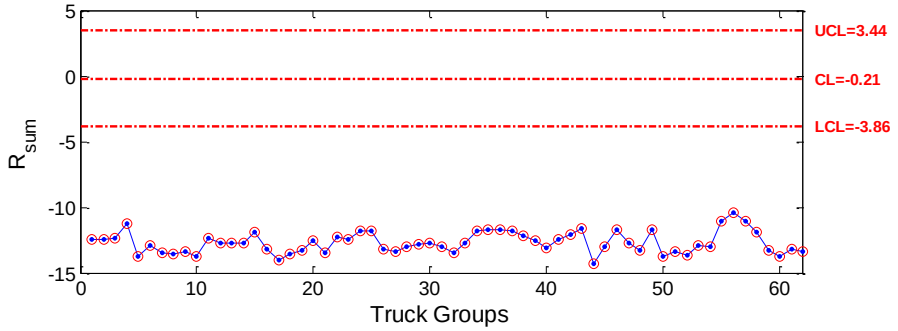

d. Sensor 4

Figure 5.6 Post-Damage Sacrificial Specimen 2 Control Charts (1.25 in. crack)

www.manaraa.com

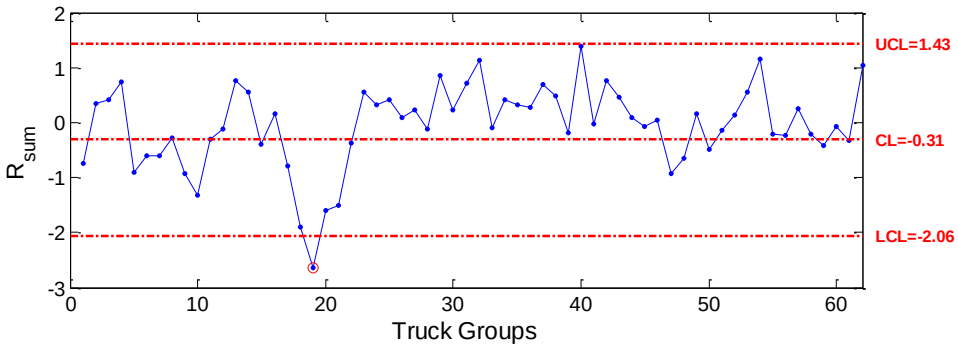

e. B-NG-BF-H

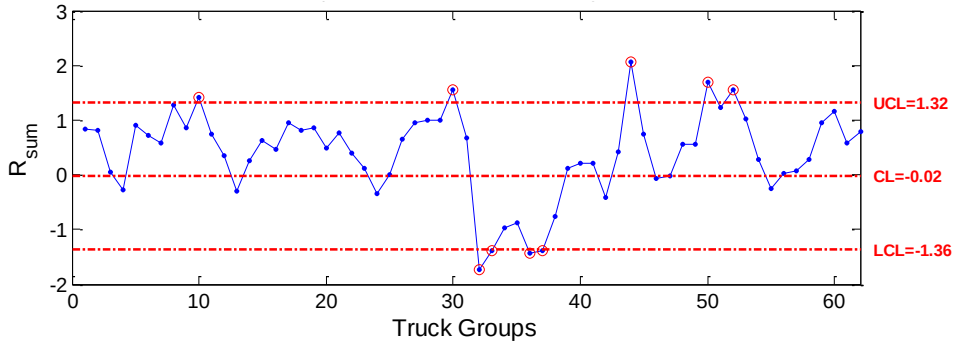

f. D-SG-BF-H

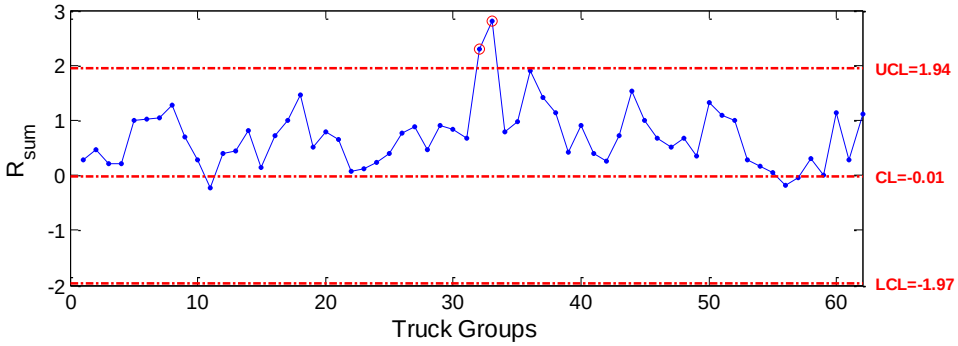

g. B-SS-BF-H

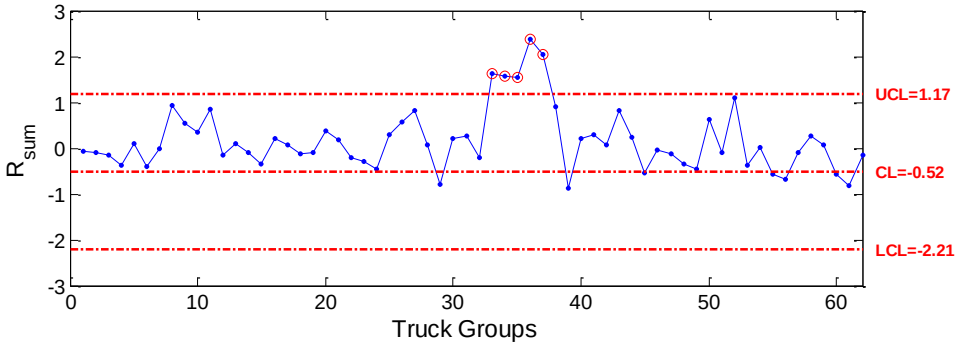

h. D-NS-BF-H

Figure 5.6 continued Post-Damage Sacrificial Specimen 2 Control Charts (1.25 in. crack)

www.manaraa.com

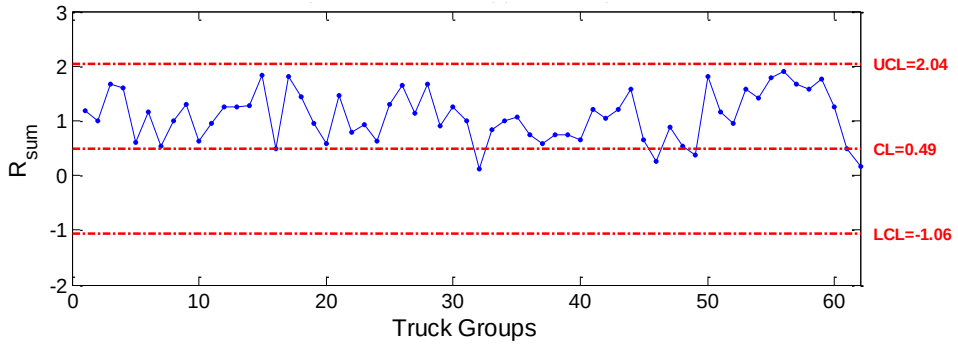

i. C-SG-CB(1)-V

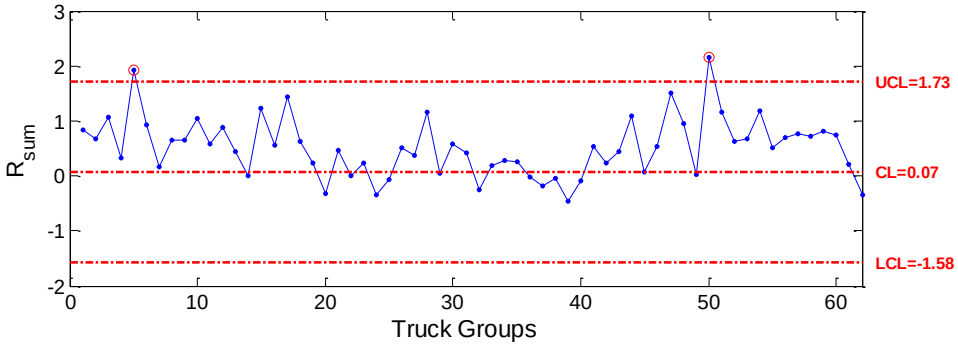

j. C-SG-CB(5)-V

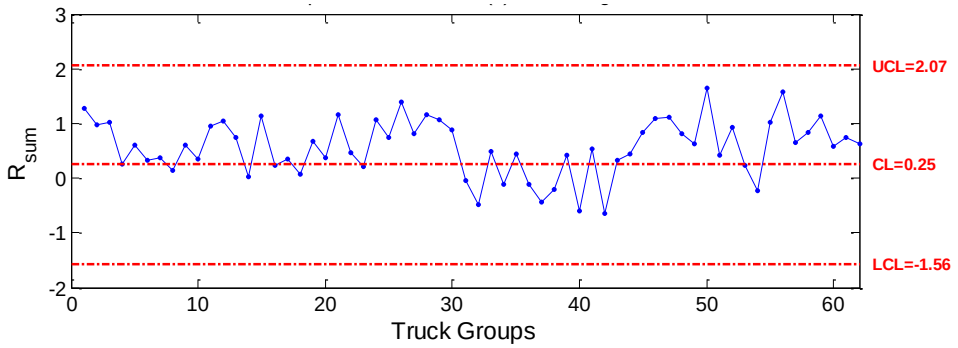

k. E-SG-CB(1)-V

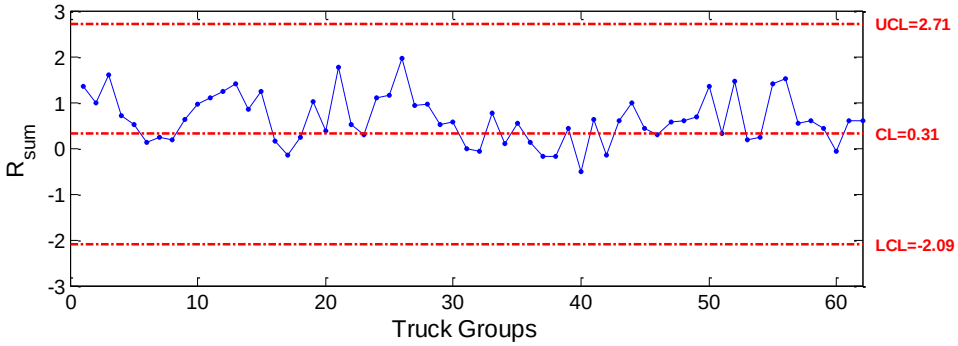

l. E-SG-CB(5)-V

Figure 5.6 continued Post-Damage Sacrificial Specimen 2 Control Charts (1.25 in. crack)

www.manaraa.com

On March 5, 2010 sacrificial Specimen 2 was vibrated at an average resonant frequency of 63 Hz for approximately 2 minutes (6,600 cycles) to extend the crack from 1.25 in. to 1.50 in. long. Data were then collected from March 6, 2010 to March 12, 2010 and a total of 551 heavy, 5-axle, right-lane trucks were detected.

For comparison to the undamaged state, the control limits in Figure 5.7 match the control limits for in Figure 5.4. As with the 1.25 in. crack condition the data points for sensor 4 are again below the LCL indicating damage. A few R-sum data from sensors two and three, as shown in Figure 5.7b and Figure 5.7c, are above the upper control limit (UCL). This suggests that with increasing damage severity the damage can be detected with sensors located further away. It is not fully understood why in Figure 5.6 the trend for sensors 2 and 3 was toward the LCL and in Figure 5.7 the trend is toward the UCL. It is speculated that experimental procedures may be the source. The control charts for the additional sensors in Figure 5.7e through Figure 5.7l show very few R-sum values outside the control limits indicating that no damage has occurred near these sensor locations. The control chart for sensor B-NG-BF-H (Figure 5.7e) shows five R-sum values above the control limits (9.1%). This may again be due to the skewed values of the column and row-sum calculations discussed previously.

On April 1, 2010 sacrificial Specimen 2 was vibrated at an average resonant frequency of 73 Hz for approximately 3.25 minutes (14,400 cycles) to extend the crack from 1.50 in. to 1.75 in. long. Data were collected from April 2, 2010 to April 16, 2010 and a total of 952 5-alxe, heavy, right-lane trucks were detected.

The control charts corresponding to the 1.75 in. crack are shown in Figure 5.8. All of the data points for sensors 3 and 4 are below their respective LCLs again indicating damage detection. The data point trends for sensors 1 and 2 (Figure 5.8a and Figure 5.8b) both shifted down opposite of the results from the 1.50 in. crack but similar to those for the 1.25 in. crack. This shift could be due to slightly differing loading conditions from placing the load transferring vertical strut in a different location than it was previously but does not have any adverse affects on the damage identifying capabilities of the control charts.

www.manaraa.com

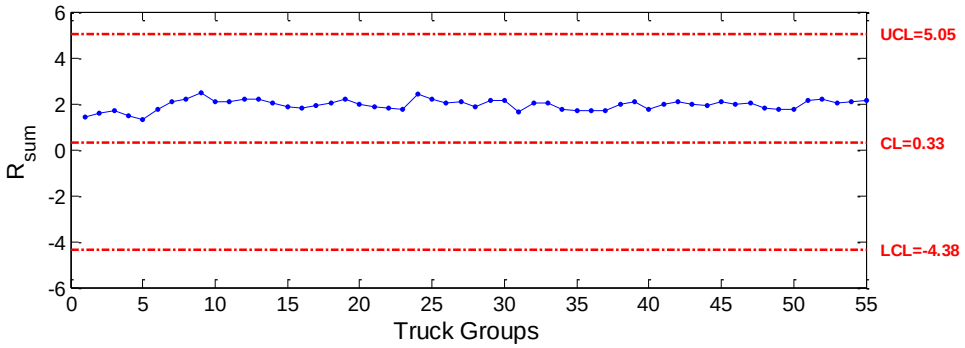

a. Sensor 1

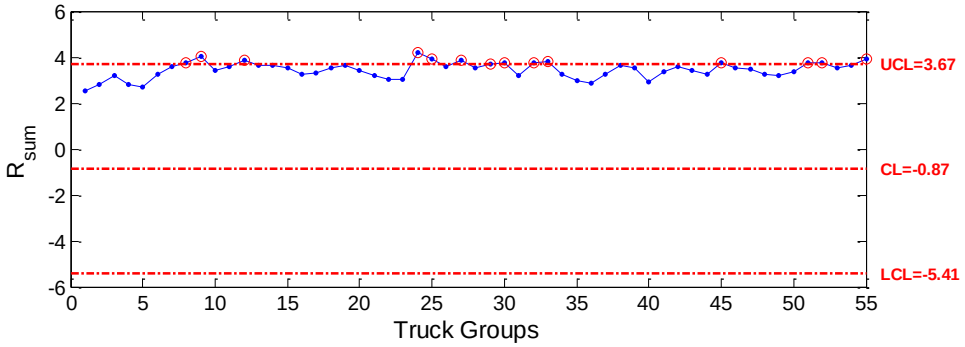

b. Sensor 2

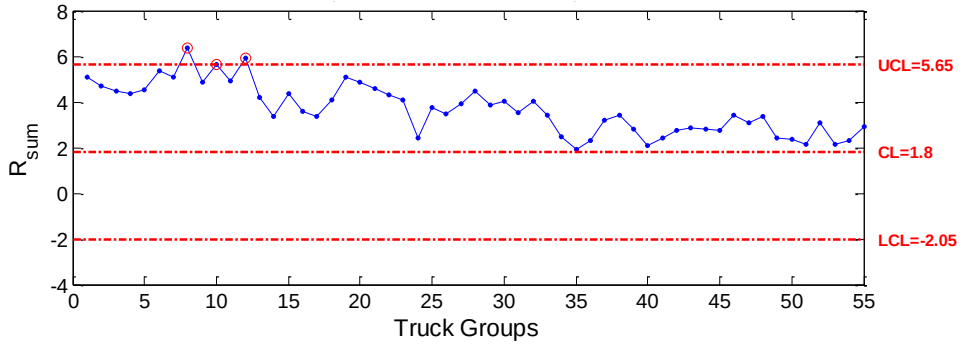

c. Sensor 3

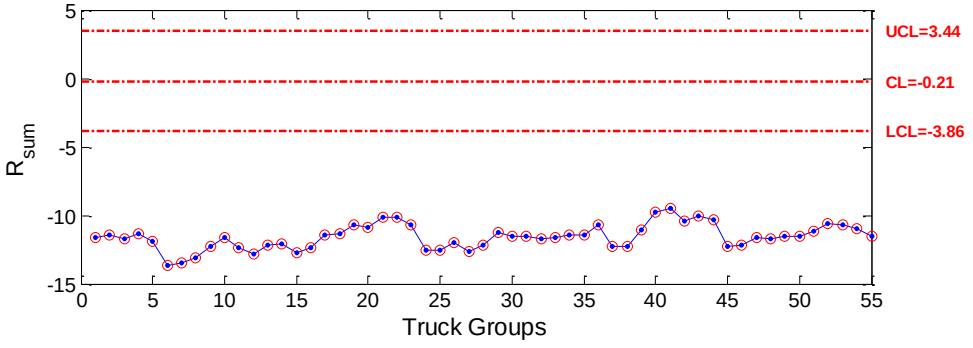

d. Sensor 4

Figure 5.7 Post-Damage Sacrificial Specimen 2 Control Charts (1.50 in. crack)

www.manaraa.com

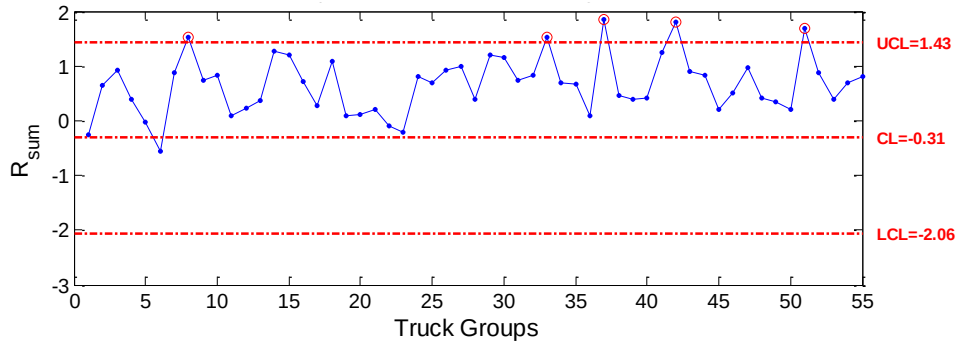

e. B-NG-BF-H

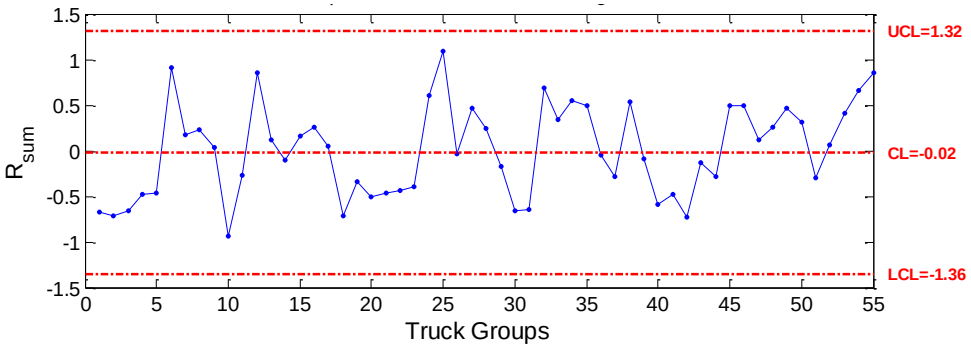

f. D-SG-BF-H

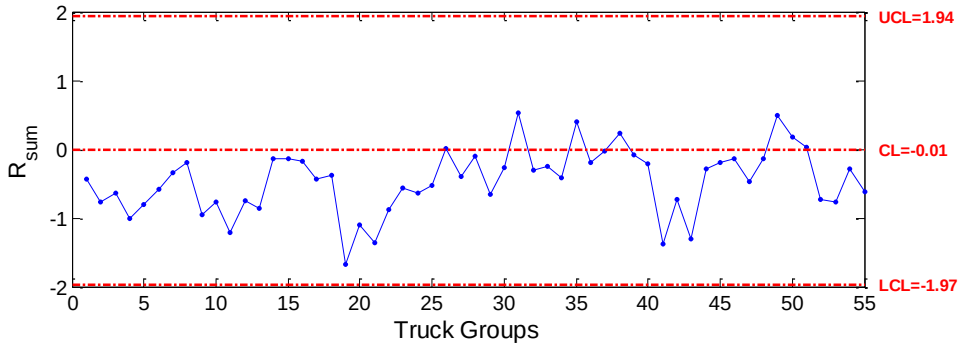

g. B-SS-BF-H

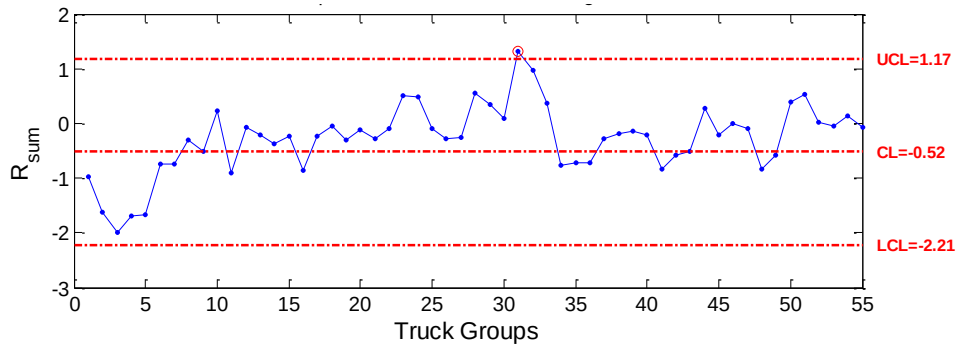

h. D-NS-BF-H

Figure 5.7 continued Post-Damage Sacrificial Specimen 2 Control Charts (1.50 in. crack)

www.manaraa.com

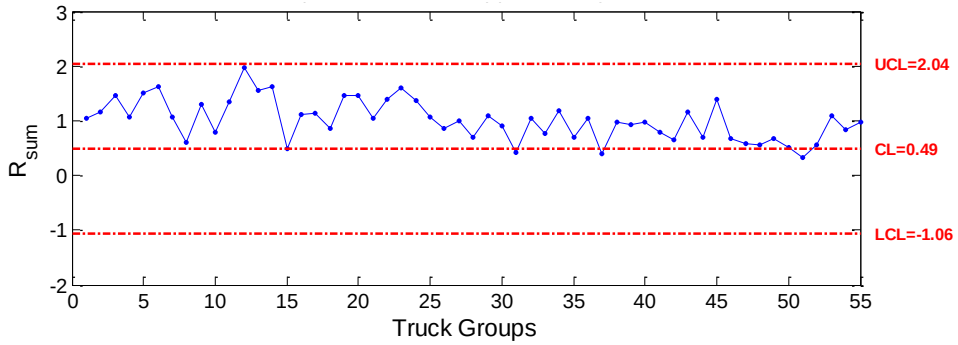

i. C-SG-CB(1)-V

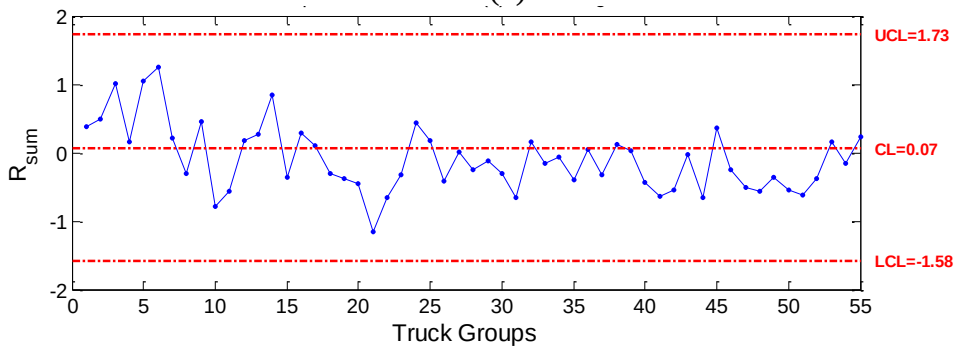

j. C-SG-CB(5)-V

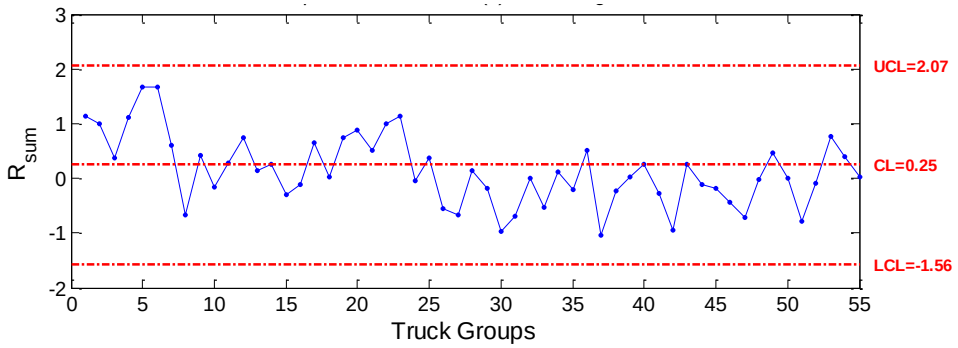

k. E-SG-CB(1)-V

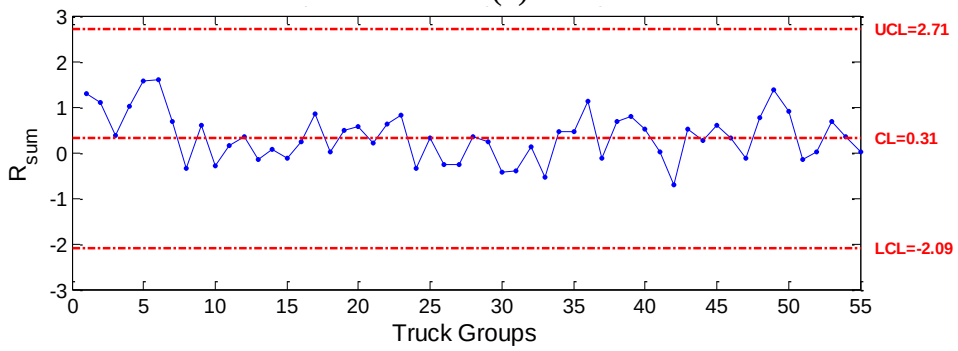

l. E-SG-CB(5)-V

Figure 5.7 continued Post-Damage Sacrificial Specimen 2 Control Charts (1.50 in. crack)

www.manaraa.com

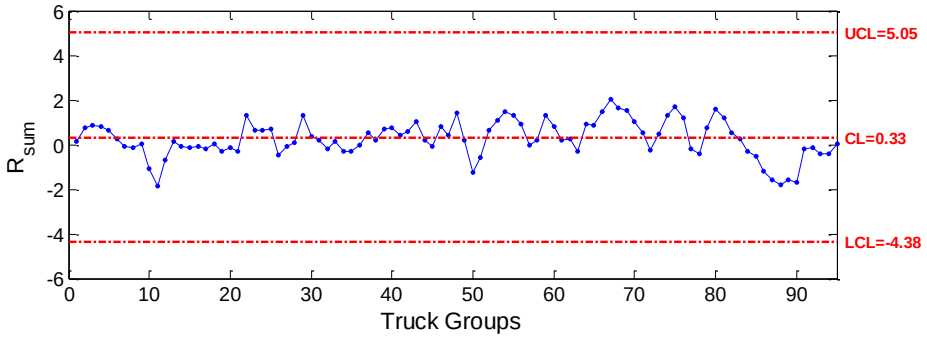

a. Sensor 1

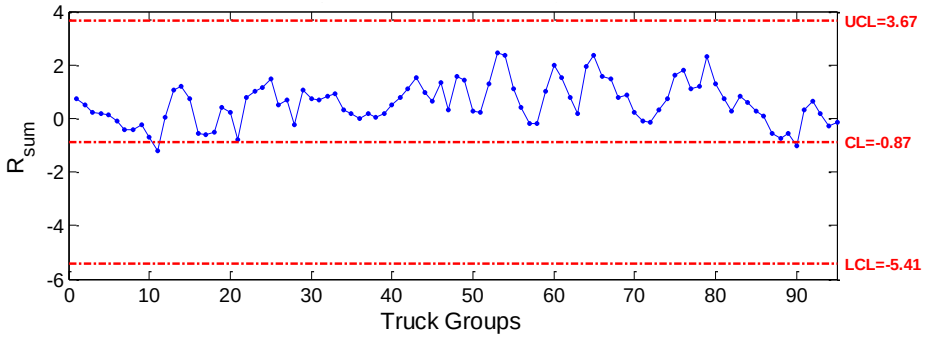

b. Sensor 2

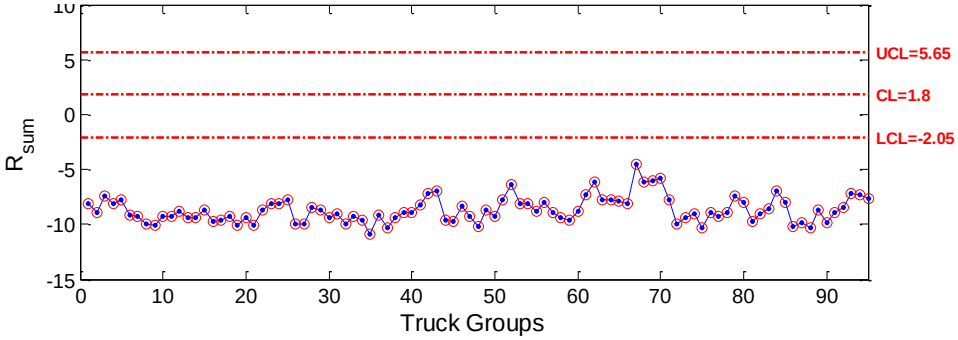

c. Sensor 3

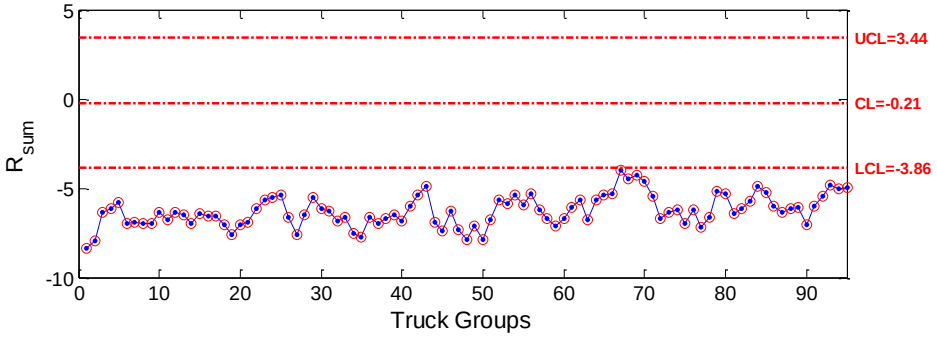

d. Sensor 4

Figure 5.8 Post-Damage Sacrificial Specimen 2 Control Charts (1.75 in. crack)

www.manaraa.com

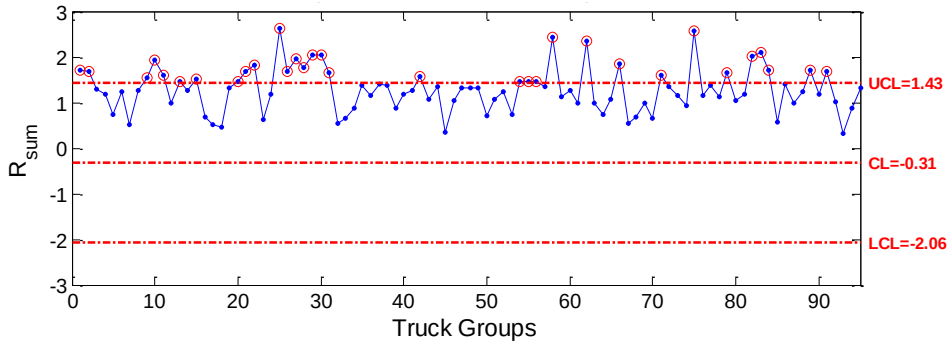

e. B-NG-BF-H

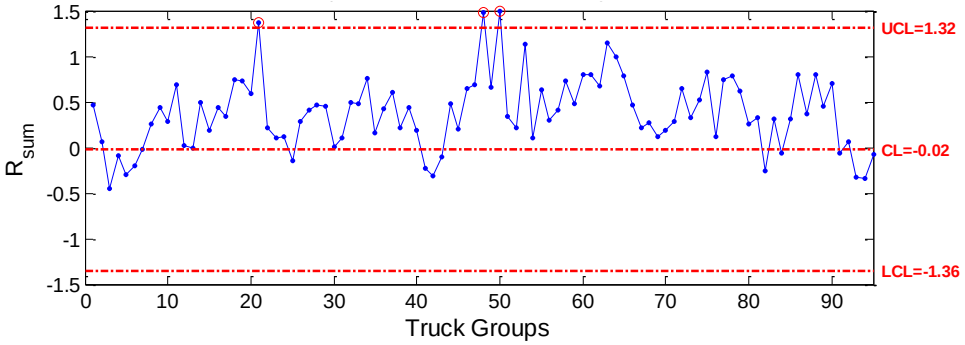

f. D-SG-BF-H

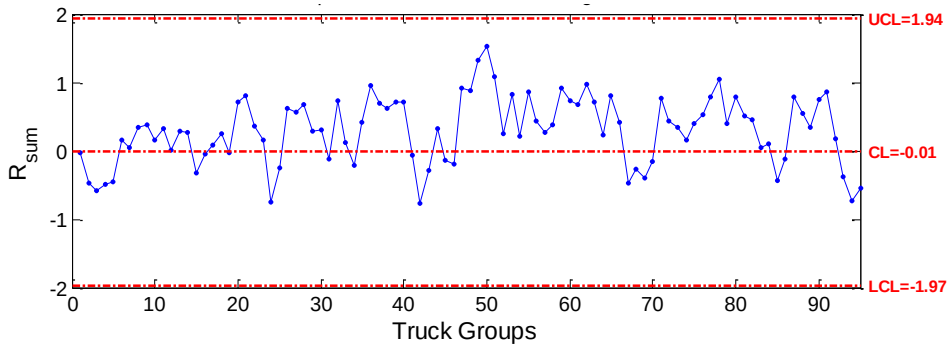

g. B-SS-BF-H

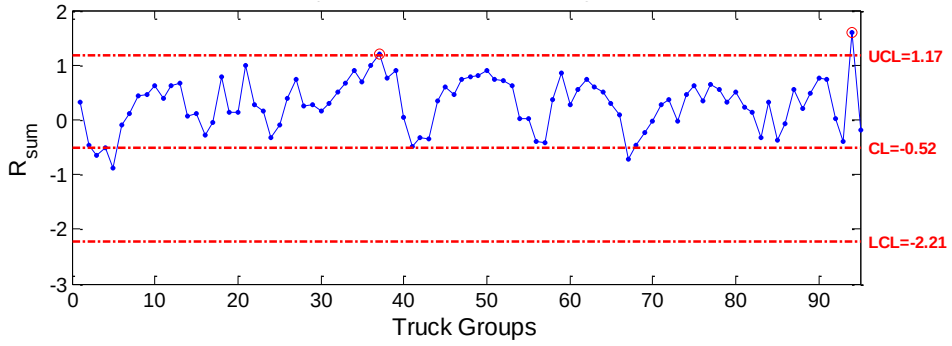

h. D-NS-BF-H

Figure 5.8 continued Post-Damage Sacrificial Specimen 2 Control Charts (1.75 in. crack)

www.manaraa.com

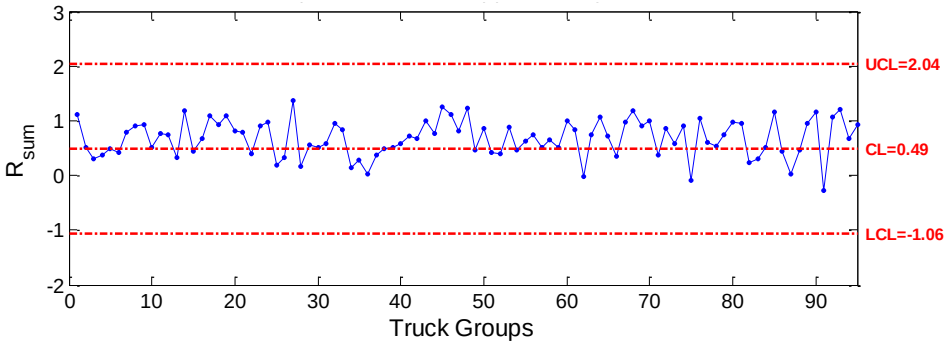

i. C-SG-CG(1)-V

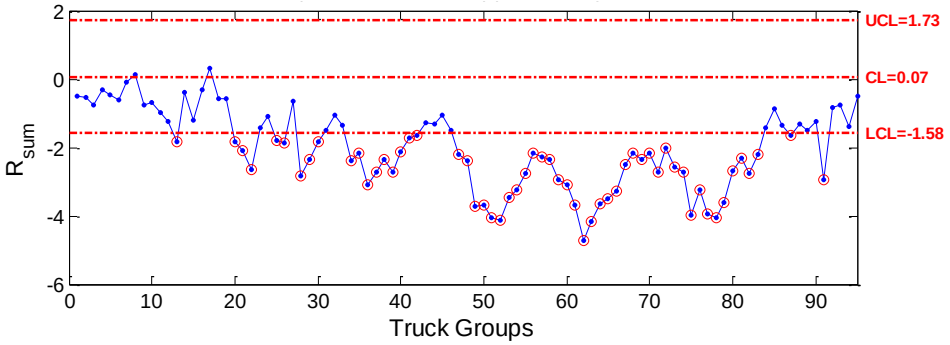

j. C-SG-CG(5)-V

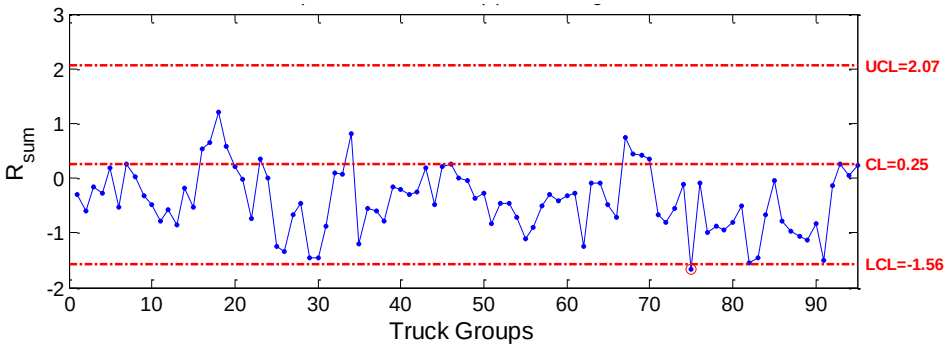

k. E-SG-CB(1)-V

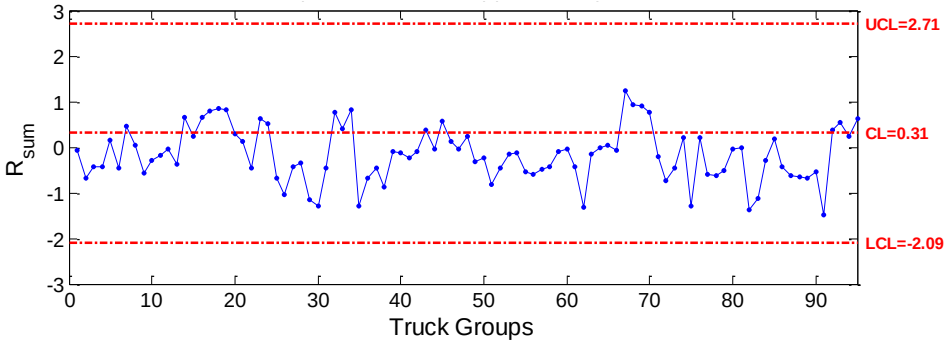

l. E-SG-CB(5)-V

Figure 5.8 continued Post-Damage Sacrificial Specimen 2 Control Charts (1.75 in. crack)

www.manaraa.com

The control charts for the sensors not on Specimen 2 are shown in Figure 5.8e through Figure 5.8l. All of these control charts show an acceptable number of R-sum values outside the control limits except for sensors B-NG-BF-H and C-SG-CB(5)-V in Figure 5.8e and Figure 5.8i respectively. Figure 5.8e shows a high percentage (33.7%) of R-sum values above the upper control limit and also shows an upward shift of the entire set of R-sum values. Figure 5.8i also shows a large percentage (60%) of R-sum values below the lower control limit as well as a downward moving shift of the R-sum values. Again, the data in both of these cases were influenced by the residual values from the sensors on Specimen 2 in the column and row-sum calculations. Further modifications to the damage detection algorithm are needed to address the high false-positive rate.

5.2.3 Percentage of Points outside the Control Limits

To aid in studying the relationship between data, the control limits, and the severity of the damage that occurred, a bar chart was constructed that displays the percentage of points outside the control limits for the sensors on Specimen 2. This chart (Figure 5.9) is a summary of the twelve control charts in Figure 5.6, Figure 5.7, and Figure 5.8. One can look at the chart and determine the location of the damage; the largest bars are those closest to the damage. For example, by investigating the 1.25 in. crack condition, the sensor with the largest percentage of points outside the control limits is sensor 4, suggesting that the damage occurs near sensor 4. The 1.25 in. crack occurred near sensor 4 so the conclusion reached from Figure 5.9 is correct. The suggested crack location may also be found for sensors 2, 3, and 4 following a similar procedure.

The cracking in sacrificial Specimen 2 occurred nearest to sensor 4 and is displayed in Figure 5.9 as the bars nearing 100% of the points outside the control limits. As the size of the crack increases to 1.75 in., the percentage of points outside the control limits of sensor 3 also starts to increase, as was expected. This increase in points outside of the control limits of sensor 3 for the 1.75 in. crack again confirms that more severe damage can be detected by sensors further away from the damage. The location of the damage, although, may be harder to detect as it becomes more severe.

www.manaraa.com

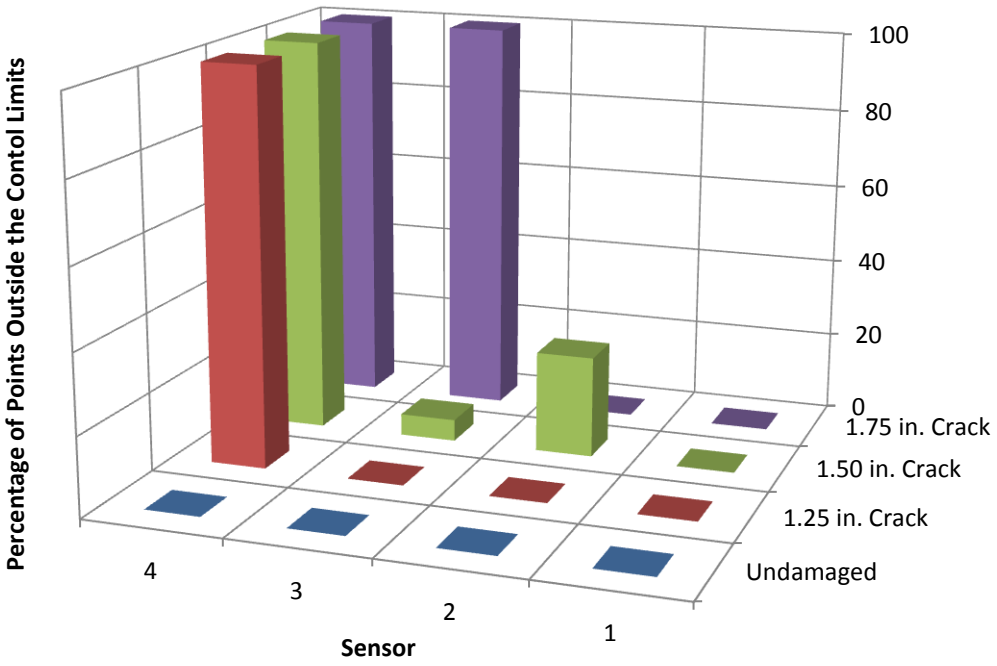

Figure 5.9 Percentage of Points outside the Control Limits: Sacrificial Specimen 2 Cracking

For example, in the case of the 1.50 in. crack, one can determine that that damage occurs near sensor 4 since the bar is the largest for that sensor (i.e., 100% of points fall outside of the control limits). But, if one examines the 1.75 in. crack case, the damage may be located near either sensor 3 or sensor 4.

5.2.4 Corrosion Testing Results

After fatigue cracking sacrificial Specimen 2 to a crack size of 1.75 in., new training data for the corrosion damage testing were collected from April 15, 2010 to April 29, 2010. A total of 2,544 heavy, right-lane, five-axle trucks were detected and used for control chart construction and false alarm testing. The resulting control charts are shown in Figure 5.10.

Only one of the points (1.67%) for either the training or testing data fell outside the control limits (Figure 5.10b, k and l). Unlike previous undamaged control chart construction, there appears to

www.manaraa.com

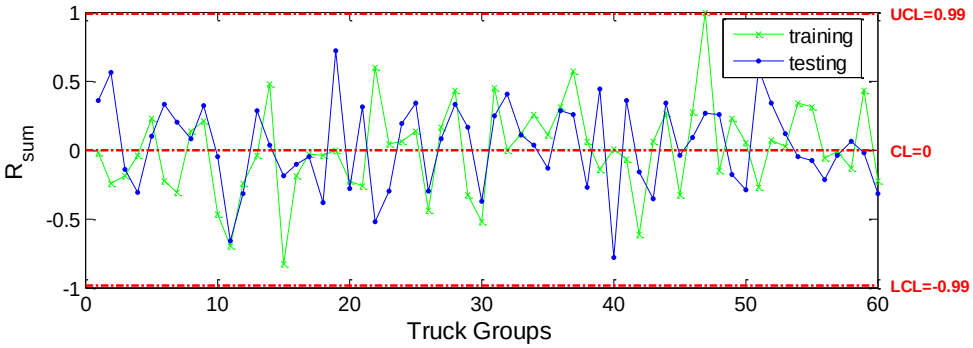

a. Sensor 1

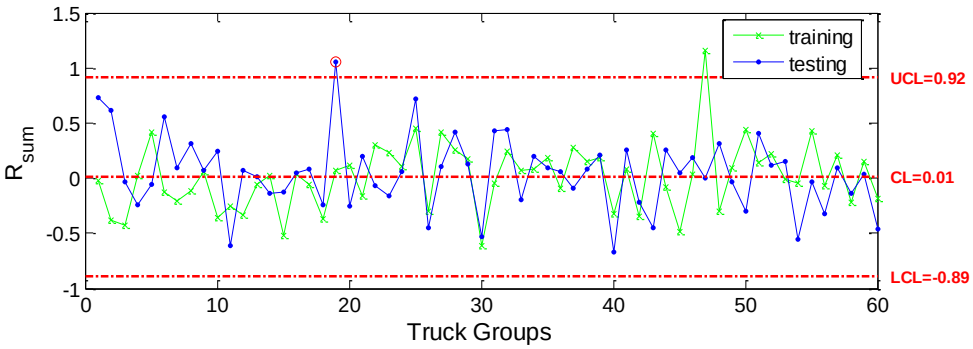

b. Sensor 3

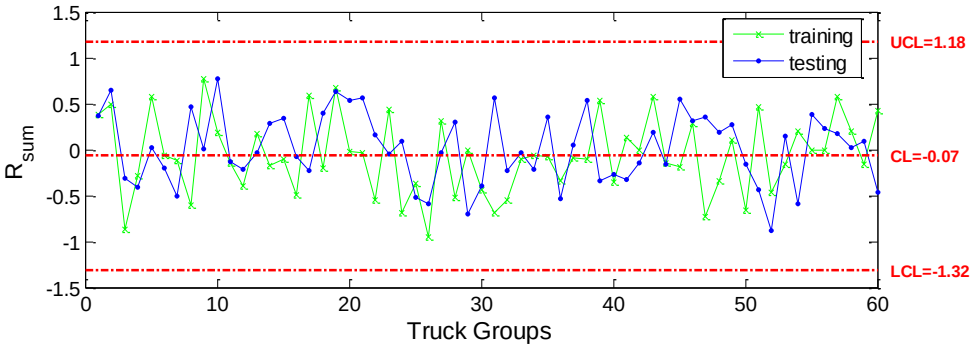

c. Sensor 3

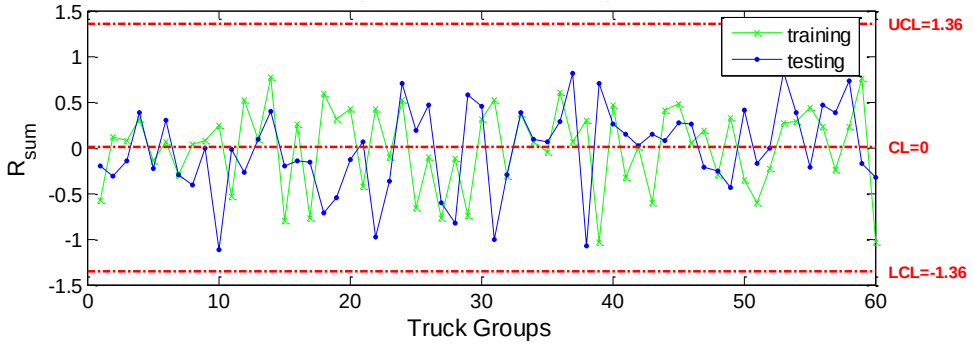

d. Sensor 4

Figure 5.10 Sacrificial Specimen 2 Corrosion Control Charts

www.manaraa.com

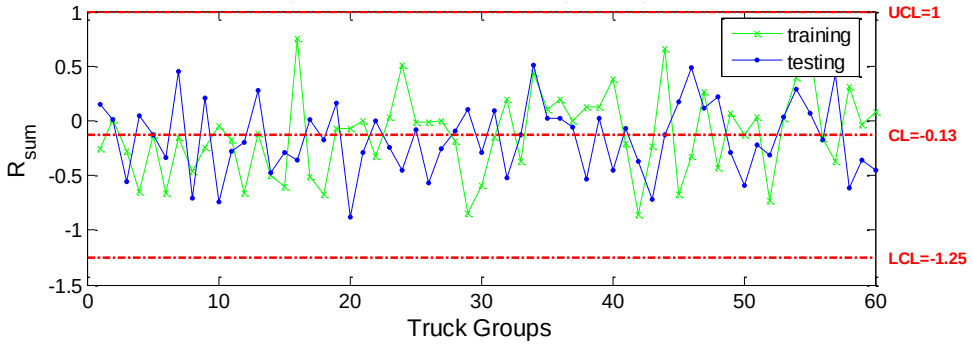

e. B-NG-BF-H

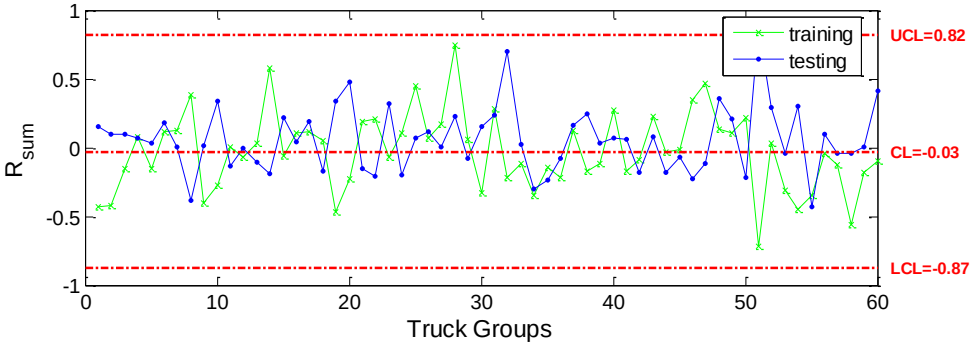

f. D-SG-BF-H

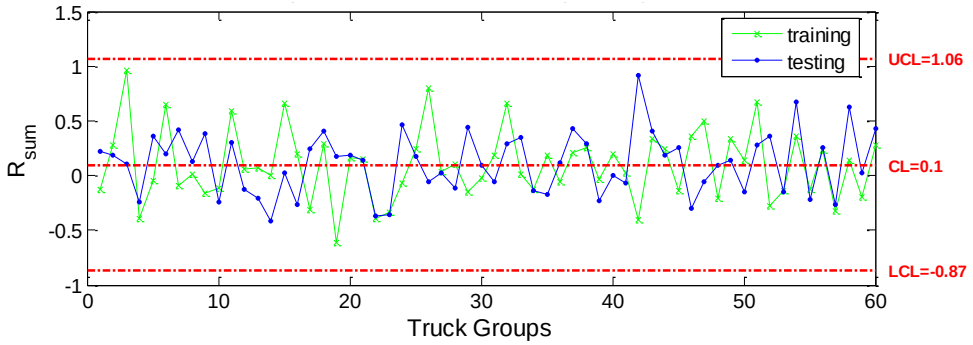

g. B-SS-BF-H

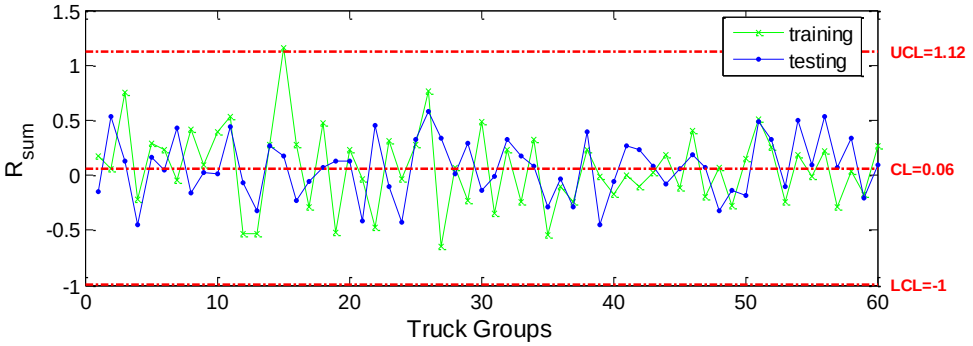

h. D-NS-BF-H

Figure 5.10 continued Sacrificial Specimen 2 Corrosion Control Charts

www.manaraa.com

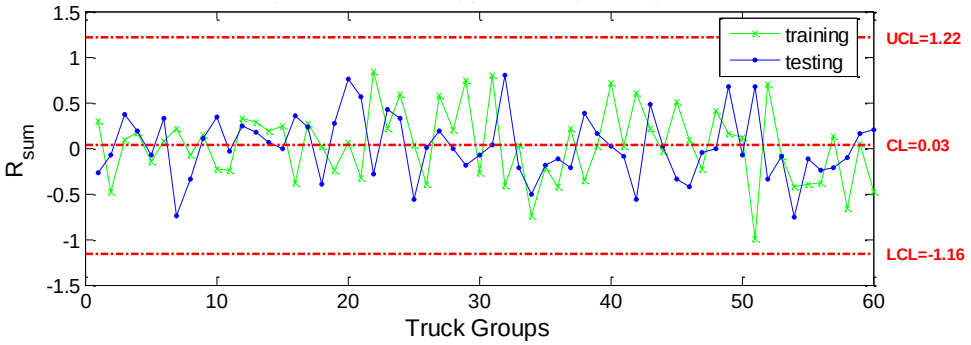

i. C-SG-CB(1)-V

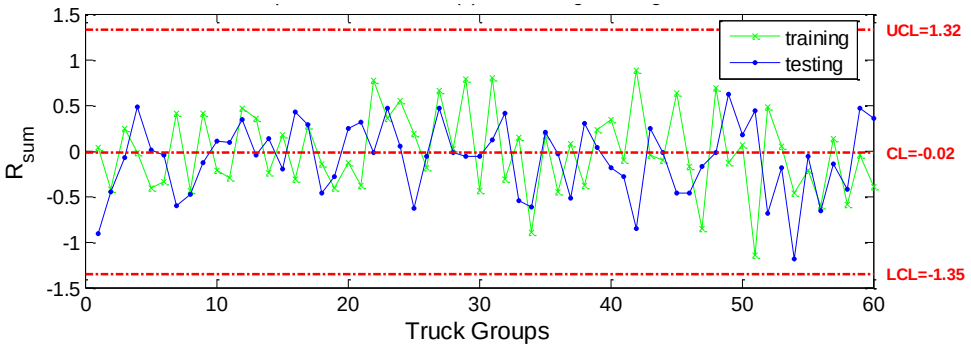

j. C-SG-CB(5)-V

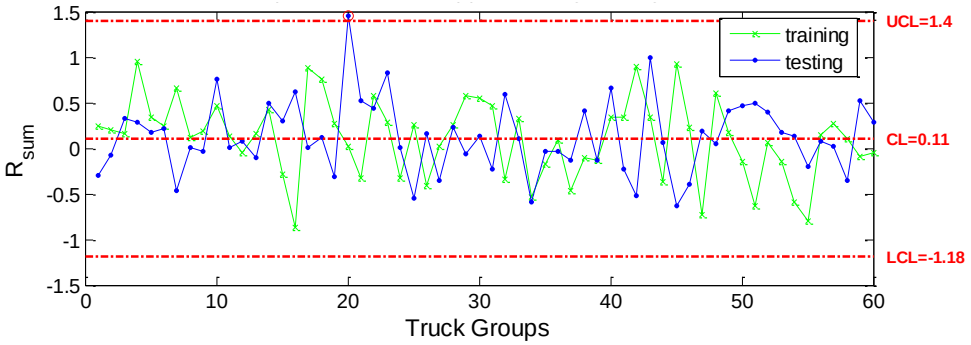

k. E-SG-CB(1)-V

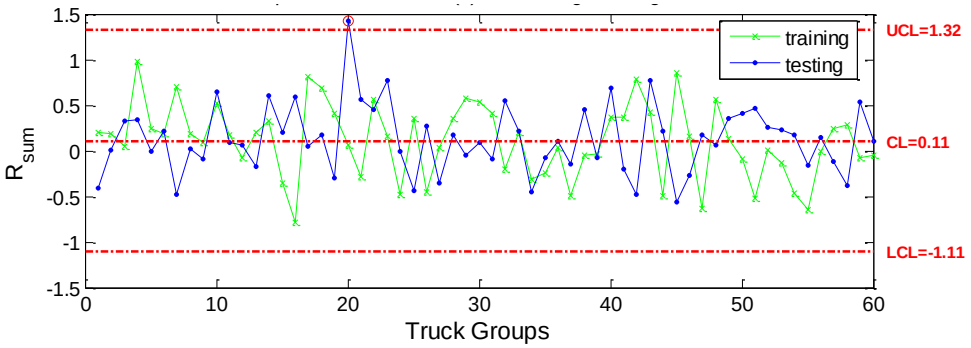

l. E-SG-CB(5)-V

Figure 5.10 continued Sacrificial Specimen 2 Corrosion Control Charts

www.manaraa.com

be a large amount of variation of the residuals. Although the reasons for this could be quite varied, the likely explanations include: influence from previous fatigue crack damage, unusual variability in truck traffic configuration, or environmental influences.

Following the collection of the training data, roughly five percent of the total plate thickness in a 1 in. by 3 in. section centered over Sensor 1 was removed. The location was centered over Sensor 1 to determine the effects of the corrosion when directly over a sensor and when in close proximity to other sensors. The locations of the simulated corrosion area and measurement points are shown in Figure 5.11. To measure the decrease in plate thickness, an additional steel plate was placed over each point and the distance from the top to the top plate was recorded. After grinding, this process was repeated and the percent decrease was calculated for each measurement point, the measurements are tabulated in Table 5.1

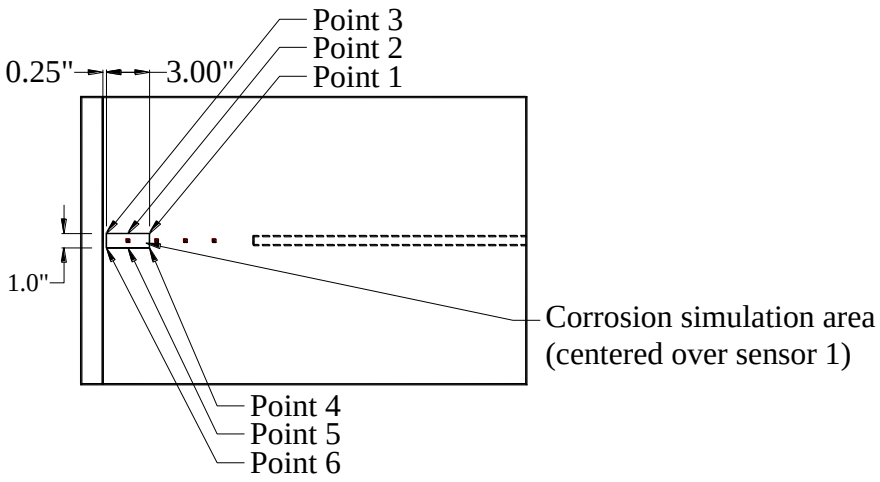

Figure 5.11 Corrosion Simulation Area Details

www.manaraa.com

Table 5.1 Simulated Corrosion Measurements Details

Measurement Point	Start (in.)	Finish (in.)	Difference (in.)	% Difference of Plate Thickness
1	0.396	0.438	0.042	9.6
2	0.396	0.412	0.016	3.7
3	0.395	0.418	0.023	5.3
4	0.393	0.429	0.036	8.2
5	0.390	0.412	0.022	5.0
6	0.396	0.420	0.024	5.5

Damage data were then collected from the corrosion simulated sacrificial Specimen 2 from May 1, 2010 to May 8, 2010. From the collected data, 497 heavy, five-axle, right-lane trucks were detected with the resulting control charts shown in Figure 5.12. Multiple points (42.9%) are below the LCL for sensor 2, indicating damage detection near sensor 2. Recall that the damage simulation area was centered over sensor 1. However, sensor 2 seemed to be more sensitive to the damage due to the higher percentage of material removed as shown in Table 5.1. The damaged control charts from sensors 1 and 3 remained similar relative to the undamaged control charts; there is a large amount of variation of the residuals within the control limits but very few points are outside of the control limits. The damaged control chart for sensor 4 differs from its undamaged control chart; specifically the mean of the damaged data is shifted up and is close to the UCL. This shift could be caused by the effects of the double curvature on the damage near sensor 2. Further damage may place more data points for sensor 4 outside the UCL giving a false reading on where the damage occurred. The control charts for sensors not on Specimen 2 are shown in Figure 5.12e through Figure 5.12l and show very few R-sum values outside of the control limits. Because the damage to Specimen 2 was small in this case, there are no large adverse affects to the R-sum values in the control charts for the sensors not on Specimen 2 as previously discussed.

www.manaraa.com

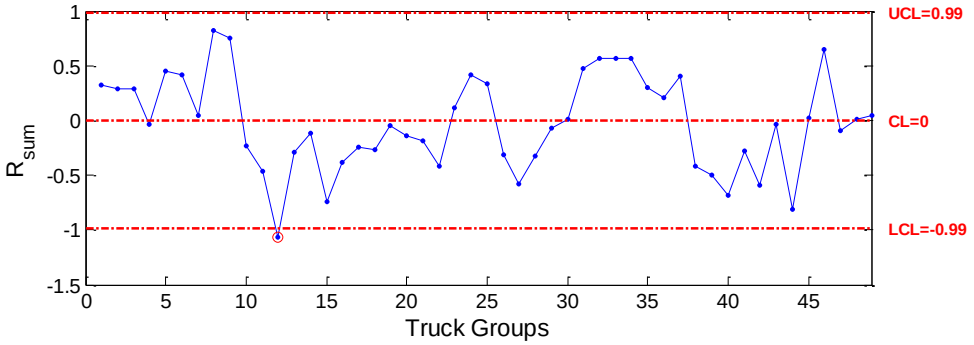

a. Sensor 1

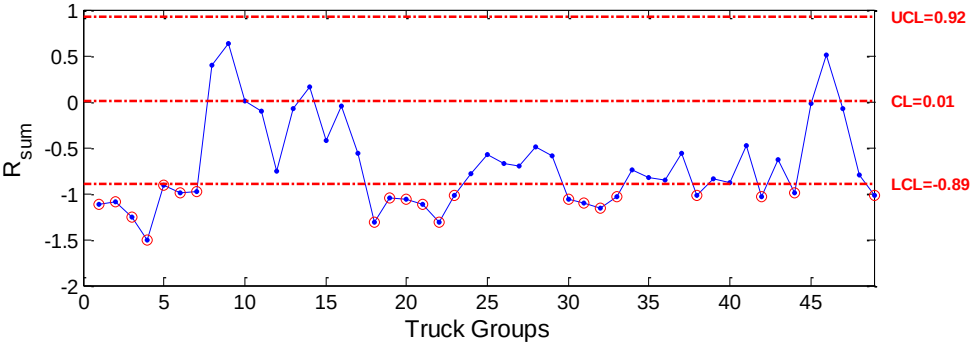

b. Sensor 2

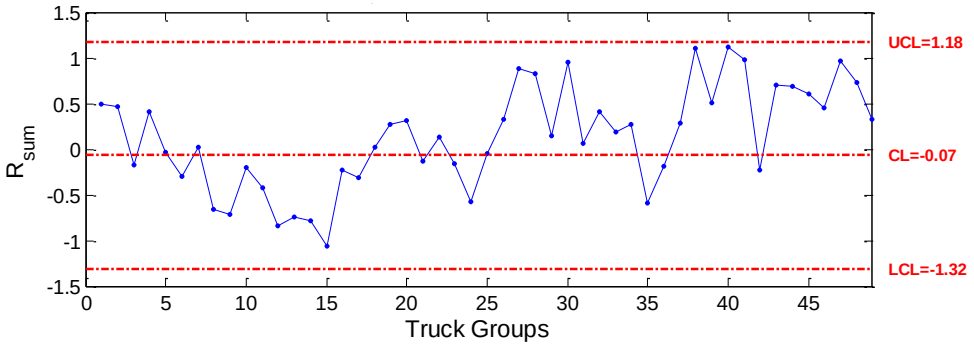

c. Sensor 3

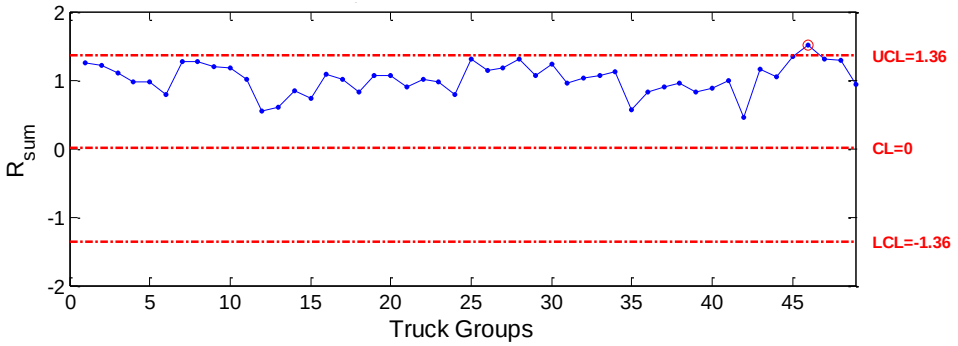

d. Sensor 4

Figure 5.12 Post-Corrosion Sacrificial Specimen 2 Control Charts

www.manaraa.com

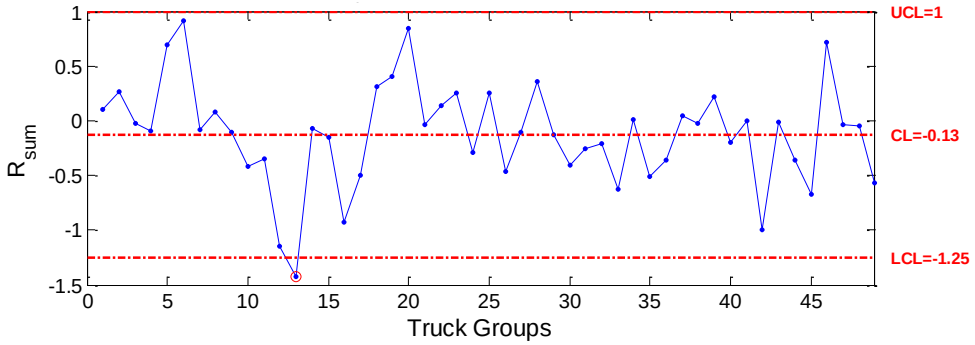

e. B-NG-BF-H

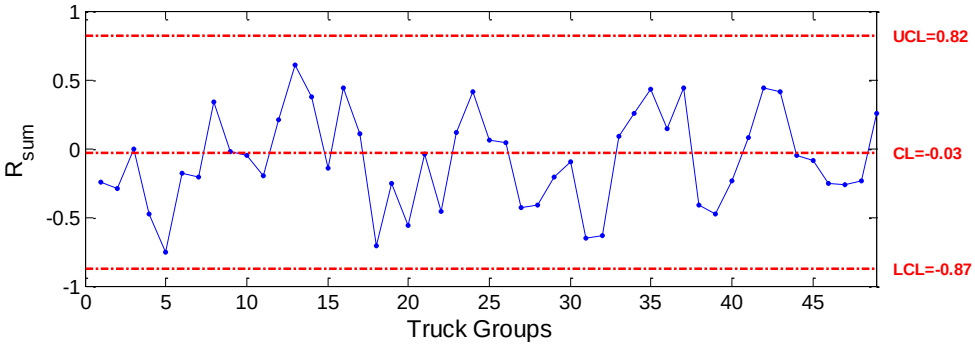

f. D-SG-BF-H

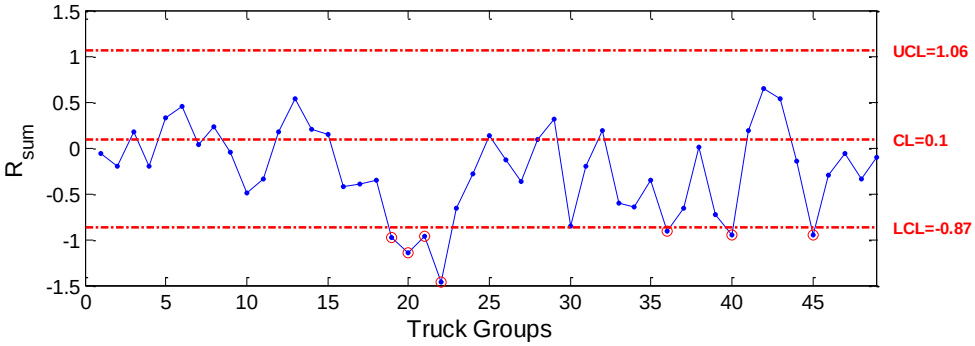

g. B-SS-BF-H

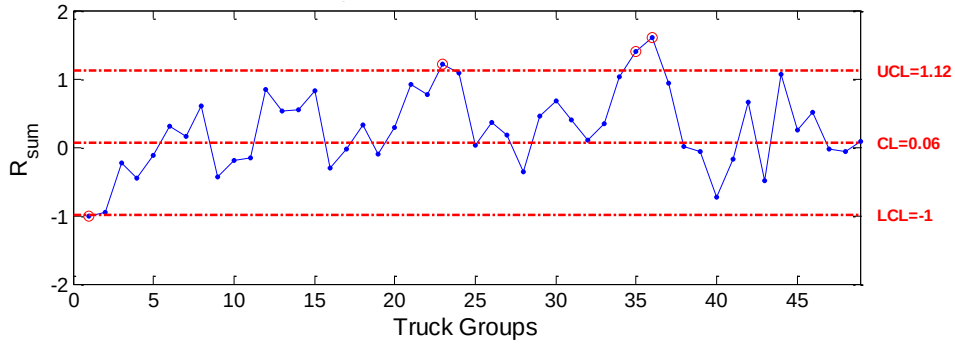

h. D-NS-BF-H

Figure 5.12 continued Post-Corrosion Sacrificial Specimen 2 Control Charts

www.manaraa.com

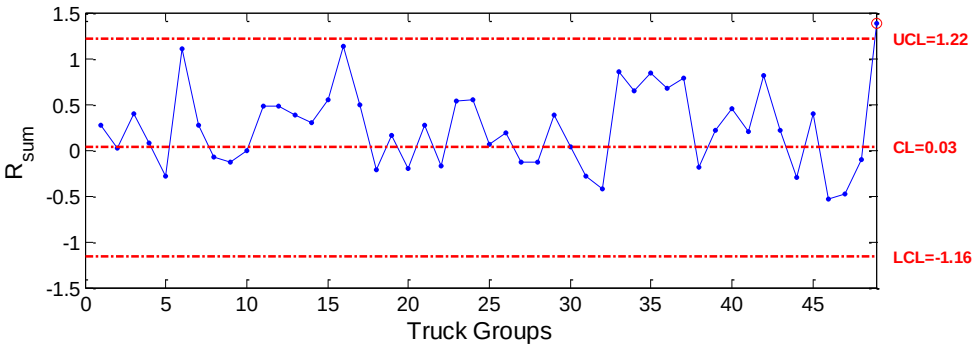

i. C-SG-CB(1)-V

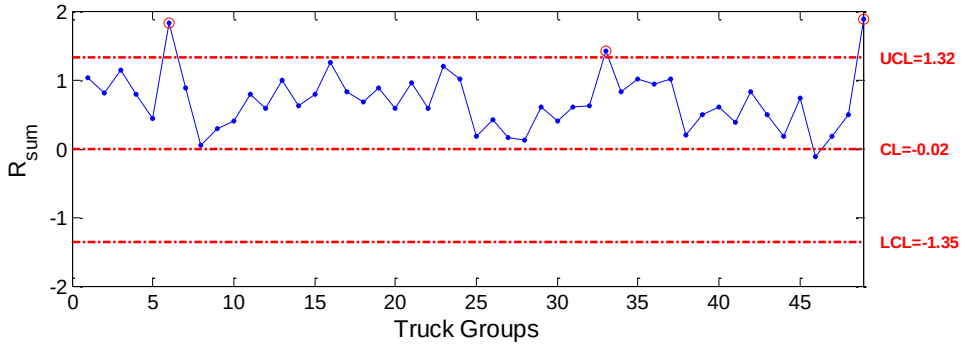

j. C-SG-CB(5)-V

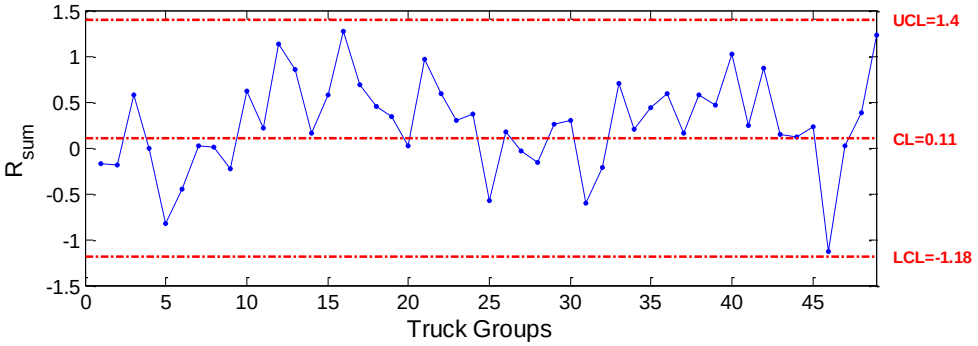

k. E-SG-CB(1)-V

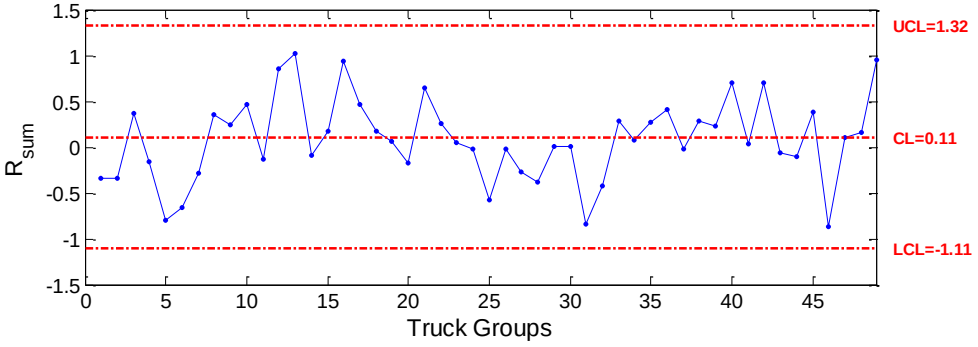

l. E-SG-CB(5)-V

Figure 5.12 continued Post-Corrosion Sacrificial Specimen 2 Control Charts

www.manaraa.com

CHAPTER 6. SUMMARY, CONCLUSIONS, AND FUTURE WORK

In this chapter a summary of the methods used and the results achieved in the experimental validation of the SHM damaged detection algorithm and the investigation into sensor attachment to concrete as presented. Conclusions are also given along with recommendations for algorithm improvement.

6.1 Summary

In previous projects a SHM system that can monitor bridges remotely and a damage detection algorithm were developed and theoretically validated. Numerous fiber-optic strain gauges were placed at different locations on the US30 bridge including fracture-critical areas. A damage detection system was created by Doornink (Doornink 2006) which uses matched event extrema to create a scatter plot. Limits were set by the user and points outside the limits are considered indications of detected damage. Damage was induced in a computer model of the US30 bridge and theoretical strains from the model were used to evaluate the damage detection approach initially developed by Doornink (Doornink 2006) and further refined by Lu (Lu 2008). As part of the refinement, it was determined that additional strain gauges on the underside of the concrete deck were needed for truck characterization. Over time, multiple gauges lost their bond with the concrete and produced erroneous results. An investigation into different sensor attachment techniques to concrete was completed using thin steel plates as the medium between the gauge and the concrete. Results of the testing showed that the strain transfer from the concrete to the gauge was not reliable and that further study was needed.

To validate the accuracy of the previously developed detection system multiple field tests were completed in this project. Located on the more than 50 fracture-critical bridges similar to the US30 bridge over the South Skunk river are multiple locations sensitive to fatigue damage, called the web-gap area. It was the desire to detect damage in these areas that was the precipitous for this work. Since damage introduction into the US30 bridge was prohibited, a sacrificial specimen which modeled the web-gap area in the US30 bridge was designed. The plate thicknesses and welds of the sacrificial specimen were similar to those found on the US30 bridge. The flanges of the sacrificial specimen were mounted to a concrete abutment pedestal.

www.manaraa.com

Double curvature bending was induced in the sacrificial specimen by attaching a steel strut to the sacrificial specimen and a bridge stringer. In this way the sacrificial specimen was exposed to ambient traffic loading.

To validate the accuracy of the damage detection algorithm, damage in the form of cracks and loss of thickness were introduced into two sacrificial specimens. Cracking was induced by vibrating the sacrificial specimen with a rotary shaker. At resonance, the sacrificial specimen was subjected to a large amount of cycles at high levels of strain which produced cracks in a relatively short period of time. Multiple sacrificial specimens with different crack sizes were evaluated. Thickness loss was created by removing material with a hand-held rotary grinder.

Following training, sacrificial Specimen 1 was damaged with a large crack at the edge of the connection plate of both the top and bottom plates. Damage data were then collected and plotted on previously constructed control charts. Every post-damage R-sum value for the three sensors closest to the damage was outside the control limits indicating damage had been detected. Unfortunately multiple R-sum values were outside the control limits for sensors not near the damage, giving false positive readings. Upon further evaluation it was concluded that these R-sum values were influenced by the large magnitude of the residuals from the sensors near the damage.

Specimen 2 was fabricated and tested similarly to Specimen 1. Specimen 2 was installed at the US30 bridge, training data were collected, control charts were constructed, and the sacrificial specimen was vibrated until a 1.25 in. long crack appeared in the top plate. Damage data were then collected and plotted on the control charts; this process was repeated with the crack further propagated to 1.50 in. and then 1.75 in. In all cases, all data points for the sensor closest to the damage were outside the control limits, indicating that damage had been detected. As with Specimen 1, multiple R-sum values for sensors far from the damage were outside the control limits giving multiple false-positives.

After damaging Specimen 2 with the 1.75 in. long crack, new training data were collected and new control charts were constructed. To determine the detectability of corrosion, an area of the top plate was ground off to simulate thickness loss associated with the corrosion process.

www.manaraa.com

Damaged data were collected and plotted on the control charts. The sensor closest to the section with the highest percentage of plate thickness ground off had numerous data points outside the control limits indicating that thickness loss can be detected.

6.2 Conclusions

Based upon the work summarized herein, the following conclusions were made:

1. Damage can be autonomously detected by the damage detection algorithm as long as the sensor is "close enough" to a sensor. It is not known how close is "close enough."

2. There is a loose correlation between the level of damage and the distance between the mean training data and the post-damage data. Specifically, the mean of the data collected from a smaller amount of damage (i.e., a 2.0 in. crack) is closer to the mean of the training data than the data from a larger amount of damage (i.e., 6.0 in. crack). A comparison of the means of the data collected from incremental amounts of damage proved inconclusive, however, and is further mentioned in the Future Work section.

3. The damage detection algorithm has a relatively high false positive detection rate. It was determined that the residual values for the sensors nearest to the damage influence the R-sum values for the other sensors during the simplification process.

4. Based on multiple loadings, plate dimensions and configuration, and loadings the investigated sensor attachment techniques should not be used in the field. All of the combinations proved unreliable and inaccurate in the strain transfer between the concrete and sensor.

6.3 Future Work

Additional work is required to further improve and verify the damaged detection algorithm including:

1. The introduction of additional and different artificial damage to the US30 bridge

www.manaraa.com

including girder corrosion and cracking in locations other than the web gap areas to further investigate the local and global detection characteristics of the damage detection algorithm.

2. The development of further algorithm improvements that:

    a. Reduces the false-positive rate by excluding the residuals from the sensors located near the damage in the matrix simplification procedure. Through a computational process, each sensor in each column and row in the residual matrix will be evaluated to determine the overall percentage each contributes to the column and row-sum values. Once the sensors which contribute the highest percentage to the sum have been identified, they will be excluded from the construction of the control charts for the sensors located further away from the damage. This will allow the control charts for the sensors located further away from the damage to be free of the influence from the sensors near the damage reducing the false-positive rate.

    b. Quantifies damage levels by comparing orthogonally fit lines through both the training and damaged data. In a statistical test called the F-Test, a comparison between two models is completed using one data set. Using multipliers to exclude or include training or damaged data, the first model, called the full-model is constructed. The full model uses training and damaged data separately to create two orthogonally fit lines that pass through both the training and damaged data separately but are considered one model. A reduced model is constructed which orthogonally fits a line through a combination of both data sets. Differences between the orthogonally fit lines for both the full and reduced models should remain small for a sensor not located near damage. Differences between the orthogonally fit lines for the full and reduced models should be larger and detectable through the F-Test which compares the residual sum of the squares for a sensor located near the damage.

www.manaraa.com

REFERENCES

Betz, B C, W J Staszewski, G Thursby, and B Culshaw. "Multi-Functional Fibre Bragg Grating Sensors for Fatigue Crack Detection in Metallic Structures." *Institution of Mechanical Engineers: Journal of Aerospace Engineering.* Professional Engineering Publishing Ltd., 2006. 453-461.

Caicedo, Juan M, and Shirley J Dyke. "Experimental Validation of Structural Health Monitoring for Flexible Bridge Structures." *Structural Control and Health Monitoring*, 2005: 425-443.

Chintalapudi, Krishna, et al. "Monitoring Civil Structures with a Wireless Sensor Network." *IEEE Internet Computing*, 2006: 26-34.

Doebling, Scott W, Charles R Farrar, Michael B Prime, and Daniel W Shevitz. "Damage Identification and Health Monitoring of Structural and Mechanical Systems from Changes in their Vibration Characteristics: A Literature Review." 1996.

Doornink, J D. "Damage Detection in Bridges through Fiber Optic Structural Health Monitoring." *Proceedings of SPIE - The International Society for Optical Engineering.* Boston, Ma: SPIE, 2006.

Galvanetto, Ugo, Cecilia Surace, and Alessandra Tassotti. "Structural Damage Detection Based on Proper Orthogonal Decomposition: Experimental Verification." *AIAA Journal*, 2008: 1624-1630.

Guan, Hong, Vistasp M Karbhari, and Charles S Sikorsky. "Long-Term Structural Health Monitoring System for a FRP Composite Highway Bridge Structure." *Journal of Intelligent Material Systems and Structures*, 2007: 809-823.

Hoult, Neil A, Paul R A Fidler, Ian J Wassell, Peter G Hill, and Campbell R Middleton. "Wireless Structural Health Monitoring at the Humber Bridge UK." *Proceedings of the Institute of Civil Engineers: Bridge Engineering.* Thomas Telford Services Ltd, 2008. 189-195.

Kim, Hansang, and Hani Melhem. "Damage Detection of Structures by Wavelet Analysis." *Engineering Structures*, 2004: 347-362.

Kim, Jeong-Tae, and Norris Stubbs. "Nondestructive Crack Detection Algorithm for Full-Scale Bridges." *Journal of Structural Engineering*, 2003: 1358-1366.

Kim, Sukun, et al. "Health Monitoring of Civil Infrastructures Using Wireless Sensor Networks." *Proceedings of the Sixth International Symposium on Information Processing in Sensor Networks.* Cambridge, MA: Association for Computing Machinery, 2007. 254-263.

Lu, Ping. *A Statistical Based Damage Detection Approach for Highway Bridge Structural Health Monitoring.* Ames, Ia: Iowa State University, 2008.

www.manaraa.com

Ng, C T, and M Veidt. "A Lamb-Wave Based Technique for Damgage Detection in Composite Laminates." *Smart Materials and Structures*, 2009.

Olund, Josh, and John DeWolf. "Passive Structural Health Monitoring of Connecticut's Bridge Infrastructure." *Journal of Infrastructure Systems*, 2007: 330-339.

Panigrahi, S K, S Chakraverty, and B K Mishra. "Vibration Based Damage Detection in a Uniform Strength Beam Using Genetic Algorithm." *Springer Online*, 2009.

Saadat, Soheil, Mohammad N Noori, Gregory D Buckner, Tadatoshi Furukawa, and Yoshiyuki Suzuki. "Structural Health Monitoring and Damage Detection Using an Intelligent Parameter Varying (IPV) Technique." *International Journal of Non-Linear Mechanics*, 2004: 1687-1697.

Salah el Din, A. S., and J. M. Lovegrove. "A Gauge for Measuring Long-Term Cyclic Strains on Concrete Surfaces." *Magazine of Concrete Research*, 1981: 123-127.

Vis, James Martin. *Evaluation of a Structural Health Monitoring System for Steel Girder Bridges.* Creative Component Report, Ames, Iowa: Iowa State University, 2007.

Wang, Shanshan, Qingwen Ren, and Pizhong Qiao. "Structural Damage Detection Using Local Damage Factor." *Journal of Vibration and Control*, 2006: 955-973.

Wipf, Terry J., Brent M. Phares, and Justin D. Doornink. *Monitoring the Structural Condition of Fracture-Critical Bridges Using Fiber Optic Technology.* Ames, IA: Center for Transportation Research and Education: Iowa State University, 2007.

Yin, An, Bingwen Wang, Zhuo Liu, and Xiaoya Hu. "Design and Implementation of the Structure Health Monitoring System for Bridge Based on Wireless Sensor Network." *6th International Symposium on Neural Networks.* Wuhan, China: Springer Verlag, 2009. 915-922.

Yuan, Shenfang, Xiaosong Lai, Xia Zhao, Xin Xu, and Liang Zhang. "Distributed Structural Health Monitoring System Based On Smart Wireless Sensor and Multi-Agent Technology." *Smart Materials and Structures*, 2005: 1-8.

www.manaraa.com